Durability of Concrete Incorporating Blended Binders and Alkali-Activated Materials to Sulfuric Acid Environments

By

Mohamed Ramadan Hussien Mahmoud

A Thesis submitted to the Faculty of Graduate Studies of

The University of Manitoba

In partial fulfillment of the requirements of the degree of

Master of Science

Department of Civil Engineering

University of Manitoba

Winnipeg, MB, Canada

Abstract

Acidic attack on concrete imparts unique set of damage mechanisms and manifestations compared to other durability issues of concrete. Sulfuric acid attack limits the service life of concrete elements and, thus, results in increased expenditures for the repair or in some cases replacement of the whole structure. To date, there is lack of standardized tests for specifically evaluating the resistance of concrete to sulfuric acid attack, which has caused great variability, for example in terms of solution concentration, pH level/control, etc., among previous studies in this area. Accordingly, there are conflicting data about the role of key constituents of concrete (e.g. supplementary cementitious materials [SCMs]), and uncertainty about building codes' stipulations for concrete exposed to sulfuric acid. Hence, the first objective of this thesis was to assess the behaviour of the same concretes, prepared with single and blended binders, to incremental levels (mild, severe and very severe) of sulfuric acid solutions over 36 weeks. The test variables included the type of cement (general use [GU] or portland limestone cement [PLC]) and SCMs (fly ash, silica fume and nano-silica). The severe (1%, pH of 1) and very severe aggression (2.5%, pH of 0.5) phases caused mass loss of all specimens, with the latter phase providing clear distinction among the performance of concrete mixtures. The results showed that the penetrability of concrete was not a controlling factor, under severe and very severe damage by sulfuric acid attack, whereas the chemical vulnerability of the binder was the dominant factor. Mixtures prepared from PLC performed better than that of counterparts made from GU. While the quaternary mixtures comprising GU or PLC, fly ash, silica fume and nanosilica showed the highest mass losses after 36 weeks, binary mixtures incorporating GU or PLC with fly ash had the lowest mass losses.

Several studies reported that the improved chemical resistance of alkali-activated materials (AAMs) over concrete based on portland cements. However, AAMs have technical limitations, which might deter its widespread use in cast-in place applications. These limitations include need for heat curing, slow setting, and slow strength development, which might be mitigated by further improving the reactivity of AAMs during early-age with nanoparticles; however, this area remains largely unexplored. Hence, the second objective of this thesis was to develop innovative types of AAMs-based concrete [alkali activated fly ash (AAFA), alkali activated slag (AAS) and their blends incorporating nanosilica] and evaluate their resistance to two different sulfuric acid exposures over 18 weeks for potential use in repair of concrete elements vulnerable to acidic attack. While AAFA specimens, produced without heat curing, experienced rapid ingress of the acidic solution and a significant reduction in the bond strength with substrate concrete, fly ash based AAMs comprising slag and or nanosilica (AAFA-S and AAFA-S-NS) had improved performance due to discounting the ingress of acidic solution and continued geopolymerization reactivity. Comparatively, specimens from the slag group exhibited high levels of swelling, internal cracking and mass loss due to chemical deterioration. The overall results suggest that AAFA-S and AAFA-S-NS mixture, without heat curing, may be a viable option for repair applications of concrete elements in acidic entrainments, but field trials are still needed to further verify their performance.

To Mom and Dad,
I hope this achievement gets me a step closer to making you proud of me.

Acknowledgements

I would like to express my sincere gratitude and appreciation to my supervisor Dr. Mohamed T. Bassuoni, P.Eng., Associate Professor, Department of Civil Engineering, University of Manitoba, for his unremitting guidance and cordial support in all stages of this research accomplishment. I do also deeply convey my sincere thanks to him for his encouragement and help to organize my ideas and interests, and also express my deep appreciation for what I have learned from him during my study.

I highly appreciate the financial support from Natural Sciences and Engineering Research Council of Canada (NSERC), John Glanville Memorial Scholarship, and Graduate Enhancement of Tri-Council Stipends (GETS). The IKO Construction Materials Testing Facility at the University of Manitoba in which these experiments were conducted.

Many thanks to Chad Klowak, P.Eng., W.R. McQuade Heavy Structures Laboratory Manager, University of Manitoba, for his technical assistance and valuable guidance.

I would like to thank my colleagues for their continuous support specially Ahmed Gaber, Mohammad Tiznobaik, Mohamed Sakr and Mohamed El Gendy whose comments and suggestions were remarkable.

Finally, I would like to thank my mother and my father for their endless support throughout this significant part of our life. Thank you all, without your sincere support I would not be here to make this achievement.

Table of Contents

Abstract i
Acknowledgements iv
Table of Contents v
List of Tables vii
List of Figures viii
Abbreviations/Nomenclature xi
Chapter 1: Introduction 1
1.1. Overview 1
1.2. Need for Research 2
1.3. Objectives 6
1.4. Scope of Work 7
1.5. Thesis Outline 8
Chapter 2: Literature Review 9
2.1. General Features of Sulfuric Acid Attack 9
2.2 Standardized Test Methods and Methods of Quantifying Degradation 13
2.3. Role of the Type of Cement, SCMs, Nanoparticles and Limestone Fillers in Resisting Acidic Attack 15
2.3.1 Role of the Type of Cement 15
2.3.2 Role of SCMs and Nanoparticles 16
2.3.3 Role of Limestone Filler 17
2.4. Alkali-Activated Materials 18
2.4.1 Review 18
2.4.2 Alkali-Activated Fly Ash 19
2.4.3 Alkali-Activated Slag 20
2.4.4 Alkaline Activator 21
2.4.5 Curing, fresh and Hardened Properties 24
2.4.6. Durability of AAMs to Sulfuric Acid Attack 28
2.5. Code Provisions 29
2.6. Closure 33
Chapter 3: Experimental Program 35
3.1 Experimental Program for Concrete Mixtures Incorporating SCMs and Nanosilica under Incremental Acidic Attack 35

3.1.1 Materials and Mixtures 35
3.1.2 Acid Exposure 37
3.1.3 Tests 39
3.2 Experimental Program for Concrete with AAMs under Different Acidic Exposures 44
3.2.1 Materials and Mixtures 44
3.2.2 Procedures of Mixing 46
3.2.3 Acid Exposure 48
3.2.4 Tests 50
Chapter 4: Results and Discussion for Concrete Mixtures Incorporating SCMs and Nanosilica under Incremental Acidic Attack 54
4.1 Penetrability and Porosity 54
4.2 Visual Assessment 56
4.3 Mass Loss 58
4.4 Thermal and Microstructural Analyses 63
Chapter 5: Results and Discussion for Concrete with AAMs under Different Acidic Exposures 72
5.1 Absorption Test 72
5.2 Visual Assessment 73
5.3 Neutralization Depth 75
5.4 Mass Loss and Pull-off Test 77
.5 Discussion 80
Chapter 6: Summary, Conclusions and Recommendations 90
6.1. Summary 90
6.1.1 Conclusions of Concrete Mixtures Incorporating SCMs and Nanosilica under Incremental Acidic Attack 90
6.1.2. Conclusions of Concrete with AAMs under Different Acidic Exposures 92
6.2 Recommendations for Future Work 93
References 95

List of Tables

Table 2. 1: Typical Ms and Na_2O dosage based on sodium silicate activators for AAFA 23

Table 2. 2: Typical Ms and Na_2O dosage based on sodium silicate activators for AAS 24

Table 3. 1: Chemical and physical properties of cement and SCMs 36

Table 3. 2: Proportions of mixtures per cubic meter of concrete 37

Table 3. 3: Chemical composition and physical properties of fly ash, slag and nanosilica 44

Table 3. 4: Proportions of the mixtures per cubic meter 46

Table 4. 1: Results from RCPT and MIP 55

Table 4. 2: Portlandite (420-440ºC) contents in specimens stored in the curing chamber 64

Table 4. 3: Enthalpies (J/g) of the main phases in the cementitious matrix after acid exposure . 65

List of Figures

Fig. 2. 1: a) gypsum depositions and b) aggregate disintegration after exposure to 2.5% concentration of sulfuric acid in a laboratory test. 1

Fig. 3. 1: Incremental aggression of the sulfuric acid exposure: phase I, II and III 1

Fig. 3. 2: Incremental aggression of the sulfuric acid exposure: phase I, II and III 1

Fig. 3. 3: RCPT apparatus. 1

Fig. 3. 4: MIP apparatus. 1

Fig. 3. 5: Drying the specimens in laboratory conditions after taking them out of the solution. ... 1

Fig. 3. 6: Weighing the specimens after drying to calculate the relative mass change. 1

Fig. 3. 7: The DSC instrument 1

Fig. 3. 8: The sample chamber of SEM where the fracture pieces were mounted. 1

Fig. 3. 9: Spraying the top surfaces of the mixtures after casting by a curing compound. 1

Fig. 3. 10: Wire brushing the surface of the substrate slabs after casting. 1

Fig. 3. 11: Casting the repair layer (AAMs) on the substrate slabs and spraying the top surface of the mixtures with the curing compound 1

Fig. 3. 12: Test set-up for the slabs before ponding with the sulfuric acid solution. 1

Fig. 3. 13: Partial coring of the slabs. 1

Fig. 3. 14: The pull-off test. 1

Fig. 3. 15: XRD instrument in which the powder samples were test 1

Fig. 4. 1: Features of damage of GU specimens immersed in the sulfuric acid solutions after Phases: (a) I, (b) II, and (c) III. 1

Fig. 4. 2: Neutralization depth of concrete specimens immersed in the sulfuric acid solutions after: a) Phase I (pH of 4.5), and b) Phase III (pH of 0.5) 1

Fig. 4. 3: Average mass loss with time for specimens from groups: a) GU, and b) PLC. 1

Fig. 4. 4: Cumulative mass loss for GU and PLC groups after: a) 24 weeks, and b) 36 weeks..... 1

Fig. 4. 5: Penetrability of specimens vs. their total mass losses after: a) Phase II, and b) Phase III 1

Fig. 4. 6: Exemplar micrographs from a GU specimen after Phase I showing gypsum in the reaction zone infilling air voids with higher magnification (x 3000). 1

Fig. 4. 7: Micrographs of SEM and EDX analyses for a GUSF specimen after Phase II: (a) deteriorated surface, and (b) gypsum formation in the reaction zone (left) with corresponding EDX (right). 1

Fig. 4. 8: SEM and EDX analyses after Phase III for a GU specimen: (a) deteriorated surface showing gypsum formation in the reaction zone (left) with corresponding EDX (right), and (b) ettringite rosettes growing in an air void away from the surface (left) with corresponding EDX (right). 1

Fig. 4. 9: SEM and EDX analyses after Phase III for a PLCFSFNS specimen showing: (a) large gypsum crystals in the reaction zone, (b) deteriorated surface, and (c) cracks extending into the inner core..... 1

Fig. 4. 10: Unreacted fly ash particles within the reaction zone of a PLCF specimen (left) with corresponding EDX (right). 1

Fig. 5. 1: Absorption trends of all mixtures..... 1

Fig. 5. 2*:* Appearance of concrete specimens after 18 weeks of immersion in 10% sulfuric acid: (a) fly ash based AAMs, and b) slag based AAMs..... 1

Fig. 5. 3: Degradation of slabs at the end of the cyclic exposure with the sulfuric acid. 1

Fig. 5. 4: Neutralization depth versus time for the specimens in the full immersion exposure. ... 1

Fig. 5. 5: Progressive neutralization depth of specimens from the AAFA mixture at different ages in the full immersion exposure. 1

Fig. 5. 6: Mass loss of the fly ash and slag AAMs at the end of the combined exposure. 1

Fig. 5. 7: Bond strength of the repair assembly from the pull-off test. 1

Fig. 5. 8: XRD patterns of specimens from different mixtures before exposure. (CSH: calcium silicate hydrate; Z: zeolite; CASH: calcium aluminate silicate hydrate; G: gypsum; P: portlandite; Q: quartz; D: dolomite; C: calcite; M: mullite) 1

Fig. 5. 9: XRD patterns of specimens from different mixtures after the combined exposure. (Z: zeolite; M: mullite, G: gypsum; P: portlandite; Q: quartz; D: dolomite; C: calcite) 1

Fig. 5. 10: SEM images with EDX of deteriorated surface showing gypsum formation in the reaction zone (left) with corresponding EDX (right) after the combined exposure: (a) AAFA, and (b) AAFA-S 1

Fig. 5. 11: SEM and EDX analyses for AAS specimen showing: (a) cracks extending into the inner core, (b) small and large gypsum crystals in the reaction zone (left) with corresponding EDX (right). 1

Fig. 5. 12: DSC curves of all mixtures showing quantities of gypsum formed after the combined exposure. 1

Abbreviations/Nomenclature

RCPT = the rapid chloride permeability test

MIP = mercury intrusion porosimetry

DSC = differential Scanning Calorimetry

EDX = energy Dispersive X-ray analysis

SEM = scanning Electron Microscopy

XRD = X-ray diffraction

CH = calcium hydroxide (portlandite)

C-S-H = calcium silicate hydrate

MLt = cumulative mass loss at the end of each week (kg)

Mi = initial mass of the specimen before exposure to sulfuric acid (kg)

Mt = mass of the specimen at time *t* (kg)

PLC = portland-limestone cement

GU = general use cement

SCMs = supplementary cementitious materials

AAMs = alkali-activated materials

SF= silica fume

NS = nanosilica

FA or F = fly ash

S = slag

AAFA = alkali-activated fly ash

AAS = alkali-activated slag

I = absorption depth of concrete at a certain point of time in mm

m_t = the difference between M_{WET} and M_{DRY} in g at a specific point of time

a = cross sectional area of the exposed surface in mm^2

d = density of fluid in g/mm^3

Chapter 1: Introduction

1.1. Overview

Chemical attack of concrete by sulfuric acid is a chief durability concern worldwide, and the recent increase in the reported attacks in industrial zones, wastewater plants, sewage facilities, etc. by acidic media has drawn much attention to this topic (Attiogbe and Rizkalla, 1988; Monteny et al., 2000; De Belie et al., 2004; Gutiérrez-Padilla et al., 2010). Sulfuric acid attack limits the service life of concrete elements, which basically are constructed to meet a target life span, and thus it results in increased expenditures on the repair or in some cases replacement of the whole structure. In USA alone, the Congressional Budget Office estimated annual maintenance costs of $25 billion for wastewater systems during the period 2000-2019 (Sunshine, 2009). The most commonly known type of sulfuric acid damage occurs in concrete sewer pipes, treatment plants, pumping stations, manholes, junction chambers, etc. This type of corrosion is known by different names, such as microbial induced corrosion (MIC), biogenic sulfuric acid corrosion and hydrogen sulfide (H_2S) corrosion (Wei et al., 2013; Gutiérrez-Padilla et al., 2010; Leemann et al., 2010). Also, sulfuric acid can originate from industrial wastewater and acid rain (Chen et al., 2013; Xie et al., 2004) due to severe air pollution problems in mega cities. For example, in China, it was reported that acid rain falls over about one third of Chinese territories (Fan et al., 2010). High rise buildings made of concrete in these areas may be damaged due to exposure to frequent rain falls with high acidity for a long time (Okochi et al., 2000). In addition, sulfuric acid may be produced in groundwater and soils as a result of the oxidation of iron-sulfide minerals in the form of pyrites (Pye and Miller, 1990). Acid attack of concrete is generally classified as a chemical attack. The sulfuric acid reacts with calcium hydroxide (CH) and calcium silicate hydrate (C-S-H), the main hydration components in the cement paste, resulting in the precipitation of calcium sulfate

[gypsum] (Alexander, 2011). This reaction ultimately leads to decalcification and disintegration of the cementitious matrix (C-S-H gel, being converted ultimately to amorphous hydrous silica). Sulfuric acid has a combined attack by the proton (an acid) and sulfate attack in which the acid component enhances dissolution and thereby plays a significant role in the damage mechanism.

1.2. Need for Research

In a mild environment with adequate design, concrete made from ordinary and blended binders can be durable. However, it has been recognized that conventional concrete can suffer from degradation due to the attack from aggressive media such as sulfates and acids. Hence, looking for efficient ways to protect existing sanitary facilities from further damage or possibly even increase their life span is a more realistic approach. Also, producing concrete which has improved resistance against chemical and sulfuric acid corrosion can also be a solution. This goal may be achieved by the partial replacement of General Use (GU) by active nanoparticles or supplementary cementitious materials (SCMs). Numerous research studies (e.g. Roy et al., 2001; Papadakis, 2000; Elahi et al., 2010; Durning and Hicks, 1991; Mehta 1985; Hewayde et al., 2003; Chang et al., 2005; Tamimi, 1997; Beddoe and Dorner, 2005; Torii and Kawamura, 1994) have proposed the use of SCMs (silica fume, fly ash, slag and nanosilica, and their combinations) to generally improve durability of concrete to chemical attack, without a general agreement on their effectiveness. It should be noted that there have been no North American specific standards for assessing the resistance of concrete to sulfuric acid attack and most of these studies (e.g. Chang et al., 2005; Rostami and Ahmad-Jangi, 2011; Lotfy et al., 2016; Soroushian et al., 2009) applied the test method prescribed in ASTM C267, which is a standard test method for the chemical resistance of mortars, grouts and polymer concrete, as a general basis for evaluating the behavior of concrete exposed to sulfuric acid. In this test, the acidic medium should be replaced with a new one as often

as necessary in order to maintain the original chemical composition and concentration; however, neither a specific concentration nor a pH level was mentioned (Monteny et al., 2000). So far, there has been no consensus on the concentration, the pH level and the time of exposure that should be used to perform this test on concrete.

Many studies used high concentrations (1-5% sulfuric acid, maintaining a constant pH level at about 1) to aggravate the damage of concrete within a short period of time (usually 30 to 120 days) (e.g. Chang et al., 2005; Rostami et al., 2011; Lotfy et al., 2016; Soroushian et al., 2009; Cohen and Mather, 1991). The acidic damage disintegrates the hydrated cement paste to various levels based on the prevailing testing conditions in the accelerated tests (e.g. acid concentration and pH) and key mixture design parameters of concrete making it rather difficult to draw conclusive trends. For instance, Durning and Hicks (1991) and Mehta (1985) reported that the incorporation of silica fume improved the resistance of concrete exposed to 1% sulfuric acid attack (without reporting the corresponding pH level) due to the depletion of calcium hydroxide content and a denser microstructure through the pozzolanic activity. Comparatively, Hewayde et al. (2003) found that the resistance of concrete specimens incorporating silica fume was similar to that of reference specimens at 3% sulfuric acid with a pH level of 0.6 for 8 weeks. Durning and Hicks (1991) and Roy et al. (2001) stated that silica fume did not improve the resistance of concrete to 5% sulfuric acid solutions (30 days of exposure without controlling the pH of the solution). Other researchers (e.g. Beddoe and Dorner, 2005) stated that silica fume may have only little effect on the durability of concrete under acid attack as the penetration of hydrogen ions (in H_2SO_4) into the alkaline pore system of concrete is strongly limited by the rapid neutralization reaction at the surface. Monteny et al. (2003) reported that a refined pore structure with higher capillary suction might cause deeper penetration of acidic solutions into concrete and increase the exposed surface

area in contact with acid. It was reported that the addition of fly ash in concrete improves its acidic resistance in most cases, although to a smaller degree than that of silica fume at 2% sulfuric acid (Torii and Kawamura, 1994). Conversely, other studies (e.g. Roy et al., 2001) showed that specimens incorporating fly ash had better behavior compared to those made with silica fume when exposed to 5% sulfuric acid solution. Chang et al. (2005) and Tamimi (1997) reported that concrete mixtures made from ternary binders comprising ordinary portland cement, fly ash and silica fume had high resistance to 1% sulfuric acid solutions compared to control specimens prepared from general use cement. Furthermore, Bassuoni and Nehdi (2007) stated that specimens from mixtures with quaternary binders including ordinary cement, fly ash, silica fume and limestone filler showed the best performance in terms of less mass loss compared to that of the ternary and binary binder mixtures when exposed to 5% sulfuric acid solution with a pH threshold of 1 for six weeks.This variability among these studies may have led to different results and discrepancy in the data available about the behavior of cementitious materials susceptible to sulfuric acids. In addition, most current building codes and guidelines for concrete recommend improving the resistance of concrete to aggressive chemicals by reducing its penetrability to external agents [e.g. Canadian Standards Association (CSA) A23.1, 2014; British Research Establishment standard Special Digest 1 (BRE) , 2005)]. However, the contradictory data on the role of SCMs at improving the resistance of concrete to sulfuric acid attack does not substantiate this approach. Hence, more investigation is still required for the deterioration levels of various cementitious binders exposed to different sulfuric acid concentrations and also to recommend the concentrations that should be used to perform the test. Frequently, the acidic damage in the field develops in an incremental manner, and thus, test protocols for testing sulfate attack on concrete should be developed accordingly.

One of the options to produce durable concrete, and reduce its carbon footprint simultaneously, is the full substitution of GU cement by novel binders termed alkali activated materials (AAMs) (Pacheco-Torgal et al., 2008; Provis, 2014; Pacheco-Torgal et al., 2012a). These alternative binders are obtained through alkaline-activation of different industrial by-products and natural minerals to produce hydrates possessing cementitious properties (Davidovits, 1991) such as the alkali-activated slag (AAS) or fly ash (AAFA). It is notable that the definition of the AAMs does not include high-volume blends of pozzolans or blast furnace slag with smaller quantities of portland cements, although the latter is a source of alkalinity. Several studies reported that the improved chemical resistance is one of the major advantages of AAMs over portland cements. For example, AAFA and AAS concrete has been found durable to aggressive acid solutions (Bakharev et al., 2003; Thokchom et al., 2009; Song et al., 2005) and sulfate attack (Bakharev et al., 2002; Rangan et al., 2005, Song et al., 2005). Also, it can protect steel reinforcement from corrosion (Bastidas et al., 2008), as the very high alkalinity of these binders is favorable for the protection of embedded reinforcing steel. However, AAMs have technical limitations, which might deter its widespread use in concrete applications. These include slow setting, high porosity and subsequent slow strength development. Also, shrinkage cracking is one of the most critical drawbacks hindering the broader applications of AAS as a binder (Ye and Radlińska, 2016; Cartwright et al., 2014; Neto et al., 2010). Mitigation of these properties is essential in order to increase the use of AAMs and benefit from their high chemical resistance, for example in acidic media. Incorporating nanosilica in conventional portland cement concrete has shown promising results in terms of strength and durability, especially in systems containing high volumes of slag and fly ash (Du et al., 2014; Jalal et al., 2012; Ghafari et al., 2015). Correspondingly, incorporating nanosilica in AAMs may enhance their properties. For instance, the addition of nanosilica increased

compressive strength and reduced the sorptivity of AAFA (Adak et al., 2014; Deb et al., 2016). Also, nanosilica increased the strength of alkali activated slags (Gao et al, 2015). Previous studies (Rodríguez et al., 2013; Gao et al., 2015; Hou et al., 2012; Adak et al., 2017; Khater et al., 2012) focused on the improvements of mechanical properties of alkali activated binders by using nanosilica. Studies on the durability of AAMs incorporating nanosilica in aggressive chemical environments are scarce in literature.

On the other hand, the properties of concrete prepared with AAMs (Hardjito et al., 2004; Hardjito and Rangan, 2005) such as the modulus of elasticity, Poisson's ratio, and the tensile strength are similar to those of conventional concrete, which might show good compatibility with the substrate layer if AAMs used in repair applications. Moreover, concrete from AAMs can be applied using the same equipment and practices used for conventional concrete to repair deteriorated infrastructure (Montes et al., 2013). It may represent an attractive alternative to epoxy resins since they are stable at high temperature (Pacheco-Torgal et al., 2012b). All these merits may make AAMs concrete a promising candidate for repair of concrete affected by acidic media; however, this area remains largely unexplored.

1.3. Objectives

The primary objectives of this thesis are to:

Develop a test protocol for assessing the resistance of concrete to acidic attack, based on incremental levels of damage.

Investigate the physical and the chemical responses of different types of concrete made with general use or portland limestone cement [PLC] without or with SCMs (fly ash, silica fume and nanosilica) to progressive levels of exposure to sulfuric acid attack.

Develop innovative types of AAMs-based concrete (AAFA, AAS and their blends incorporating nanosilica) and evaluate their resistance to acidic attack for potential use in repair of concrete elements vulnerable to acidic attack.

1.4. Scope of Work

This study was divided into two experimental parts. In the first part, a test protocol based on incremental levels of sulfuric acid attack was developed to evaluate the response of different concrete mixtures to progressive sulfuric acid attack for nine months, to better understand the mechanism of the attack. Therefore, a wide range (fourteen) concrete mixtures was prepared with various proportions of SCMs such as silica fume and fly ash (Class F) with or without the incorporation of different dosages of nanoparticles (6% nanosilica). The tests in this part of research included rapid chloride penetrability (RCPT), visual inspection, neutralization depth, mass change, and mercury intrusion porosimetery (MIP) and the microstructure was tested by thermal analysis and microscopy.

In the second part, a total of six AAMs-based concrete mixtures including: AAFA with different types of additives (slag and nanosilica) as well as AAS with and without nanosilica were prepared by using a combination of sodium hydroxide (NaOH) and sodium silicate (Na_2SiO_3) solutions as alkaline activators. The durability of these concrete mixtures was evaluated under severe chemical attack (10% sulfuric acid solution) and alternating wetting-drying and freezing-thawing cycles for 18 weeks. Also, to evaluate the bond strength of these mixtures, mini-scale slabs were cast to simulate a repair configuration in the field, and subsequently, the repair mixtures were placed on the top surface. The pull-off test was used to investigate the bond strength before and after 18 weeks of successive wetting/drying and freezing/thawing cycles with chemical attack. The

alteration of microstructure in deteriorating specimens was investigated by microscopy, thermal and mineralogical analyses.

1.5. Thesis Outline

The thesis is organized into five chapters, as describes below:

Chapter one contains introduction which provides information on acid attack of concrete, lack of test standards, the motivation for developing AAMs as an alternative binder for concrete, objectives and scope of the work.

Chapter two presents a literature review of acidic attack on conventional concrete. This includes a discussion of the reaction products formed, influential factors, damage mechanisms, available standards, durability characteristics of various blended binders and code provisions relevant to such exposures. In addition, it presents information on alkali activation of supplementary cementitious materials (geopolymers) as an alternative to conventional binders in developing concrete with superior durability properties, especially in the case of acidic attack.

Chapter three describes the experimental program including: materials and mixtures, procedures of mixing, exposures, and tests.

Chapter four presents result and discussion for the incremental sulfuric acid exposure including mechanisms of damage and effects of various SCMs on sulfuric acid resistance of concrete.

Chapter five provides test results and discussion for the bond characteristics and durability properties of concrete with AAMs under different acidic exposures.

Chapter six provides conclusions of the research program based on the test results with recommendations for future research.

Chapter 2: Literature Review

2.1. General Features of Sulfuric Acid Attack

Sulfuric acid [$H_2(SO_4)$] attack on concrete may be characterized by a chemical reaction between the acidic media and cement hydration products and, if soluble, the aggregate particles, results in excessive formation of gypsum (**Fig. 2.1**). The nature of attack of sulfuric acid on concrete is manifold. Acid attack can occur under static or flowing conditions at different temperatures and pressures in structures such as containers for liquid manure, silage, deicing agent run-off at airports as well as cooling towers and sewers etc. (Alexander et al., 2013).

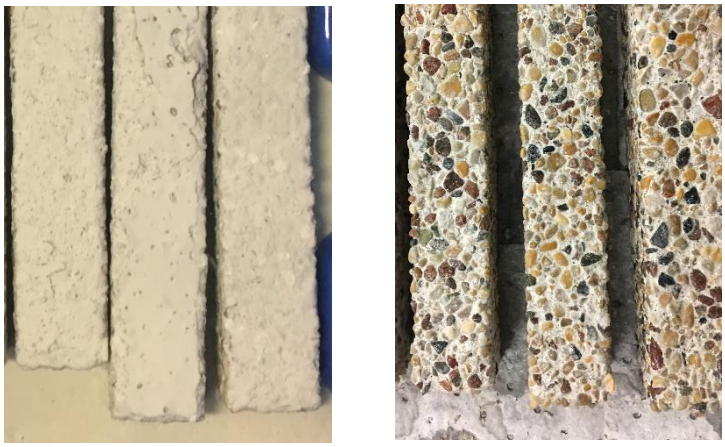

(a) **(b)**

Fig. 2. 1: a) gypsum depositions and b) aggregate disintegration after exposure to 2.5% concentration of sulfuric acid in a laboratory test.

Based on the origin of the acid itself, sulfuric acid attacks on concrete can be classified as biogenic/microbial or chemical attack (De Belie et al., 2004; Monteny et al., 2000; Monteny et al., 2001). The biogenic sulfuric acid attack necessitates the presence of H_2S, moisture, and acidophilic microorganisms to form sulfuric acid (House and Weiss, 2014). According to the authors, microbially induced corrosion (MIC) is a multistage degradation process. Five species of acidophilic microorganisms (Thiobacillus) have been found affecting MIC in concrete waste water

networks: T. thioparus, T. novellus, T. neapolitanus, T. intermedius, and T. thiooxidans (House and Weiss, 2014). Numerous studies have well documented MIC in wastewater collection and treatment systems in most developed areas of the world including: North America (Gutierrez-Padilla, 2007; U.S. EPA, 1991), Europe (Diercks et al., 1991), Australia (Thistlethwayte, 1972; Parker, 1951), South Africa (Alexander and Fourie, 2011), and the Middle East (Saricimen et al., 2003). In contrast, the chemical sulfuric acid attack can originate from acid rain, chemical reactions within the concrete components, or simply accidental spillage of the acid itself. The origin of sulfuric acid can also be assorted as 'external' or 'internal', potentially with different damage manifestations. For instance, in a field case study on some sewer pipes (external attack), Alexander and Fourie (2011) described biogenic sulfuric acid attack as moist corroded concrete surface with white slimy corrosion products (sulfate salts of calcium) with corrosion debris and blisters on the surface depending on mixtures designs.

Comparatively, in another field study (Tagnit-hamou et al., 2005), the petrographic analysis showed direct links between severe deterioration (cracking) of foundations and porches of several houses in Canada after two years of construction and sulfuric acid generated due to the usage of pyrrhotite-containing aggregates in concrete. The extent of damage caused by internal attacks are noteworthy and was also reported by other researchers (House and Weiss, 2014). The most widely reported cases for an external sulfuric acid attack on concrete are in sewer pipes (e.g. House and Weiss, 2014; O'Connell et al., 2010; Parker, 1951), which belong to the category of MIC. The chemically external attack can also originate from backfill with pyratic or pyrrhotite-bearing aggregates (Tagnit-hamou et al., 2005) while the internal attack is mostly associated with using such aggregates in concrete (Tagnit-hamou et al. 2005). In an external attack of concrete, acids can enter the pores of cementitious matrix convectively by capillary suction and/or diffusion

due to a pH gradient in the pore solution between the attack front and inner concrete. In an internal attack of concrete, oxidation of pyratic or pyrrhotite-bearing aggregates in presence of water produces sulfuric acid. The formed sulfuric acid reacts with the calcium-bearing phases (primarily portlandite and C-S-H, in the absence of portlandite) in hydrated cement paste to form gypsum. Also, ettringite possibly could be formed away from the reaction zone which is similar to conventional sulfate attack. If carbonates are present, thaumasite formation is also possible. Thus, the damage manifestations of concrete in the latter cases are typified by expansion, cracking and softening (Tagnit-hamou et al., 2005; Monteny et al., 2000).

Irrespective of the nature of attack, at pH values below 6.5 the neutralisation reaction may, as far as stoichiometry is concerned, be thought of as a reaction between the acid and $Ca(OH)_2$, i.e. the consumption of two protons in the pore solution by the hydroxyl ions transfers one calcium ion to the pore solution (Beddoe and Dorner, 2005). Calcium ions are released from the solid matrix (Portlandite, calcium silicate hydrates and, to a lesser extent, in hydrated aluminate, ferrite and sulphate phases in the hydrated binder). The neutralization reaction is much rapid than the penetration of protons into the undamaged alkaline pore system. The dissolved calcium reacts with acid anions to produce gypsum which barely has no strength (Gutberlet et al., 2015). The corrosion process also results in extreme coarsening of the pore size distribution and a large increase in porosity thus boosting the transport of ions in the corroded layer, which governs the acid diffusion towards the uncorroded material. Investigations at the Centre for Building Materials (Dorner and Beddoe, 2002) showed that effective diffusion coefficients of corroded mortar are more than an order of magnitude larger than the values for the uncorroded material. However, the precipitation of gypsum from dissolved calcium and acid anions can reduce the porosity of the degraded layer and hence affects the transport of the acid species through the degraded layer into the sound

material and consequently the rate of degradation. However, the formation of an excessive amount of gypsum (Torii and Kawamura, 1994) can produce sufficient pressure to overcome the tensile strength of the weakened paste matrix results in the failure of the pore structure and consequently loss of surface material. According to observations, gypsum is a kind of softy gel with no structural strength (Vincke et al., 2000), and a porosity of 0.85 to 0.92 (Jahani et al., 2001). Therefore, as the reaction products precipitate, the pores will be filled with gypsum. Since gypsum gel is compressible (Azam, 2007), it is assumed that gypsum will be compressed after a complete filling of pores. The gypsum accumulation leads to pressure increase until the inner pressure exceeds the ultimate bearing capacity of the pore. If so, the pore structure will be damaged. The damaged zone, where the pore structure is damaged by inner pressure, should be treated as uncompressed gypsum with unreacted solid compounds (such as silica gel, remaining cement hydrates, etc.). Apart from the surface, ettringite can form away from the acidic front (Tagnit-hamou et al., 2005).

However, given the complex chemistry that makes different cementitious systems unique (e.g. variable amount of portlandite, C-S-H, physical penetrability, and their role in the process), it is quite difficult to clearly define all cementitious systems by one degradation mechanism in sulfuric acid exposures. Evidently, the corrosion resistance of concrete is a function of the type and, in turn, the chemical composition of the cement as well as the pH of the acid under consideration (Dorner, 2000). Therefore, both the rate and mechanism of degradation are affected by the concentration of the acid along with composition and amount of the hydration products exposed to the reaction. Not all the hydration products react with the acids at the same time. Progression of acidic corrosion of concrete is linked to the stability of the components of hydrated cement and reaction products, which depends on the pH level of the attacking media. According to O'Connell et al. (2010), the formation of reaction products, their quantities and their specific

effects on the cement matrix are still debatable. As the pH values decrease to 12.6, 10.7, and 10.5, CH, ettringite, and C-S-H decompose, respectively, until a silica gel residue is obtained at pH values below roughly 2. Hence, it can be deduced that the damage features of acidic attack may vary based on the severity of attacking solutions.

2.2 Standardized Test Methods and Methods of Quantifying Degradation

Up till now, there have been no North American standards for specifically assessing the resistance of concrete to sulfuric acid attack. Previous studies (e.g. Chang et al., 2005) applied the test method prescribed in ASTM C267 (2012), which is a standard test method for the chemical resistance of mortars, grouts and polymer concrete, as a general basis for evaluating the behavior of concrete exposed to sulfuric acid. In this test, the acidic medium should be replaced with a new one as often as necessary in order to maintain the original chemical composition and concentration; however, neither a specific concentration nor pH level is stipulated. In general, quantifying degradation may comprise mass loss, thickness change, pH change of liquid, linear or volumetric expansion, residual strength, calcium released in liquid, hydrogen ion consumption, loss of elastic modulus, etc. These measurements may be supplemented by SEM or XRD analysis to examine the microstructure. Bertron et al. (2004) used Phenolphthalein as an indicator of the pH change in the concrete pore solution to measure the depth of neutralization, in relation to the time of exposure of five organic acids. This indicator shows a magenta colored region on the concrete surface where the pH level exceeds about 9 and a colorless region where the pH level is less than 9. Schmidt et al. (2006) investigated the usage of a non-destructive method by using ultrasonic surface waves (leaky Rayleigh waves) to examine the degradation of mortar samples in sulfuric acid solutions.

It should be mentioned that the choice of the method of quantifying the degradation may lead to different conclusions with respect to the relative performance of different concrete types.

For instance, De Belie et al. (2004) used both mass loss and thickness change as key parameters to evaluate the deterioration of concrete samples in microbiological tests. They reported samples with limestone aggregates showed a higher mass loss relative to the samples with inert aggregates; however, their thickness change was lower than those with inert aggregate. This effect could be partly illustrated by considering the density of the concrete constituents into account. For concrete with limestone aggregates, the removed material consisted of concrete (aggregates and cement mortar) with a density of about 2,400 kg/m^3. By contrast, the removed material for the concrete contained inert aggregates consisted of cement mortar with a density of around 2,000 kg/m^3. This explicate the reason why limestone concrete with a lower average attack depth, exhibit a higher mass loss. This trend may probably disappear when degradation proceeds and large aggregates are disintegrated from the matrix. This could also imply that concrete with limestone aggregates experience larger expansion compared to concrete with inert aggregates. Hence, one single parameter may not be stuffiest to evaluate the degradation properly. Mass change parameter may be used in case of no secondary products precipitate, otherwise it may be the result of a combination of several phenomena. For example, mass gain may occur at the beginning of testing such as the degradation mechanisms in case of acids and sulfates, due to the formation of secondary reaction products. Hence, it is recommended to use numerous relevant indicators to investigate the concrete resistance to a particular degradation mechanism (Bassuoni et al., 2006; Cohen and Mather, 1991). Mass changes, expansion, dynamic modulus of elasticity and flexural strength can be monitored. De Belie et al. (2004) investigated the biogenic sulfuric acid degradation in terms of the thickness using an automated laser profilometer, mass loss, and calcium and sulfate concentrations in the microbial suspension.

2.3. Role of the Type of Cement, SCMs, Nanoparticles and Limestone Fillers in Resisting Acidic Attack

2.3.1 Role of the Type of Cement

The Canadian Standards Association (CSA) A3001 (2013), has specified six types of portland cement. These six types of cement are as follows: general use (GU), moderate sulfate resistance (MS), moderate heat of hydration (MH), high early strength (HE), low heat of hydration (LH), high sulfate resistance (HS), and white Portland cement. The ASTM C1157 (2017) has equivalent designations for the five types of portland cement used in the United States. Many studies have been performed to evaluate the durability of concrete exposed to sulfuric acid attacks. In most of these studies (Fattuhi and Hughes, 1988; Fattuhi et al., 1988), concrete produced by 100% GU cement was used as the reference mixture. This type of concrete has shown inferior performance in comparison with the mixtures blended with SCMs. HS cement has a low quantity of tricalcium aluminate (C3A) which improves the durability of concrete against different kinds of sulfate attacks. According to previous studies, maintaining low content of C3A (less than 5% by weight) resulted in improvement in the performance of concrete in aggressive environments (Mindess et al. 2003). Although, sulfuric acid intrusion is mostly more acidic than sulfate attack; however, the expansion which can arise from secondary ettringite formation may be accompanied by sulfuric acid attacks (Monteny et al., 2000). Monteny et al. (2003) investigated a concrete mixture with HS cement soaked in a 0.5% sulfuric acid solution. HS cement-based concrete showed a better performance than concrete that contained silica fume; however, its resistance was less than the concrete produced with blending slag and some other polymer modified concretes. Bassuoni et al. (2007) reported that self-consolidating concrete made with 100% GU has comparable behaviour

to that made of HS cement after exposure to 5% sulfuric acid solution which was attributed to the existence of a large amount of CH and C-S-H (vulnerable to low pH acidic solutions).

2.3.2 Role of SCMs and Nanoparticles

There is a lack of a general consensus concerning the effectiveness of substituting cements with supplementary cementitious materials (SCMs) in resisting attack caused by acidic media. The difference in opinion expected since the parameters based on which the studies were conducted vary widely from each other. Numerous research studies have been conducted to investigate the effects of supplementary cementitious materials (SCMs) on mitigating sulfuric acid attack on concrete, without a general agreement on their effectiveness. The acidic damage disintegrates the hydrated cement paste to various levels based on the prevailing testing conditions in the accelerated tests (e.g. acid concentration and pH) and key mixture design parameters of concrete making it rather difficult to draw conclusive trends. For instance, Durning and Hicks (1991) and Mehta (1985) reported that the incorporation of silica fume improved the resistance of concrete exposed to 1% sulfuric acid attack (without reporting the corresponding pH level) due to the depletion of calcium hydroxide content and a denser microstructure through the pozzolanic activity. Comparatively, Hewayde et al. (2003) found that the resistance of concrete specimens incorporating silica fume was similar to that of reference specimens at 3% sulfuric acid with a pH level of 0.6 for 8 weeks. Durning and Hicks (1991) and Roy et al. (2001) stated that silica fume did not improve the resistance of concrete to 5% sulfuric acid solutions (30 days of exposure without controlling the pH). Other researchers (e.g. Beddoe and Dorner, 2005) stated that silica fume may have only little effect on the durability of concrete under acid attack as the penetration of hydrogen ions (in H_2SO_4) into the alkaline pore system of concrete is strongly limited by the rapid neutralization reaction at the surface. Monteny et al. (2003) reported that a refined pore

structure with higher capillary suction might cause deeper penetration of acidic solutions into concrete and increase the exposed surface area in contact with acid.

It was reported that the addition of fly ash in concrete improves its acidic resistance in most cases, although to a smaller degree than that of silica fume at 2% sulfuric acid (Torii and Kawamura, 1994). Conversely, other studies (e.g. Roy et al., 2001) showed that specimens incorporating fly ash had better behavior compared to those made with silica fume when exposed to 5% sulfuric acid solution. Chang et al. (2005) reported that concrete mixtures made from ternary binders comprising ordinary portland cement, fly ash and silica fume had high resistance to 1% sulfuric acid solutions compared to control specimens prepared from general use cement. Furthermore, Bassuoni and Nehdi (2007) stated that specimens from mixtures with quaternary binders including ordinary cement, fly ash, silica fume and limestone filler showed the best performance in terms of less mass loss compared to that of ternary and binary binder mixtures when exposed to 5% sulfuric acid solution with a pH threshold of 1 for six weeks. On the other hand, the advent of nanoparticles to the concrete industry has a promising impact to improve the long-term performance of concrete infrastructure. However, research on nano-modified concrete is still in its infancy and has mainly focused on hydration kinetics and physico-mechanical properties. To date, there is dearth of information on the durability characteristics of nano-modified concrete, specially its resistance to acidic exposures.

2.3.3 Role of Limestone Filler

The durability of concrete mixtures incorporated limestone fillers (LF) exposed to sulfuric acid attacks has been studied by numerous researchers. One of these studies has been performed on self-consolidating concrete that comprised 47% LF to 1% sulfuric acid (Al-Tamimi and Sonebi,

2003). Cylindrical specimens were submerged into a 1% acidic solution for 18 weeks exposure period. Mass loss and visual inspection were used as key parameters to evaluate the performance of different specimens relative to those of conventional concrete which contained only portland cement subjected to the same testing method. The final results showed that conventional concrete had experienced severe degradation and lost 21% of its mass in comparison to only 9% for those made with SCC mix with limestone powder at the end of the immersion period. The better performance of the LF concrete was ascribed to the neutralization effect offered by limestone powder (Al-Tamimi and Sonebi 2003). Bassuoni et al. (2007) studied different groups of concrete mixtures subjected to a sulfuric acid solution with a concentration of 5%. One of their mixtures comprised 50% Portland cement, 15% LF, 20% slag and 15% fly ash. At the end of 6 weeks with pH threshold of 1 in sulfuric acid solution, the mixture with four binders which contained 15% LF, had a 42% reduction in mass loss in comparison to the control mixture (the best performance). Shi and Stegemann (2000) studied the acid resistance of limestone fly ash cement (80% commercial hydrated high calcium lime with 20% class F fly ash), alkali-activated slag cement, portland cement and high alumina cement and found that limestone fly ash cement had the best performance.

2.4. Alkali-Activated Materials

2.4.1 Review

The term alkali activation is used to imply that alkali source is used as an activator to catalyze the pozzolanic reaction or release the latent cementitious properties of fine inorganic materials including mainly industrial by-products materials which primarily consists of silicates, alumina-silicates and calcium (Provis, 2014). Alkali-activated materials (AAMs), including the materials referred to as ‘geopolymers’, have attracted much interest in academic and commercial spheres

over the past decade or more. The name geopolymer was introduced by Davidovits (1991), and is used to distinguish the geopolymer reaction from other types of AAMs (e.g. alkali-activated slag) as the reaction product is more polymer than C-S-H gel. Alkali-activation is gaining increasing recognition and interest as several authors reported that AAMs had high chemical resistance which is one of the major advantages of AAMs over conventional concrete (Davidovits, 1991; Bakharev et al., 2003). In addition, these binders offer the potential for greenhouse emissions savings when compared with Portland cement (van Deventer et al., 2012), because the majority of the materials used to produce AAMs are generally derived from industrial by-products, to which little environmental footprint is usually attributed. Palomo et al. (1999) assorted alkali activation into two different models. The first model includes the activation of fly ash, comprising primarily silicate (Si) and aluminates (Al), using a high concentration alkali solution and second, the activation of slag, comprising primarily silicate (Si) and calcium (Ca), involving a low to mild alkali solution.

2.4.2 Alkali-Activated Fly Ash

Alkali-activated fly ash (AAFA) or fly ash-based geopolymer or simply geopolymer involves the formation of an inorganic cementitious like material through a polymerisation process designated as a geopolymer reaction (Li et al., 2002). The research on alkali-activated alumina-silicate (Fly ash) was first introduced by Glukhovsky in the 1950's (Shi et al., 2006). Nevertheless, the research on the AAFA received a great interest after the term geopolymer was introduced by Davidovits (1991). AAFA are formed when alumino-silicates dissolve in a strong alkaline media, reorganize and precipitate in a hardened state (e.g. Davidovits, 1991). Many studies (Provis, 2009) have reported that the main reaction product of such systems is a highly cross-linked amorphous aluminosilicate gel: 3D polymeric chain and a structure of Si-O-Al-O bonds. Also, the reaction

products may contain areas of semi-crystalline zeolite-like phases such as sodalite, gismondine, and chabazite (Bakharev, 2005a; Ryu et al., 2013). Properties are very similar to conventional concrete produced from portland cement when formed under suitable conditions (Sofi et al., 2007), although the microstructure of the AAFA is different compared to ordinary Portland cement-based concrete. The geopolymerisation reaction starts with the dissolution mechanism which results in initial attack by alkaline media on the fly ash particles (Fernández Jiménez et al., 2005). The reaction products are generated both inside and outside the shell of the sphere, until the fly ash particles are entirely consumed. The precipitation process occurs with the dissolution process simultaneously. The alkaline solutions penetrate and react with the smaller fly ash particles inside the larger spheres and fills the interior space with reaction product, forming a dense matrix (Fernández-Jiménez, and Palomo, 2005). However, due to the massive precipitations of reaction products, some portions of the smaller fly ash spheres are covered with a layer of the reaction products (Fernández-Jiménez, and Palomo, 2005). Consequently, this growing layer provides a crust which consequently prevents the ingress of the alkaline medium resulting in un-reacted fly ash particles which leads to deceleration of the reaction rate. The geopolymerization process is not uniform but varies locally depending on the particle size distribution and the chemical composition of fly ash particles. The result is several morphologies in a single paste of geopolymer comprising un-reacted particles, partially dissolved particles attacked by the alkaline solution and fully dissolved particles (Fernández Jiménez et al., 2005).

2.4.3 Alkali-Activated Slag

Research on utilizing slag as an alternative material to cement was started when Feret (1939) and Purdon (1940) described the reaction of alkalis on slag; however, it was not until the works of Glukhovsky in the late 1950's when the idea became widespread (Roy, 1999). Ground granulated

blast-furnace slag (GGBS) is an ideal candidate for AAMs due to its latent hydraulic properties. Alkali-activated slag (AAS) has been used in Ukraine in the 1960's (Fernández Jiménez et al., 1999), China and Scandinavian countries due to environmental issues driving a search for an alternative binder for concrete (Escalante-Garcia et al., 2003;Wang et al., 1994; Talling et al., 1989; Brough and Atkinson, 2002; Fernández Jiménez et al., 1997; Collins and Sanjayan, 2000; Bakharev, 2000; Al-Otaibi, 2008). The hydration product of AAS is totally different from that formed in AAFA. As reported by many research works, the calcium silicate hydrate (C-S-H) is the major component of hardened AAS pastes (Bakharev, 2000, Brough and Atkinson, 2002, Escalante-Garcia et al., 2003), similar to that formed in OPC. However, the ratio of Ca/Si in C-S-H is much lower than that from the hydration of portland cement (Chen and Brouwers, 2007). According to Taylor (1997), the type of C-S-H gel in AAS has a ratio of Ca/Si below 1.5, while the C-S-H gel resulting from hydration of ordinary portland cement has a Ca/Si ratio of approximately 2.0. Brough and Atkinson (2002) reported the existence of two different types of C-S-H gel in AAS. According to the authors, the inner regions of the AAS hydrates contained a C-S-H gel with a Ca/Si ratio of approximately 0.9 with high Mg, compared to a Ca/Si ratio of approximately 0.7 in the outer regions with low Mg.

2.4.4 Alkaline Activator

Glukhovsky et al. (1980) classified the alkaline activators into six groups according to their chemical compositions, where M is an alkali ion:

(1) Caustic alkalis, MOH.

(2) Non-silicate weak acid salts, M_2CO_3, M_2SO_3, M_3PO_4, MF.

(3) Silicates, M_2O . $nSiO_3$.

(4) Aluminates, M_2O . nAl_2O_3.

(5) Alumino-silicates, M_2O . Al_2O_3 . (2–6)SiO_2.

(6) Non-silicate strong acid salts, M_2SO_4.

Many researchers have widely reported that the activation with sodium silicate or sodium silicate blended with sodium hydroxide resulted in the best strength for AAFA and AAS specimens (Fernández Jiménez and Palomo, 2005; Bakharev, 2005a; Fernández Jiménez et al., 2003; Shi, 1996; Wang et al., 1994). For AAFA, many authors have reported that the activator concentration (in terms of NaOH molarity) is a key parameter (Hardjito and Rangan, 2005). However, this approach can not consider the effect of the concentration of Na^+ ions in the mixture especially when the activator includes both sodium hydroxide and sodium silicate. Adam (2009) recommended the use of the activator dosage (the mass ratio of total Na_2O in the activator solution to fly ash) as the main indicator of the Na^+ concentration to take into consideration the effect of the alkali concentration in the mix. Similarly, Bakharev (2005a) adopted using an activator dosage (the mass ratio of Na^+ to fly ash). According to the author, the mass ratio of Na_2O to fly ash in the activator solution for the sodium silicate based activator is more suitable since the grade of sodium silicate solution is usually specified by the ratio of SiO_2 to Na_2O which makes the mix calculation easier. For AAS specimens, it was reported (Wang et al., 1994) that both the Na_2O dosage and activator modulus (Ms), which is the mass ratio of the SiO_2 to the Na_2O in the alkaline activator, have a significant effect on the strength development of AAS.

However, for both alkali-activated fly ash/slag, there is a threshold value of Na_2O dosage above which there will be no further notable increase in strength (Krizan and Zivanovic, 2002; Wang et al., 1994). Moreover, in blended sodium silicate and sodium hydroxide, there is a competing effect of the Na_2O dosage and (Ms) which results in an optimum value for both the Na_2O dosage and that of (Ms). The typical Na_2O dosage and Ms for AAFA and AAS specimens

adopted by several authors are presented in Table 1 and Table 2, respectively. It can be deduced that for AAFA, a higher dosage of Na_2O was required (5.3% - 16.3%) than that for AAS specimens (3% - 7%). This is attributed to the polymerisation process which requires highly alkaline solutions to dissolve the silica and alumina ions in the fly ash precursor. The extent of dissolution of Si and the Si/Al ratio in fly ash are significant factors in the geopolymerisation reaction (Davidovits, 1991).

Table 2. 1: Typical Ms and Na_2O dosage based on sodium silicate activators for AAFA

Authors	Specimen Type	Activator Modulus (Ms)	Na_2O dosage (%)
Talling (1989)	Mortar	N/A	3.0 – 5.0
Wang et al. (1994)	Mortar	0.75 – 1.50	3.0 – 5.5
Shi (1996)	Mortar	1.50	6.0
Fernández Jiménez et al. (1997)	Mortar	1.50	4.0
Bakharev et al. (1999)	Paste	0.87 – 1.30	4.8 – 12.0
Krizan et al. (2002)	Mortar	0.60 – 1.50	3.0 – 4.0
Escalante-Garcia et al. (2003)	Mortar	2.00	6.0
Adam (2009)	Mortar	0.75 – 1.25	3.0 – 5.0
Adam (2009)	Concrete	0.75 – 1.25	5.0

Table 2. 2: Typical Ms and Na_2O dosage based on sodium silicate activators for AAS

Authors	Specimen	Activator Modulus (Ms)	Na_2O dosage (%)
Fernández-Jiménez and Palomo (2005)	Mortar	0.037 – 1.23	5.55 – 14.90
Hardjito and Rangan (2005)	Concrete	1.31 – 1.36	5.30 – 5.70
Wallah and Rangan (2006)	Concrete	1.31	5.70
Sumajouw and Rangan (2006)	Concrete	1.09	6.80
Adam (2009)	Mortar	1.00 – 1.50	10.0 – 15.0
Adam (2009)	Concrete	0.75 – 1.25	7.50

2.4.5 Curing, fresh and Hardened Properties

For AAFA, several factors such as reactivity of the source materials (Diaz et al., 2010), the type of alkaline activator (Palomo et al., 1999), alkaline activator to source material ratio (Nath and Sarker, 2015; Deb et al., 2014) and curing temperature affect the geopolymerization process. Selection of the binder compositions is an important factor affecting the properties of fresh and hardened AAFA (Nath and Sarker, 2015). AAFA based on low calcium fly ash cured at ambient temperature require very long time to set and it develops low strength relative to those cured at elevated temperature such as at 60C°. Hence, most research works have been adopted curing temperatures ranging from 30C° to 85C° and about 95% relative humidity (Palomo et al., 2004; Van Jaarsveld and Van Deventer, 1999). Consequently, curing times may differ from several hours to several days. A comparative study of different curing conditions (Krivenko et al., 2002) reported that temperature and humidity constitute a significant role in the development of the microstructure and consequently the properties of AAFA materials. Unsuitable curing conditions may lead to carbonation at a very early stage (Criado et al., 2005), in turn, lower pH levels and as a result substantially retarding the ash activation rate and mechanical strength.

According to Palomo et al. (1999), adopting high curing temperature for long curing period led to increasing the compressive strength. Also, it was reported that alkaline activator that consisted of soluble silicates led to increasing the reaction rate of AAFA relative to alkaline activators that consisted only of hydroxide (Palomo et al., 1999). Similarly, according to Bakharev (2005a), AAFA exhibited higher mechanical strength development when heat curing was adopted. Winnefeld et al. (2010) also concluded that heat curing is significantly effective in developing the strength of AAFA. The authors also reported that 80C° is the ideal curing temperature; however, curing temperature above 80C° led to decreasing the compressive strength. In addition, Rowles

and O'connor (2003) have shown that the mechanical properties of AAFA are significantly influenced by the chemical composition of the fly ash in terms of the availability of silicate (Si), aluminate (Al) and sodium (Na). According to Rowles and O'connor (2003), the compressive strength of AAFA is influenced by the Si/Al and Na/Al molar ratio. It was concluded that Si/Al ratio of 2.5 and Na/Al ratio of 1.3 results in a better strength development. The authors also suggested that the bonding network in the amorphous aluminosilicate differs with the change of the chemical composition of the fly ash. Similarly, Steveson et al. (2005) reported that using high silicate content with a Si/Al ratio of approximately 3.9 and a Na/Al ratio of approximately 1.0 led to high strength AAFA which own dense microstructure with low porosity. The authors also reported that the initial strength development can be attributed to the charge-balancing role of the alkali cations in the fly ash formulations relative to the initial alkali dissolution reaction of the aluminosilicate fly ash particles. Also, they stated that the Si/Al ratio has an impact on the setting time. According to Silva et al. (2011), the amount of Al available in the fly ash has a significant effect of controlling the setting time, and increasing the Si/Al ratio led to a longer setting time. This was attributed to the alteration of the properties of the AAFA during condensation.

Sagoe-Crentsil and Weng (2007) concluded that in a geopolymeric system with a high Si concentration, the condensation stage starts with formation of oligomeric silicates results in a poly(sialate)-siloxo or poly(sialate)-disiloxo 3D rigid polymeric structures, while using low Si concentration will end up forming a poly(sialate) polymer structure. The poly(sialate) polymer structure is formed by the condensation and reaction between the aluminate and silicate species. However, an increase in the Si content produces oligomeric silicates (a condensation and reaction between silicate species) and forms poly(sialate)-siloxo or poly(sialate)-disiloxo. Ivan Diaz-Loya et al. (2011) reported that although silicate and aluminate are the main contributors to the AAFA

reaction, CaO components from the fly ash precursors significantly affect the strength. The setting time was found to increase as the CaO content decrease. The decrease in CaO leads to reducing the compressive strength of the resulting geopolymer. Previous studies (Deb et al., 2014; Nath and Sarker, 2015) showed that the setting and strength development of low-calcium AAFA can be improved by a small percentage of ground granulated blast furnace slag (GGBFS) or ordinary portland cement in the binder. In addition, improvements in the fresh and hardened properties of AAFA matrix by the addition of nano materials were reported by previous studies. It was reported by Adak et al. (2014) that addition of 6% nanosilica increased the compressive strength of AAFA. The addition of 6% nanosilica showed appreciable improvement in compressive, flexural and tensile strength at 28 days under ambient temperature curing. The water absorption and the penetrability are also seemed to be comparatively less for 6% addition of nanosilica modified AAFA mortar. Such improvement of nanosilica modified AAFA mortar is due to transformation of amorphous compound to crystalline compound. Similarly, It was found (Deb et al., 2016) that addition of 2% nanosilica in AAFA mortars alone or fly ash blended with 15% GGBFS or 10% OPC improved the compactness of microstructure by reducing porosity.

For AAS specimens, Wang et al. (1994) stated that the mechanical strength is influenced by numerous factors, i.e. the dosage of Na_2O, the alkali modulus (Ms), the type and the fineness of slag precursors. The authors stated that the optimum dosage of Na_2O was within the range of 3.0-5.5%, with an alkali modulus of 0.75-1.50. Also, the authors reported that the fineness and the type of slag precursors play a significant role as increasing the fineness of slag within its optimum range results in higher strength and the type of slag significantly affects the strength development at higher alkali modulus (Ms > 1.00). Krizan and Zivanovic (2002) also reported that the dosage of alkali modulus has a significant effect on the hydration process of AAS. AAS activated with

sodium silicate with an alkali modulus between 0.6 and 1.5 results in a higher ultimate strength compared to portland cement. However, the author argued that increasing the Ms as well as the dosage of sodium silicate increased the drying shrinkage Krizan and Zivanovic (2002). Similarly, Adam (2009) mentioned that Na_2O dosage and Ms has a significant effect on the strength development of AAS concrete. The author concluded that a Na_2O dosage of 5% with a Ms of 1.00 led to optimum strength; however, with any further increase of alkali modulus results in reducing the strength. Wardhono et al. (2015) stated that the standard regime used for curing cement-based concrete can be applied to the AAS, as both have a similar characteristic in terms of the hydration product (C-S-H gel). Bakharev et al. (1999) investigated the effect of curing temperature on microstructure and compressive strength of AAS concrete. Heat treatment considerably accelerates the strength development of AAS concrete, but at later age, compressive strength of the materials is reduced compared to a concrete cured at room temperature. On the other hand, cracking generated by shrinkage is one of the most critical drawbacks for broader applications of AAS binder (Cartwright et al. 2014). The chemical activator species and dosage, slag fineness, curing conditions were found to have a significant effect on its shrinkage. Bakharev et al. (1999) investigated the effect of curing temperature on shrinkage of AAS concrete. They concluded that heat curing considerably reduced shrinkage of AAS concrete, making it comparable with shrinkage of OPC concrete. Palacios and Puertas (2007) investigated the effect of shrinkage-reducing admixture on reducing the shrinkage of AAS. They concluded that shrinkage-reducing admixture based on polypropylenglycol reduced autogenous shrinkage by 85% and drying shrinkage by 50% in AAS mortars. Recent studies modified AAS by incorporating a different type of fibers (steel, polyvinyl alcohol, polypropylene, and carbon fiber) to overcome shrinkage issues (Kim et al., 2015; Aydın and Baradan, 2013).

2.4.6. Durability of AAMs to Sulfuric Acid Attack

AAFA has been widely advertised as showing potential for commercially attractive properties are in applications requiring chemical (acid) resistance or high-temperature resistance (Bakharev, 2005b). These properties are generally achieved through the presence of an alkali aluminosilicate gel, as opposed to a C-S-H type gel; the highly crosslinked (Q4) nature of the aluminosilicate 'geopolymer'-type gel (Bakharev, 2005a), and the resulting low bound water content, provide these properties to low calcium alkali-activated binders. Some higher-calcium AAFA can also show good chemical durability (Shi et al., 2000). Bakharev, (2005b) studied the resistance of AAFA against 5% sulfuric acid up to 5 months exposure and reported that these materials have better resistance than ordinary cement counterparts. Song et al. (2005) conducted an accelerated test to assess the durability of geopolymer concrete soaked in a 10% sulfuric acid solution for 56 days and reported its high durability. Wallah and Rangan, (2006) have shown that geopolymer composites possess excellent durability properties in a study conducted to evaluate the long-term properties of fly ash based geopolymers. Deb et al. (2016) examined the acid resistance of AAFA mortar with 2% nanosilica. The geopolymer mortar specimens were immersed in 3% sulfuric acid solution for 90 days and then the changes in mass were recorded. It was reported that the mass loss after 90 days of acid exposure for alkali activated flyash specimen without nanosilica was 5.41% as compared to 1.9% for the mix with 2% nanosilica. Also, relatively more damages were observed of the specimens without NS and some minor erosion was noticed in case of nanosilica incorporated specimens. Moreover, the strength loss of the specimens without nanosilica ranged from 30% to 41% while that of the specimens with 2% nanosilica ranged from 9% to 11% after 90 days of immersion. Therefore, the acid resistance of geopolymer mortars significantly enhanced with the addition of 2% nanosilica.

AAS was reported to have better durability compared to ordinary portland cement-based concrete (Bakharev et al., 2003). However, there are scarce data available in the literature on the durability of AAS to sulfuric acid. It was reported that AAS concrete showed a strength reduction of about 33% as compared to the 47% reduction of its counterparts conduced using ordinary Portland cement in an acetic acid environment (pH 4) after a time of one year (Bakharev et al., 2003). The high resistance of AAS to an acid attack was attributed to the low Ca content (40% CaO) of the slag compared to Portland cement (~65% CaO) and to the presence of glassy slag, which is practically insoluble in an acid solution (Bakharev, 2005; Bakharev et al., 2003).

2.5. Code Provisions

To date, very general recommendations are found in the latest version of the American Concrete Institute (ACI) 201.2R-08 (2016): Guide to Durable Concrete on acidic attacks. The only clear recommendation made in the American stipulation is the usage of silica fume to increase the resistance of concrete to acids and appropriate protective-barrier system (ACI 515.1R, 1985). The document states that "no hydraulic-cement concrete, regardless of its composition, will long withstand water of high acid concentration (pH of 3 or lower)". Table 6.2 in the same document recommends an increased cementitious material content for better protection against acids; however, the exact range for the cementitious materials was not specified. The damage mechanism in this document oversimplifies the attacks by different types of acids while completely overlooks the sulfate acid attacks caused by ammonium sulfate and ammonium nitrate exposures. An example of such over simplification is that the code recommends that "a dense concrete with a low w/cm provides a degree of protection against mild acid attack" but whether this is applicable for acids producing soluble reaction products (HCL and HNO_3), insoluble reaction products (sulfuric acid) or both, is not understood from this statement. Again, Table 6.1 in this document postulates

damage by aluminum chloride as more severe than ammonium sulfate and nitrate; however, reference to such comparison is absent in that document. Nevertheless, this document provides general guidelines for improving the resistance of concrete to classical sulfate attack, which as the literature suggests, cannot be reliably applied to the specific case of sulfuric acid attack (since the attack mechanisms and reaction products are quite different) or even the other mineral acids (HCL and HNO_3).

In contrast, Canadian standard CSA A23.1/A23.2-14 (2014), states that sulfate-resistant cements, like other portland or blended hydraulic cements, are 'not' resistant to most acids or other highly corrosive substances. The Canadian standard gave a good explanation and guidance on the impact of iron sulphides in concrete aggregate that might oxidise and cause an internal sulfuric acid attack. Upon exposure to water and oxygen, sulphide minerals oxidize to form acidic, iron, and sulphate-rich by-products. Pyrrhotite that is reported to have caused the most damage and was found to react much faster in alkaline concrete environments than other iron sulphides. The Canadian stipulation recommends that when pyrrhotite, is detected in the aggregate, the aggregates should not be used. The CSA A23.1/A23.2-14 (2014) reveals examples of rocks where the sulphide sulphur content may exceed 0.10% and have satisfactory field performance (excluding potential alkali reactivity) include Ordovician limestones and dolostones of the St. Lawrence Lowlands (Quebec) and Lake Ontario area that contain significant amounts of minute cubic pyrite. The presence of other forms of sulfides in the aggregate, such as pyrite and marcasite which are less dangerous compared to pyrrhotite, has also been considered problematic as its oxidation is accompanied by a large increase in volume or the release of sulphate that produces sulphate attack upon the cement paste, or both can occur. The code mentioned that there is no accelerated physical test method (performance test) to assess the potential for expansion of concrete due to the oxidation

of iron sulphides. The code concludes that new and unproven sources of concrete aggregates should be tested for sulphur content. If the sulphide sulphur content is less than 0.10%, the aggregate may be used without further investigations. Otherwise, the nature of the sulphide mineral present should be determined.

French standard, NF P18-301 (1983), limited the total sulphur content to 1% as SO_3 (0.4% as S). This threshold was increased in the context of European standardization as NF EN 12 620 (2003) specified that the total sulfur content (S) of the aggregates and fillers, when required, shall not exceed; (a) 2% S by mass for air-cooled blast-furnace slag; and (b) 1% S by mass for aggregates other than air-cooled blast-furnace slag. For concrete exposed to aggressive industrial chemicals, fertilizers, agricultural wastes, and other chemicals, CSA A23.1/A23.2-14 (2014) recommends the use of supplementary cementing materials, penetrating sealers, protective coatings, or other means (information for protective treatment was referred to PCA IS001.11 (2007)). The CSA A23.1/A23.2-14 (2014) also classifies the sewer pipe (the 'crown'; most vulnerable part to sulfuric acid attack) as A-XL and limits the requirements for concrete as maximum w/c of 0.4, minimum specified compressive strength of 50 MPa within 56 days, air content of 3-9% based on aggregate size, a certain curing type and a chloride ion penetrability of less than 1000 coulombs in 91 days. Thus, both the ACI 201.2R-08 (2016) and CSA A23.1/A23.2-14 (2014) recommend reducing the physical penetrability of the concrete to encounter against acid attacks (especially sulfuric acid).

Likewise, British standards correlate the ability of cementitious systems to resist the chemical attack to the impermeability (BRE Special Digest 1, 2005). British standard practices of designing concrete for the installation in the ground are required to be resistant to attack from commonly found chemicals, including sulfates and acids. BRE Special Digest 1 (2005) provides information on sulfuric acid attacks but without specific guidance. The British code specify an

Aggressive Chemical Environment for Concrete (ACEC) based on the type of ground, water mobility and pH. In section D5.3.2, the code also recommends super-sulfated cement and calcium aluminate cement as they have good sulfate resistance and a good reputation for acid resistance. According to the same document, well maintained mix proportions, temperature, curing conditions and w/c ratio, can give a good chemical resistance to concrete. However, the only specific criterion mentioned for acidic exposures in this code is a minimum cement content of 400 kg/m^3 and a total w/c ratio of not more than 0.40. It also recommends preventing the surface of the concrete from drying out during the first day of curing to ensure continued hydration and help to maintain the protective surface zone. In a few cases, the BRE Special Digest 1 (2005) also exercised oversimplification. For instance, the code completely dissociates expansion from acid attack which is subject to debate as discussed in previous sections. Other documents such as BS EN 206-1 (2005), indicates that a level of NH_4 of 15–30 mg/l should be regarded as slightly aggressive, 30–60 mg/l as moderately aggressive, and greater than 60 mg/l as highly aggressive. Another document from BRE Special Digest 1 (2005) recommends that excavation and removal of ammonium contaminated soils (where concrete will be placed) is not generally necessary rather, specifying a good quality concrete with a low permeability to resist ingress of ammonium ions will be enough. An exception is a case where there is a possibility of encountering high ammonium concentrations. In such cases, coatings or sacrificial layers was recommended for additional protection. Various options for protective coating against chemical attacks are also discussed in BS EN 1504-2 (2004) and BS EN 1504-10 (2003).

On the other hand, AAMs are not included in the current Canadian regulations and codes as alternatives for concrete; however, some other jurisdictions worldwide incorporated AAMs. In Switzerland, alkali-activated slags are explicitly incorporated into national guidelines (SIA, 2014),

and in the UK, a Publicly Available Specification (BSI PAS 8820, 2016) for AAMs and concretes has recently been published. In China, the standard GB/T 29423 (2012) describes the use of AAMs for chemical resistance applications. There is an extensive set of prescriptive standards for alkali-activated slag cements and concretes which has long been in place in Ukraine, Russia and other CIS nations derived from the work of the Glukhovsky Institute in Kiev (Kavalerova et al., 2014). In Australia, the state roads authority of the state of Victoria (VicRoads) has updated four of their standard specifications to explicitly include AAMs: Sections 703 (general concrete paving), 701 (drains and pipes), 705 (drainage pits), and 711 (safety barriers), with additional possible allowances for use of these materials under Section 610 (structural concrete) (Andrews-Phaedonos, 2014).

2.6. Closure

In light of the literature available till date, extensive research has been conducted on sulfuric acid attack on concrete. However, evolution of code provisions to this concrete durability issue has also been insufficient. For instance, there have been no North American specific standards for assessing the resistance of concrete to sulfuric acid attack. Numerous research studies have been conducted to investigate the effects of SCMs on mitigating sulfuric acid attack on concrete, without a general agreement on their effectiveness. The contradictory data on the role of SCMs in improving the resistance of concrete to sulfuric acid attack is likely due to the variability in testing conditions (concentration and pH level). Given the variability of testing parameters reported in the literature and the lack of standard test methods, one of the objectives of this study is to investigate the effect of incremental levels of sulfuric acid attack on concrete mixtures incorporating SCMs to systematically evaluate the response of the same type of concrete to each level of aggression. The

protocol developed herein may better correlate to field conditions, where acidic attack of concrete is progressive.

On the other hand, although AAMs are a promising alternative to conventional concrete as an acid resistant materials and might impact the long-term performance of concrete infrastructure, AAMs have technical limitations, which might hinder their widespread use in concrete applications. Mitigation of these properties is essential in order to increase the use of AAMs and benefit from their high chemical resistance. The incorporation of nanoparticles (e.g. nanosilica) probably has a promising impact to improve the long-term performance of AAMs. However, research on AAMs incorporated nanosilica is dearth and has mainly focused on the hydration kinetics and mechanical properties. In addition, there is lack of information on the durability characteristics of AAMs containing nanosilica. Also, AAMs are a promising candidate for repair of concrete exposed to acidic media; however, this area also remains largely unexplored. Hence the feasibility of using AAMs incorporated nanosilica as a repair material, in acidic environment was investigated in this study.

Chapter 3: Experimental Program

This chapter describes the experimental program including: materials and mixtures, procedures of mixing, exposures, and tests adopted in this research program. The experiments were divided into two parts: experimental program for concrete mixtures incorporating SCMs and nanosilica under incremental acidic attack, and experimental program for concrete with AAMs under different acidic exposures.

3.1 Experimental Program for Concrete Mixtures Incorporating SCMs and Nanosilica under Incremental Acidic Attack

3.1.1 Materials and Mixtures

General use cement (GU) and portland limestone cement (PLC) have been used in this study, which meet CSA A3001 (CAN/CSA-A3001, 2013) specifications. SCMs including Type F fly ash (abbreviated as FA), silica fume (abbreviated as SF) conforming to CSA A3001 (2013) and nanosilica sol (abbreviated as NS), were used as replacements of the total binder to prepare 14 concrete mixtures. In order to improve the workability, a high-range water reducing admixture, based on polycarboxylic acid and complying with ASTM C494/C494M13 Type F (2016) was added to all mixtures to achieve a slump range between 75 and 125 mm. **Table 3.1** shows the chemical and physical properties of the cement and SCMs. The coarse aggregate was well-graded natural gravel (9.5 mm) containing a small fraction (about 10% by mass) of carbonaceous aggregate with a specific gravity and absorption of 2.65 and 1.6%, respectively. The fine aggregate was well-graded river sand with a specific gravity, absorption, and fineness modulus of 2.53, 1.5% and 2.9, respectively. The total binder content and water-to-binder ratio (w/b) for all mixtures were kept constant at 390 kg/m^3 and 0.40, respectively. Single binder (control) mixtures were prepared from 100% GU or PLC. The binary binders incorporated GU or PLC with either 30% fly ash, 5%

nanosilica or 5% silica fume. Ternary binders were prepared from 65% GU or PLC with 30% fly ash and either 5% nanosilica or silica fume. Quaternary binders consisted of 60% GU or PLC with 30% fly ash, 5% nanosilica and 5% silica fume. **Table 3.2** shows the mix proportions for all mixtures. Concrete was mixed in a mechanical mixer to prepare three replicates of prismatic (50×50×285 mm) and cylindrical (100×200 mm) specimens, which were cured at standard conditions (22±2°C and 98% RH) for 28 days according to ASTM C192 (2016).

Table 3. 1: Chemical and physical properties of cement and SCMs

Chemical Composition (%)	**GU**	**PLC**	**FA**	**SF**	**NS**
SiO_2 %	19.8	19.2	55.2	92.0	99.17
Al_2O_3 %	5.0	4.4	23.1	1.0	0.38
Fe_2O_3 %	2.4	2.6	3.6	1.0	0.02
CaO %	63.2	61.5	10.8	0.3	--
MgO %	3.3	2.4	1.1	0.6	0.21
SO_3 %	3.0	3.4	0.2	0.2	--
Na_2O_{eq} %.	0.1	0.2	3.2	0.2	0.20
Specific Gravity	3.17	3.11	2.12	2.22	1.40
Mean Particle Size (µm)	13.15	11.81	16.56	0.15	35×10^{-3}
Fineness (m^2/kg)	390	453	290	20000	80000
Viscosity (Cp)	--	--	--	--	8
pH	--	--	--	--	9.5

Table 3. 2: Proportions of mixtures per cubic meter of concrete

Mixture ID.	Cement (kg/m^3)	Water (kg/m^3)	FA (kg/m^3)	SF (kg/m^3)	NS (kg/m^3)	Coarse Aggregate (kg/m^3)	Fine Aggregate (kg/m^3)	28 Day Compressive Strength (MPa)	28 Day Splitting Strength (MPa)
GU group									
GU	390	156	--	--	--	1228	614	55	4.6
GUF	273	156	117	--	--	1200	600	46	4.2
GUSF	370	156	--	20	--	1212	606	65	4.8
GUNS	370	137	--	--	39	1224	612	58	5.3
GUFSF	254	156	117	20	--	1196	598	54	5.5
GUFNS	254	137	117	--	39	1196	598	53	5.9
GUFSFNS	234	137	117	20	39	1180	590	52	6.1
PLC group									
PLC	390	156	-	-	-	1228	614	60	4.8
PLCF	273	156	117	-	-	1200	600	47	4.4
PLCSF	370	156	-	20	-	1212	606	62	5.0
PLCNS	370	137	-	-	39	1224	612	70	5.4
PLCFSF	254	156	117	20	-	1196	598	48	5.4
PLCFNS	254	137	117	-	39	1196	598	70	5.6
PLCFSFNS	234	137	117	20	39	1180	590	56	6.0

3.1.2 Acid Exposure

After curing, the concrete specimens were immersed into consecutive levels of aggression in sulfuric acid solutions, as shown in **Fig. 3.1**, with concentrations of 0.0001, 1.12 and 2.5% and corresponding initial pH of 4.5, 0.35 and 0, respectively (Phases I, II and III). The time interval was 12 weeks for each phase, i.e. a total exposure period of 36 weeks (**Fig. 3.2**). These exposure periods conformed to the common time intervals reported in the literature on accelerated tests of sulfuric acid attack. The aggression level of Phase I was selected in compliance with the exposure classes in BRE Special Digest 1 (2005) (class of exposure DS-1) and European code EN 206 (2005) (class of exposure XA2). However, in many applications (e.g. wastewater and sewage facilities) the level of aggression level may yield more severe levels. Hence, higher concentrations and lower pH levels were chosen for Phases II and III. In addition, in the field, concrete is

customarily exposed to progressive levels of acidic attack. Therefore, to make the aggression level incremental and avoid shocking the specimens with the higher concentrations, the first two weeks of Phases II and III comprised a ramping transition period from the lower to higher concentration, as depicted in **Fig. 3.2**. The test procedure was carried out at room temperature and humidity (approximately 22±2°C and 60%, respectively). In order to keep the level of aggression constant during each phase, the pH values were kept at constant thresholds of 4.5, 1 and 0.5, for Phase I, II and III, respectively. The pH values of the solutions were observed daily and adjusted to the threshold phase by adding small aliquots of diluted sulfuric acid solutions. The solution-to-specimens' volume ratio was kept constant at two and solutions were renewed with fresh ones before each phase. Each group of (GU and PLC) of specimens had its own acid bath to provide similar acidic environments for the GU and PLC mixtures and isolate the neutralization effect (if any) to the PLC mixtures.

Fig. 3. 1: Incremental aggression of the sulfuric acid exposure: phase I, II and III

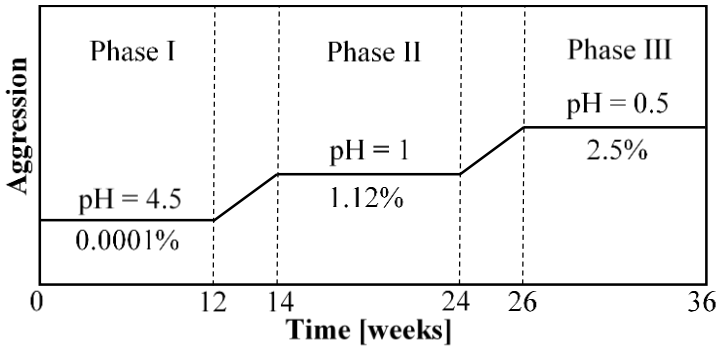

Fig. 3. 2: Incremental aggression of the sulfuric acid exposure: phase I, II and III

3.1.3 Tests

The rapid chloride permeability test (RCPT) was conducted to determine the penetrability (physical resistance) of the concrete specimens according to ASTM C1202 (2015) on discs (100×50 mm) from all mixtures, as shown in **Fig. 3.3**. To minimize the electrolysis bias of this method, the penetration depth of chloride ions/front into concrete was determined according to the procedure described by Bassuoni et al. (2005) since it better correlates to the physical characteristics of the pore structure. Following the RCPT, the discs were axially split into two symmetrical halves and then sprayed with 0.1 M silver nitrate solution which converts to white silver chloride, representing the penetration depth. To determine the porosity of concrete mixtures, the mercury intrusion porosimetry (MIP) was conducted, as shown in **Fig. 3.4**, on small samples (chucks) extracted from concrete cylinders of each mixtures. These samples were approximately 4 to 7 mm in size, and were carefully selected so that large aggregates were avoided. Before conducting the MIP, approximately 5 g of these chunks from each mixtures were oven-dried at 45±2°C until reaching a constant mass to reduce the potential of drying shrinkage cracks associated with higher temperatures.

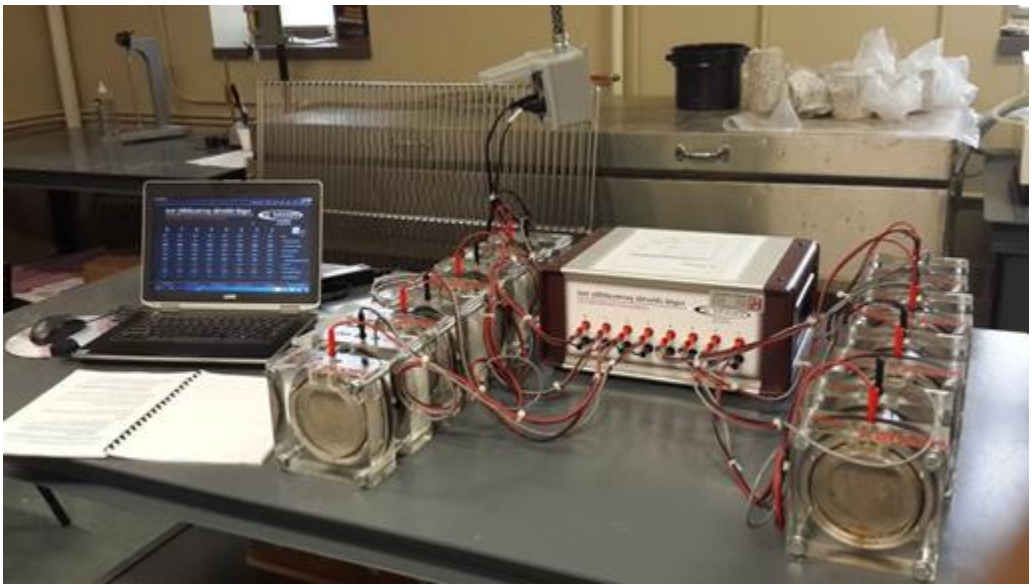

Fig. 3. 3: RCPT apparatus.

Fig. 3. 4: MIP apparatus.

Before the exposure, the mechanical properties of specimens from all mixtures were determined. The compressive and splitting tensile strengths were determined at 28 days using concrete cylinders according to ASTM C39 (2016) and ASTM C496 (2011), respectively [**Table 3.2**]. For the concrete prisms, the initial masses were recorded at 28 days to calculate the

accumulative change in mass with the time of exposure. Specimens were taken out of the solution weekly, rinsed with the same solution in the containers to remove loose reaction products and then blotted with paper towel to remove excess moisture. After drying specimens in laboratory conditions (20°C and 50% RH) for 30 min, as shown in **Fig. 3.5**, visual assessment and masses (**Fig. 3.6**), were recorded. For each specimen, the relative mass change at the end of each week (ML_t) was calculated, according to Equation 1:

$$ML_t = \frac{M_t - M_i}{M_i} \times 100 \qquad (3.1)$$

where, M_t is the mass of the specimen at time t (kg), and M_i is the initial mass (kg) of the specimen before sulfuric acid exposure.

Fig. 3. 5: Drying the specimens in laboratory conditions after taking them out of the solution.

Fig. 3. 6: Weighing the specimens after drying to calculate the relative mass change.

Phenolphthalein was used as an indicator of the pH change in the concrete pore solution to measure the depth of neutralization. The solution was sprayed on the surface of concrete cylinders freshly cut using a concrete saw, with the orientation of the cylinder perpendicular to the longitudinal axis of symmetry. This indicator shows a magenta colored region on the concrete surface where the pH level exceeds about 9 and a colorless region where the pH level is less than 9. Thermal and microstructural studies were performed to investigate the degradation products within the surface of the specimens. Differential scanning calorimetry (DSC) (**Fig. 3.7**) at a heating rate of 10C°/min was conducted on powder samples extracted from the surface (0 to 10 mm) of selected specimens exposed to the sulfuric acid solutions after Phases II and III, in comparison to companion specimens kept in the curing room. The powder samples were prepared from fracture pieces of specimens, which were pulverized to fine powder passing through sieve #200 (75 μm). The results were complemented by microanalysis from scanning electron microscopy (SEM) (**Fig. 3.8**) with energy-dispersive X-ray analysis (EDX). The fracture pieces selected for the SEM analysis were extracted from the reaction front (surface of the specimens) and were coated with a

fine layer of carbon before performing the analysis to make the surface conductive and improve the sample imaging.

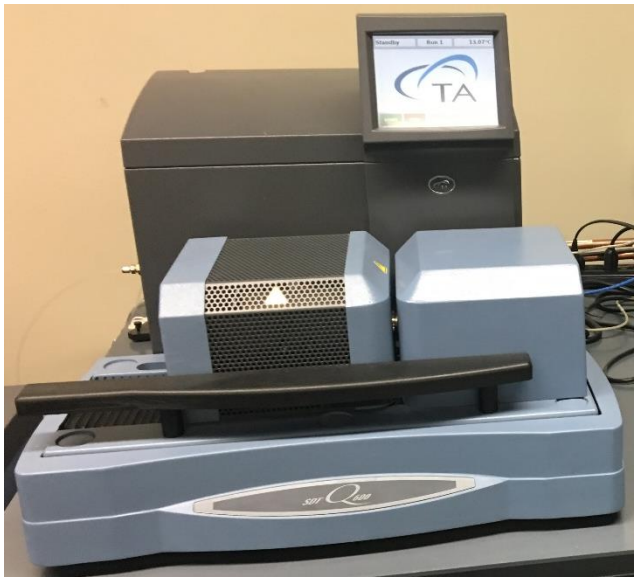

Fig. 3. 7: The DSC instrument

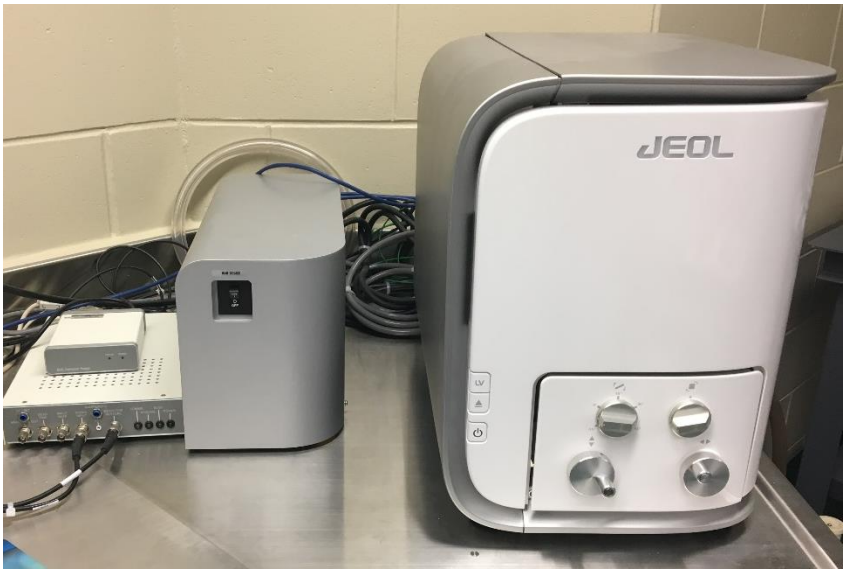

Fig. 3. 8: The sample chamber of SEM where the fracture pieces were mounted.

3.2 Experimental Program for Concrete with AAMs under Different Acidic Exposures

3.2.1 Materials and Mixtures

Class F fly ash (FA), ground granulated blast-furnace slag (S) Grade 100 and their blends were used as the main binder components for concrete tested in this study. Commercial nanosilica (NS) sol (50% solid content of SiO_2 dispersed in an aqueous solution) with an average particle diameter of 35 nm were used as an additive with a dosages of 6%. The chemical composition and physical properties of the fly ash, slag and nanosilica are presented in **Table. 3.3**. Locally available coarse aggregate (natural gravel with a maximum size of 9.5 mm) and fine aggregate (well-graded river sand with a fineness modulus of 2.9) were used. The specific gravity and absorption were 2.65 and 2%, respectively, for gravel, and 2.53 and 1.5%, respectively, for sand. A high-range water-reducing admixture (HRWRA) based on polycarboxylic acid and complying with ASTM C494/C494M13 (2016) Type F was added to maintain a slump range of 50 to 75 mm. In addition, an air-entraining admixture was used to provide a fresh air content of 6±1%.

Table 3. 3: Chemical composition and physical properties of fly ash, slag and nanosilica

	FA	**S**	**NS**
Chemical Composition			
SiO_2 %	55.20	33.4	99.17
Al_2O_3 %	23.13	13.4	0.38
Fe_2O_3 %	3.62	0.76	0.02
CaO %	10.81	42.7	--
MgO %	1.11	5.3	0.21
SO_3 %	0.22	2.4	--
Na_2O_{eq} %	3.21	0.3	0.20
Physical Properties			
Specific Gravity	2.12	2.87	1.40
Mean Particle Size, µm	16.56	14.12	35×10^{-3}
Fineness, m^2/kg	290*	492*	80000**
Viscosity, Cp	--	--	8
pH	--	--	9.5

* Blain fineness.

** Fineness was determined by titration with sodium hydroxide according to the manufacturer.

A combination of sodium hydroxide (NaOH) and sodium silicate (Na_2SiO_3) solutions was used as an alkaline activator. Two molar concentrations (8 and 12 mol) of NaOH were prepared by mixing 99% pure pallets with deionized water two days prior to mixing. In the literature, the concentration of NaOH solution varied between 8 and 16 M and it is not recommended using above or less than this limit for the formation alkali activated materials (Adak et al. 2014; Law et al. 2012; Adam 2009). The chemical composition of the Na_2SiO_3 solution consisted of 9% Na_2O, 28% SiO_2, and 63% H_2O with SiO_2-to-Na_2O ratio of 3.11. Single binder (control) mixtures (AAFA and AAS) were prepared from 100% fly ash or slag, respectively. The binary binders were prepared by incorporating either fly ash with 6% nanosilica or 10% slag, or slag with 6% nanosilica to produce AAFA-NS, AAFA-S and AAS-NS, respectively. Ternary binders (AAFA-S-NS) consisted of 84% fly ash with 10% slag and 6% nanosilica.

Table 3.4 summarizes the proportions of all mixtures. For AAFA, AAFA-NS, AAFA-S and AAFA-S-NS mixtures, the ratio of alkaline activator (NaOH and Na_2SiO_3) to fly ash was 40 % (by weight) with a Na_2SiO_3/NaOH of 2.0; however, the corresponding ratios were 30% and 1.5, respectively, for AAS and AAS-NS. These ratios were reported in previous studies to produce high rate of activation for fly ash and slag binders, respectively (Deb et al., 2015; Adak et al. 2014; Rattanasak et al., 2009; Al Bakri Abdullah et al., 2012; Wang and Scrivener, 1995; Bakharev et al., 2001; Adam 2009; Görhan and Kürklü, 2014). Due to the high quantity of solids (Na_2O and SiO_2) in the alkaline activators, the notion of water-to-solid ratio (w/s) was used for the mixture design. The w/s and total binder content for all mixtures were kept constant at 0.35 and 400 kg/m^3, respectively. The quantity of mixing water included the sum of water contained in the sodium silicate, sodium hydroxide, nanosilica and added water, while the quantity of solid was the sum of the of fly ash and/or slag, nanosilica and solid contents in the alkaline activator solution.

Table 3. 4: Proportions of the mixtures per cubic meter

Mixture ID	FA (kg)	S (kg)	NS (kg)	Aggregate (kg)		Activator (kg)		Water* (kg)	28 Day Compressive Strength (MPa)
				Sand	Coarse	Na_2SiO_3	NaOH		
Fly ash group									
AAFA	400	0	0	842	842	106.7	53.4	44.5	26.6
AAFA-NS	384	0	32	843	843	106.7	53.4	28.5	28.3
AAFA-S	360	40	0	848	848	106.7	53.4	44.5	39.4
AAFA-S-NS	344	40	32	849	849	106.7	53.4	28.5	38
Slag group									
AAS	0	400	0	917	917	72.0	48.0	63.4	24.4
AAS-NS	0	384	32	919	919	72.0	48.0	47.4	33.7

*Added water to maintain constant w/s of 0.35.

3.2.2 Procedures of Mixing

To attain homogenous dispersion of components, a specific sequence of mixing was adopted based on experimental trials to prepare six replicates of cubic (100×100×100 mm) specimens and three replicates of prismatic (100×100×350) and cylindrical (75×150 and 100×200 mm) specimens. The Na_2SiO_3 and NaOH solutions of desired quantity were mixed together with gauging water for 5-6 minutes about 24 hours before mixing with other ingredients. Right before mixing, air entraining agent, superplasticizer and nanosilica were added to the water. All dry ingredients (FA and/or S, gravel and sand) were mixed in a mechanical mixer with a speed of 60 rpm for 2 min. The premixed liquid (alkaline activator) and water with air entraining agent, superplasticizer and colloidal nanosilica simultaneously were added gradually in the mixer, and mixing continued for additional 3-5 min to achieve a uniform mixture. After mixing and casting the mixtures, a vibrating table was used to ensure good compaction of specimens. The top surface of the mixtures was sprayed by a curing compound (**Fig. 3.9**) made of high-grade hydrocarbon resins in a water-based emulsion conforming to ASTM C309 (2012) to mimic curing conditions in the field. The moulds were then stored in laboratory condition (20°C and 50% RH) until testing.

Fig. 3. 9: Spraying the top surfaces of the mixtures after casting by a curing compound.

In order to assess the bond behavior of the concrete mixtures as repair materials, two replicates slabs of 300×250 mm surface area and 70 mm thickness were cast as substrate concrete. The mixture design of these slabs comprised 400 kg high sulfate resistance Portland cement cement with 15% fly ash as a binder replacement at a w/b of 0.4 w/b, which is typical of existing/parent concrete for wastewater concrete infrastructure according to City of Winnipeg standard construction specifications for such facilities (CW 2160-R7-DIVISION 3, 2006). Right after casting the substrate slabs, the top surface (finished surface) was roughened wire brushed to improve bonding with repair concrete made from AAMs (**Fig. 3.10**). After 24 hours, the slabs were demolded and moist cured for 7 days in the curing chamber and then maintained in normal laboratory conditions to minimize the residual shrinkage in the substrate concrete. At 90 days, the mixtures were cast and placed on the top surface of these slabs with a thickness of 30 mm, following the aforementioned mixing procedure. The top surfaces of the slabs were sprayed by the curing compound, which were left in the formwork until testing (**Fig. 3.11**).

Fig. 3. 10: Wire brushing the surface of the substrate slabs after casting.

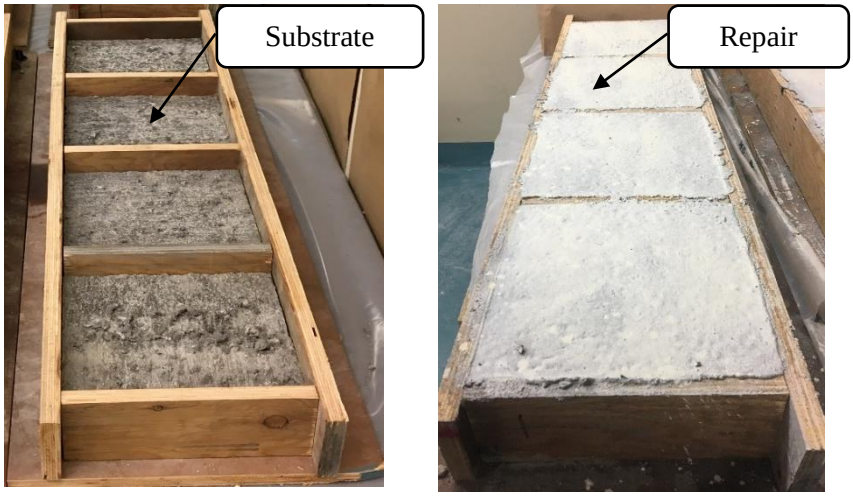

Fig. 3. 11: Casting the repair layer (AAMs) on the substrate slabs and spraying the top surface of the mixtures with the curing compound.

3.2.3 Acid Exposure

After 28 days, the cubic specimens were fully immersed in 10% sulfuric acid solution with corresponding initial pH of -0.6 for 18 weeks to monitor the corrosion/penetration depth in specimens with time. Only one surface (treated with curing compound) was exposed to the acidic solution while the other surfaces were sealed with epoxy coating. Such concentration (10%) was applied to induce very severe exposure conditions, which is twice the high concentration (5%)

typically used in previous studies for conventional concrete (e.g. Lee and Lee, 2016; Bassuoni et al., 2007; Song et al., 2005). The solution-to-specimens' volume ratio was kept constant at two and solutions were renewed with fresh ones after nine weeks.

After 28 days, the top surface of each slab was brushed to remove the curing compound (**Fig. 3.12**). Subsequently, the slabs were exposed to 18 weeks of aggressive acidic environments: four weeks of wetting/drying (W/D) cycles, four weeks of wetting (W), four weeks of freezing/thawing (F/T) cycles, and a six weeks of alternating W/D and F/T cycles (three weeks each). This customized procedure may simulate aggressive exposures in wastewater facilities, where concrete is subjected to acidic media and changing environmental conditions. For the W/D cycles, the slabs were subjected to wetting by ponding (3 to 5 mm) the surface of specimens with 10% sulfuric acid solution followed by drying. A W/D cycle (five days) consisted of wetting for three days, followed by drying at 40±2°C and 55±5% RH for two days in an environmental chamber. The W/D cycles can be initiated, for instance, by fluctuation of the wastewater level which might exacerbate the degradation effects of acid attack through ease the ingress of the acid and other synergistic effects. Also, the hot drying cycle might mimic the practical environmental conditions for wastewater facilities during periods of low flows (e.g. in sewer pipelines and acid storage tanks) and elevated ambient temperatures in hot months. The wetting stage was for four weeks at 22±2°C and 98% RH, while ponding the surface constantly with the sulfuric acid solution. The F/T cycles were applied according to the general procedures of ASTM C666 (2015) test procedure A, except that the 10% sulfuric acid solution was used instead of water and the frequency of F/T cycles per day was less to allow for chemical reactions. The duration of one F/T cycle was 12 hours: freezing at −18±1°C for 7 h and thawing at 4±1°C for 3.5 h, and 45 min. to ramp to the minimum freezing temperature or the maximum thawing temperature.

Fig. 3. 12: Test set-up for the slabs before ponding with the sulfuric acid solution.

3.2.4 Tests

In order to evaluate the resistance of the mixtures to the penetrability of aggressive ions, absorption test was conducted according to the modified absorption test introduced by Tiznobaik and Bassuoni (2017a). 50±2 mm thick slices were cut from the mid of 75×150 mm (diameter and height, respectively) cylindrical specimens after 28 days of casting under laboratory conditions (20°C and 50% RH) using a water-cooled diamond saw. The 50±2 mm concrete discs were placed in an environmental chamber at 50±2˚C and 40% RH until reaching a constant mass, and then placed in a sealed desiccator under vacuum pressure (~85 KPa) for 6 h. The initial mass of the specimens to the nearest 0.01 g were recorded and then the specimens were submerged in 4% calcium chloride ($CaCl_2$) solution for up to 360 min, and the amount of absorption of specimens after 1, 5, 10, 20, 40, 80, 160 and 360 minutes were calculated.

These results were presented as the absorption (I) of concrete specimens by:

$$I = \frac{m_t}{a \times d} \tag{3.2}$$

where:

I = absorption depth of concrete at a certain point of time in mm,

m_t = the difference between M_{WET} and M_{DRY} in g at a specific point of time,

a = cross sectional area of the exposed surface in mm^2, and

d = density of fluid in g/mm^3.

Also, the corrosion depth with time was evaluated every three weeks regular time intervals for the continually immersed cubic specimens using a phenolphthalein solution. To characterize the hardened properties of these mixtures, the compressive strength test was conducted at 3, 7, and 28 days according to ASTM C39 (2016). At the end of the acidic exposure, the slabs were evaluated qualitatively by visual examination, and quantitatively by determining mass of scaled materials. To evaluate the bond between the repair mixtures and substrate concrete as well as the resistance of the composite assembly to environmental conditions, the pull-off test was applied according to CSA A23.2-6B (2014), as shown in **Fig. 3.13** and **Fig. 3.14,** at 28 days (unexposed slabs) and after the acidic exposure with different environments (18 weeks).

Fig. 3. 13: Partial coring of the slabs.

Fig. 3. 14: The pull-off test.

Mineralogical and microscopy studies were conducted to evaluate the microstructure of the AAMs. The microscopy studies were conducted using the scanning electron microscopy (SEM), as described in section 3.1.3. The results were complemented by backscattered scanning electron microscopy (BSEM) with elemental dispersive X-ray (EDX). The mineral phases were analyzed by X-ray diffraction (XRD, Cu-Kα) (**Fig. 3.15**) with a scanning rate of 0.5°/min on powder samples extracted from the repair and substrate layers as well as the interfacial zone for exposed and unexposed (reference) slabs. Also, Thermal studies was performed to investigate the degradation products within the surface of the specimens using the differential scanning calorimetry (DSC), as described in section 3.1.3.

Fig. 3. 15: XRD instrument in which the powder samples were test

Chapter 4: Results and Discussion for Concrete Mixtures Incorporating SCMs and Nanosilica under Incremental Acidic Attack

4.1 Penetrability and Porosity

Table 4.1 shows the chloride ions penetration depth from the RCPT and the total porosity obtained from MIP for all concrete specimens prepared from the fourteen mixtures. The results of the penetration depth and total porosity were consistent, since the penetration depths were directly proportional to the corresponding total porosity. The control specimens from the PLC mixture had about 28% and 9.5% reduction in the penetration depth and porosity, respectively, compared to the control GU specimens. This is ascribed to the higher fineness (453 m^2/kg) of PLC compared to the GU cement (390 m^2/kg), which can improve the hydration process and microstructure of concrete (Ramezanianpour and Hooton, 2014). However, for the other mixtures (e.g. PLCF and PLCFSFNS, respectively vs. GUF and GUFSFNS), this trend diminished due to the addition of SCMs. For the GU and PLC groups, incorporating different types and sizes of SCMs such as silica fume, fly ash and/or nanosilica significantly reduced the penetration depth and porosity of specimens (**Table 4.1**). For example, compared to the specimens prepared with the GU cement only, adding a dosage of 30% fly ash in binary specimens (GUF) led to reduction of about 49% in the penetration depth and 19% in the total porosity. Incorporating silica fume in binary (GUSF) or ternary (GUFSF) systems led to more reduction in the penetrability of specimens (70 and 61%, respectively). Nanosilica had a significant effect when it was incorporated in binary (e.g. GUNS) and ternary (e.g. GUFNS) systems, as there were 76 and 80% reductions in the penetration depth,

respectively, with corresponding reductions of about 42 and 43% in the total porosity. The addition of fly ash, silica fume and nanosilica in a quaternary binder (e.g. GUFSFNS) led to the highest decrease in the penetrability (85%) and porosity (45%) compared to GU. These trends were also valid for the PLC group. Generally, the role of SCMs in refining and densifying the pore structure was due to the pozzolanic reactivity (e.g. fly ash), and thus discounting the penetrability of concrete [36]. Nanosilica and silica fume further reduced the penetrability of concrete owing to both chemical (pozzolanic reaction) and physical (filler action and speeding up the reaction rate) effects due to the high fineness of these materials (Said et al., 2012). However, the effect of nanosilica was magnified compared to silica fume, as nanosilica has a specific surface of 80,000 m^2/kg compared to 20,000 m^2/kg for silica fume.

Table 4. 1: Results from RCPT and MIP

Mixture ID.	Penetration Depth (mm)	Standard Error of Penetration Depth	Chloride Ions Penetrability Class (ASTM C1202)	Average Porosity (%)
GU group				
GU	17.6	0.89	Moderate	15.8
GUF	9.0	0.64	Low	12.8
GUSF	5.3	0.37	Very Low	9.5
GUNS	4.2	0.53	Very Low	9.2
GUFSF	6.8	0.74	Very Low	11.4
GUFNS	3.5	0.32	Very Low	9.0
GUFSFNS	2.7	0.92	Very Low	8.7
PLC group				
PLC	12.7	1.02	Moderate	14.3
PLCF	11.9	0.92	Low	14.0
PLCSF	5.0	0.45	Low	9.4
PLCNS	4.0	1.06	Very Low	9.1
PLCFSF	6.8	0.76	Very Low	11.4
PLCFNS	3.2	0.37	Very Low	8.9
PLCFSFNS	3.0	0.21	Very Low	8.8

4.2 Visual Assessment

Figure. 4.1 shows the visual progression of damage on the surface of concrete at different stages of exposure. At the end of Phase I (12 weeks), all the GU and PLC specimens exposed to continuous immersion in the mild acidic environment (0.0001% and pH threshold of 4.5) remained intact without visible features of damage, as shown in **Fig. 4.1(a)**. However, after immersion in the severe acidic media in Phase II (1.12% concentration and pH threshold of 1), progressive precipitation of white powdery material [identified as gypsum by DSC, **Fig. 4.1(b)]** was observed on the surface of all specimens after 24 weeks. Nevertheless, there were no distinctive differences among specimens from the single or blended binders in the GU and PLC groups throughout Phase II. At the end (36 weeks) of Phase III (2.5% concentration and pH threshold of 0.5), a significant amount of off-white residue (gypsum) deposited in the bottom of containers which implied continuous leaching of the corroded layer of concrete in this very severe acidic media. All specimens generally had uneven surfaces (due to using siliceous aggregates) surrounded by soft paste [e.g. **Fig. 4.1(c)]**, which implies that the cementitious matrix decomposed at and near the reaction zone with the acidic solution.

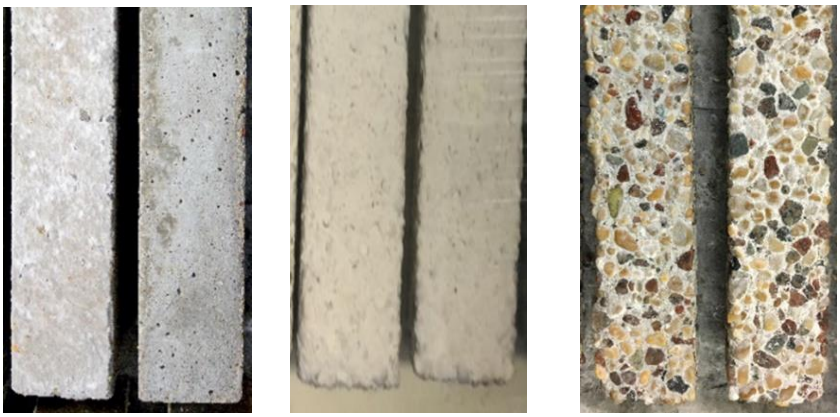

(a) **(b)** **(c)**

Fig. 4. 1: Features of damage of GU specimens immersed in the sulfuric acid solutions after Phases: (a) I, (b) II, and (c) III.

The neutralization depth can give a measure of the penetration depth of H^+ ions in the concrete specimens reflecting the degree of damage, by loss of alkalinity due to acidic attack. **Figure 4.2** shows examples for the neutralization depths after Phases I and III. At the end of Phase I, the cross section of all specimens consisted mostly of a sound core (pH > 9 as indicated by the pink color of phenolphthalein) and a thin reaction zone (0 to 2 mm; colorless part). Subsequently, the neutralization depths for all specimens showed a slight increase (4 and 6 mm) at the end of Phases II and III, respectively. It was noted that the neutralization depths were comparable for all specimens made from single and blended binders in the GU and PLC groups at the end of each phase, although the concrete mixtures tested had different penetrability as discussed in the Penetrability and Porosity section. Consequently, other physical parameters and microstructural features are needed to judge the relative performance among the mixtures.

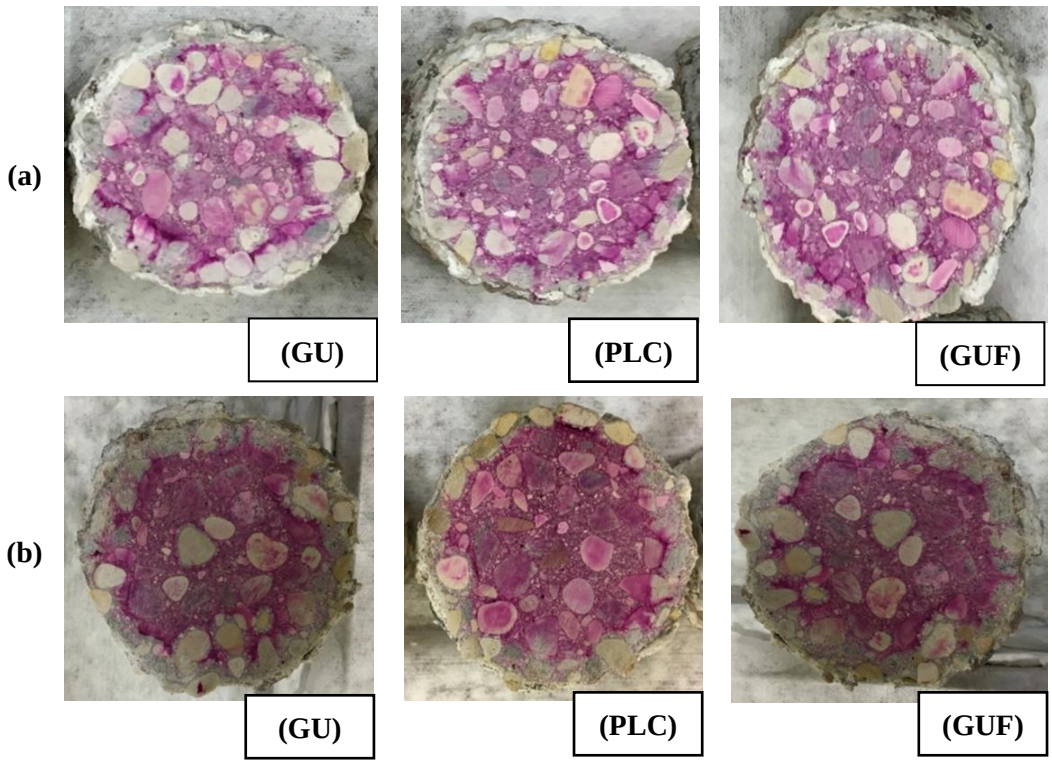

Fig. 4. 2: Neutralization depth of concrete specimens immersed in the sulfuric acid solutions after: a) Phase I (pH of 4.5), and b) Phase III (pH of 0.5)

4.3 Mass Loss

The change in mass versus time for all specimens exposed to the incremental concentrations of sulfuric acid solutions is shown in **Fig. 4.3**. Also, the total mass losses of all specimens after 24 and 36 weeks are shown in **Figs. 4.4(a)-(b)**.

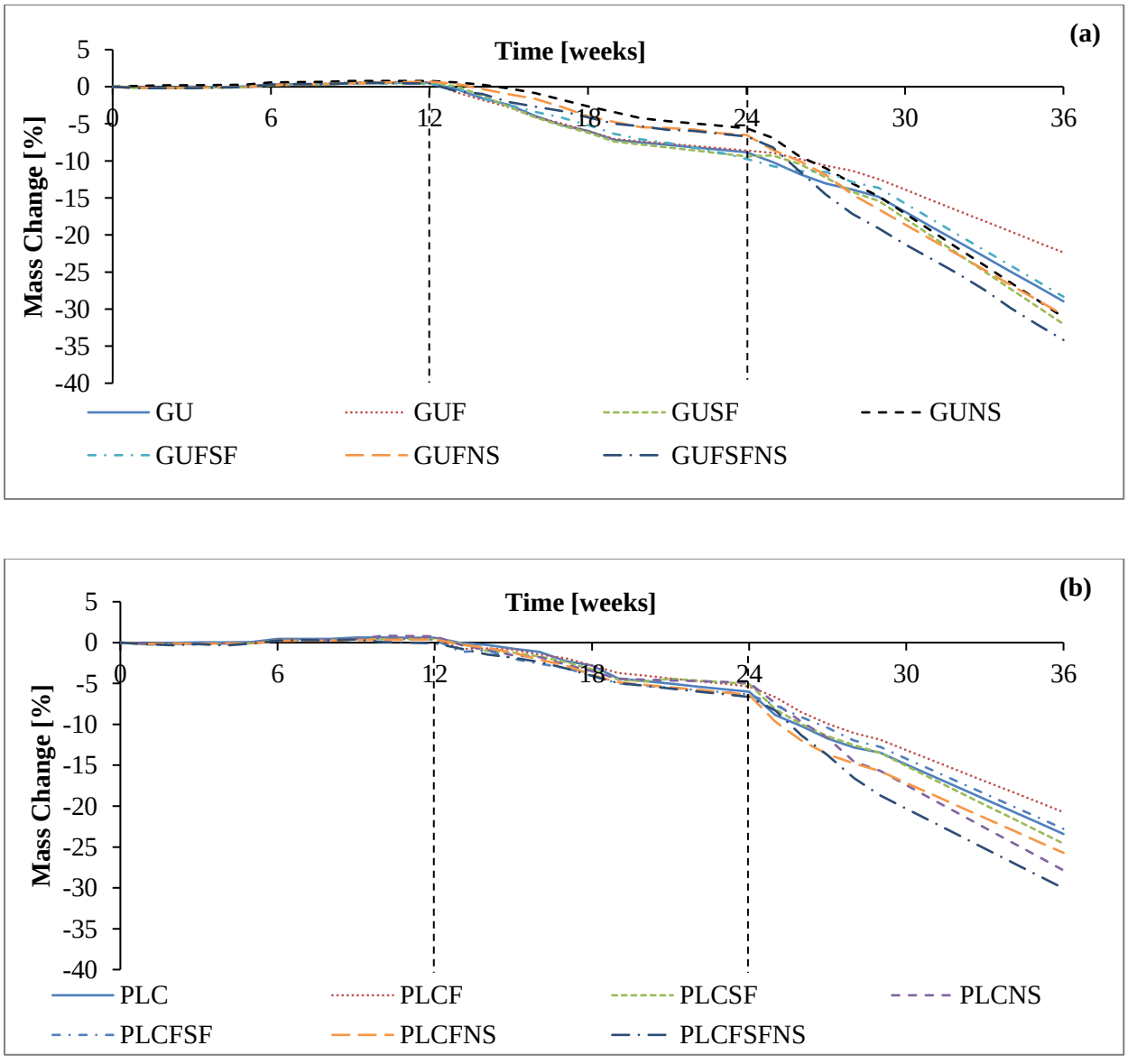

Fig. 4. 3: Average mass loss with time for specimens from groups: a) GU, and b) PLC.

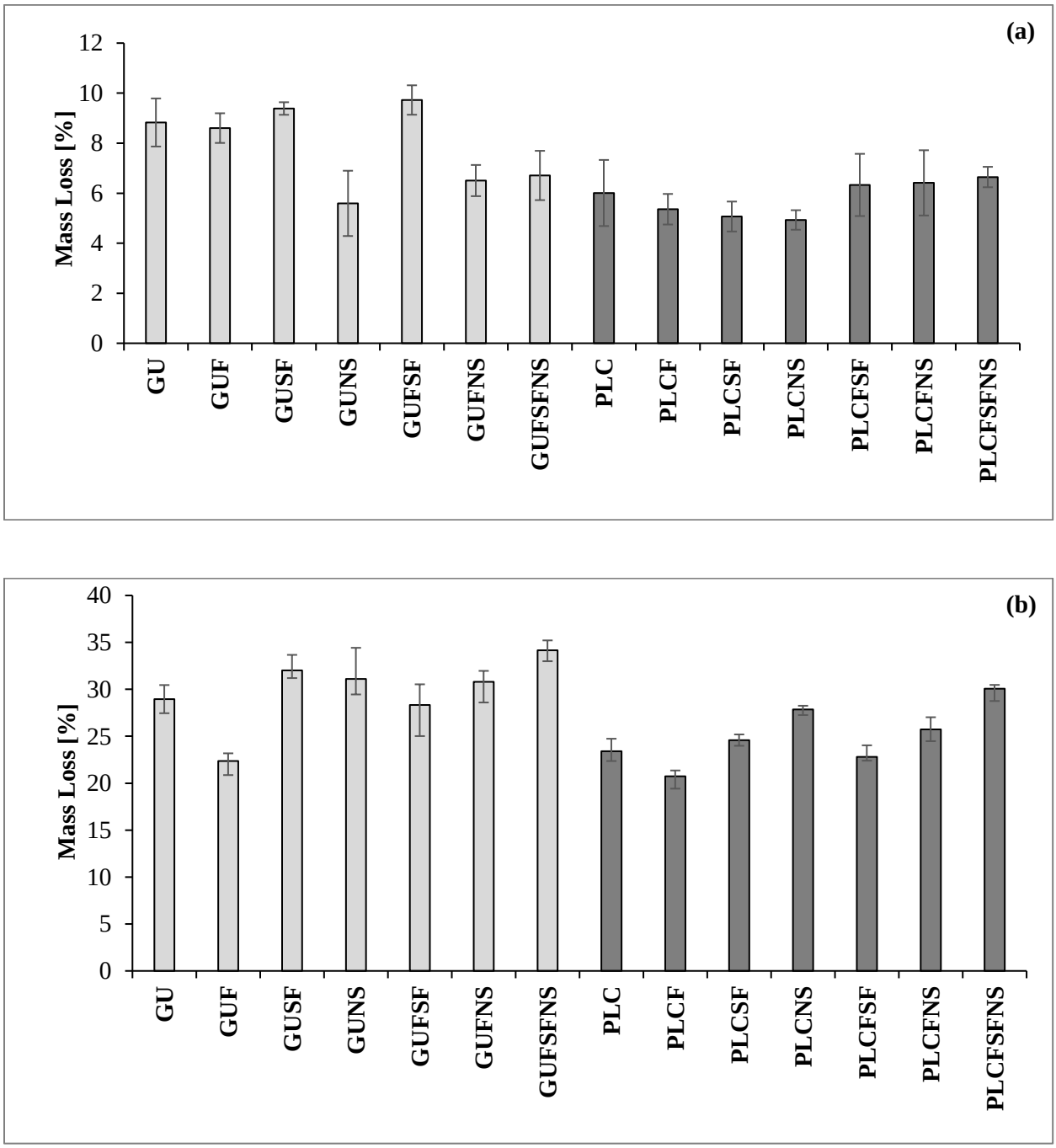

Fig. 4. 4: Cumulative mass loss for GU and PLC groups after: a) 24 weeks, and b) 36 weeks.

During Phase I, the specimens showed a slight mass gain (maximum of 0.6%) with time, without notable differences among specimens from the single and blended binders in the GU and PLC groups. This could be ascribed to the continued hydration of the cementitious paste and

absorption of solution into the specimens, which are expected at early stages of chemical immersion tests. Since no mass losses were observed among all specimens in Phase I, it appears that the mixtures tested were resistant to this mild acidic media (lower acidic concentration and higher pH) for 12 weeks.

During Phase II (severe acidic attack), all specimens exhibited continual mass loss (**Fig. 4.3**) up to the end of this phase. After 24 weeks, the total mass loss of the GU group ranged from 5.5 to 10% [**Fig. 4.4(a)**]. For binary and ternary specimens containing fly ash and/or silica fume (GUF, GUSF and GUFSF), the behavior was comparable (approximately 8.5 to 10% mass loss) to the control GU specimens (mass loss of 8.8%). However, specimens comprising nanosilica (GUNS, GUFNS, GUFSFNS) showed approximately 24 to 36% reduction of mass loss relative to the control GU specimens. Generally, specimens from the PLC group had lower mass losses (average of 24% reduction) than that of corresponding specimens from the GU group. However, there were indistinctive trends among the PLC specimens from single and blended binders, as the cumulative mass losses were in the range 5 to 6.6% at the end of Phase II [**Fig. 4.4(a)**].

During Phase III (very severe acidic attack), the mass loss rate of all specimens sharply increased (**Fig. 4.3**) up to the end of this exposure (36 weeks) showing mass losses in the range of 22 to 34% and 20 to 30% for the GU and PLC groups, respectively [**Fig. 4.4(b)**]. Concrete specimens made from the binary binder including GU and fly ash (GUF) exhibited the lowest total mass loss of about 22%, while the quaternary binder prepared with GU, fly ash, silica fume and nanosilica (GUFSFNS) experienced the highest mass loss of 34%. Correspondingly, specimens from the PLC group (PLCF and PLCFSFNS) showed mass losses of 20 and 30%, respectively. Similar to Phase II, all specimens made with PLC had relatively lower mass losses (average 15%

reduction) compared to their corresponding GU specimens. For the GU group, adding 30% fly ash in a binary system (GUF) led to a significant reduction in the average mass loss results by 23% compared to the control specimens (GU). However, ternary systems comprising fly ash and 5% silica fume (GUFSF) showed comparable results to the control specimens (GU). The results also indicated that binary systems (GUSF) containing 5% silica fume led to an increase in the mass loss of around 10% compared to GU specimens. On the contrary to Phase II trends, adding 5% nanosilica (ultrafine pozzolanic material) in either binary (GUNS) or ternary systems (GUFNS) with 30% fly ash led to increasing the mass loss (about 7%) of specimens compared to GU specimens. Incorporating nanosilica with silica fume and fly ash in the quaternary binder (GUFSFNS) led to maximizing the mass loss of specimens, which was 18% higher than that of the GU specimens. For the PLC group, incorporating 5% silica fume with PLC in binary (PLCSF) and ternary systems with 30% fly ash (PLCFSF) led to comparable results to that of the control PLC specimens. However, the incorporation of nanosilica (PLCNS), combination of fly ash and nanosilica (PLCFNS) and all three SCMs (PLCFSFNS) with PLC led to increase of mass losses by 20, 10 and 28%, respectively compared to the control (PLC) specimens.

The relationship between the penetration depths (initial physical resistance) of specimens and their cumulative mass losses after Phases II and III was explored [**Figs. 4.5(a)-(b)]**. The data patterns show mixed and discordant trends. After Phase II, some concrete specimens (e.g. GUNS, GUFNS and GUFSFNS) with low penetration depths owing to matrix densification exhibited the lowest mass loss, while after Phase III the same specimens showed the highest mass loss in the sulfuric acid solutions. Also, other specimens (e.g. GUF and PLCF) with higher penetration depths than that of systems comprising nanosilica yielded the lowest mass losses after Phase III. The trends from Phase II did not fully validate the current stipulations of building codes for concrete.

For instance, CSA A23.1 (2014) limits the maximum w/b to 0.40 and the chloride ions penetrability to less than 1000 coulombs as well as recommending incorporation of SCMs to enhance the resistance of concrete exposed to aggressively acidic environments (class of exposure A-XL), where the pH may be less than 2.0. Also, it states that the performance of concrete in such environments is primarily dependent on the resistance to the penetration of acids (CSA A23.1, 2014). In the case of the GU group, only systems with nanosilica (highest physical resistance) led to some improvement of the acidic resistance of concrete compared to control specimens; however, no such improvement was achieved for blended binary or ternary binders comprising silica fume and fly ash, in spite of their lower penetration depths (**Table 4.1**) relative to the GU specimens. Also, no distinctive trends were visible among the single and blended binders incorporating PLC, which performed better than that of GU counterparts. This might be attributed to the pronounced effect of the limestone component in PLC which led to neutralization of the acid solution in contact with the exposed surface of specimens (Belie et al., 2004). In addition, at the higher concentration of sulfuric acid (Phase III), the mass loss trends were opposite to these code specifications regarding the concept of enhancing the physical resistance of concrete. In **Fig. 4.5b**, the general pattern of data showed that as the physical resistance increased (lower penetration depths), the mass loss of specimens increased. Although the concrete mixtures tested herein complied with codes and guides (CSA A23.1, 2014; BRE Special Digest, 2005, BS EN 206-1, 2005) recommendations (w/b of 0.4 and binder content of 400 kg/m^3), with additional improvement of physical resistance by adding (silica fume and nanosilica) in binary, ternary and quaternary systems, the improvement in the acidic resistance of concrete after Phase III was particularly observed for the binary systems comprising 30% fly ash, which did not show the lowest penetrability (**Table 4.1**). Hence, in the very severe sulfuric acid exposure (2.5% and pH 0.5), the

penetrability of the cementitious matrix was not the controlling factor for the deterioration rate, and thus further investigation was performed on the microstructure of the specimens.

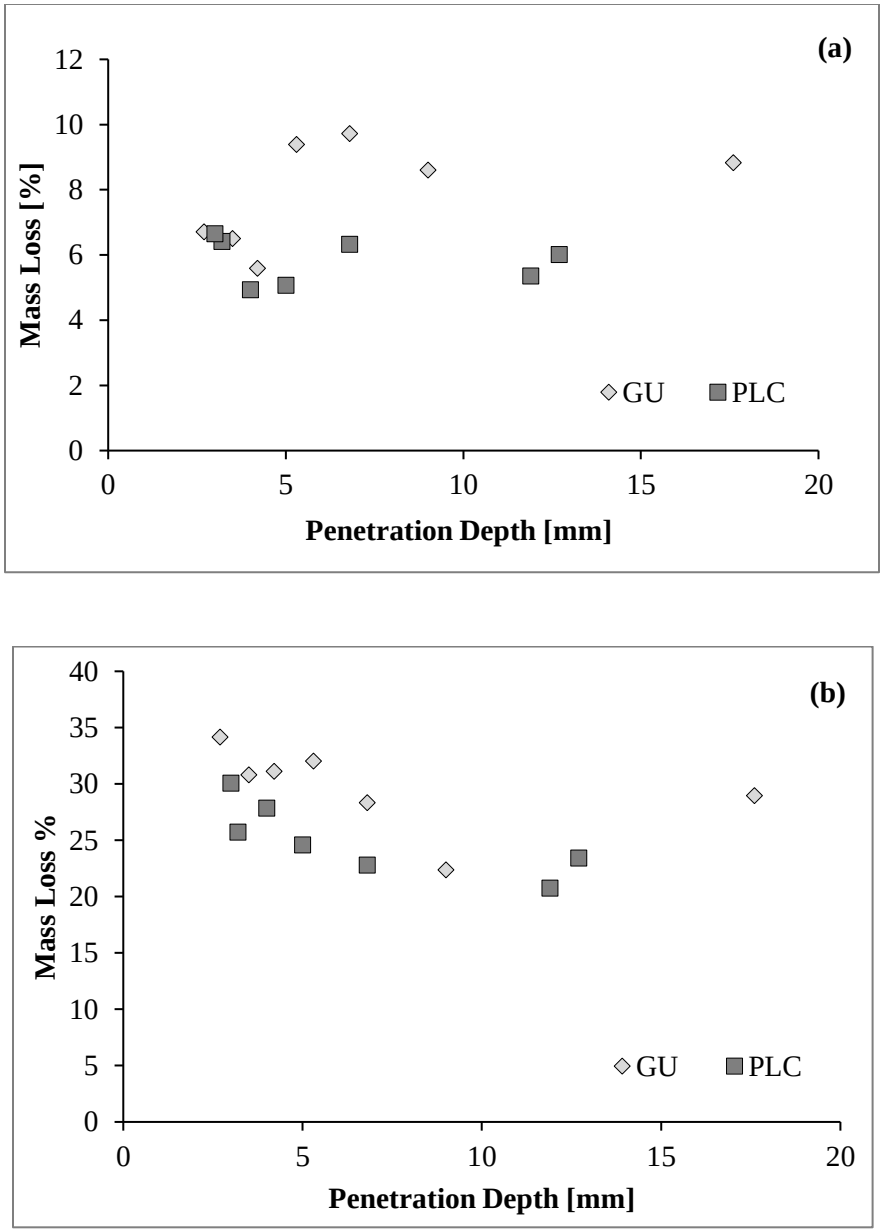

Fig. 4. 5: Penetrability of specimens vs. their total mass losses after: a) Phase II, and b) Phase III

4.4 Thermal and Microstructural Analyses

Table 4.2 provides a summary of the DSC results of the portlandite phase in the cementitious matrix of all mixtures stored in the curing chamber reflecting the progress of hydration, while

Table 4.3 provides DSC for the corresponding samples exposed to sulfuric acid solutions reflecting the deterioration of specimens and formation of reaction products. The trends from DSC were corroborated by microscopy analyses. Gypsum was identified in all specimens as the key reaction product between the sulfuric acid solution and hydrated cement paste (**Table 4.3**). However, it seems that the amount of gypsum formed in Phase I was insufficient to induce pressure to the confined pore space; thus, the specimens did not suffer from surface deterioration [**Fig. 4.1(a) and Fig 4.3**]. After Phase I, micrographs taken from fracture surfaces (0 to 10 mm from the surface) of the exposed specimens indicated that the surface of concrete was intact, and gypsum crystals were infilling some voids near the exposed surface (e.g. **Fig. 4.6**). After Phase I, the drop in portlandite contents in specimens was likely due to the neutralization reaction with acid in the limited reaction zone and progression of pozzolanic reaction, beyond this zone for blended binders.

Table 4. 2: Portlandite (420-440ºC) contents in specimens stored in the curing chamber

	Enthalpy: J/g			
Mixture ID.	**After 28 d**	**After 118 d**	**After 208 d**	**After 298 d**
GU Group				
GU	55.4	56.8	57.0	57.1
GUF	34.2	16.3	14.0	14.1
GUSF	41.9	40.1	39.8	39.8
GUNS	26.9	26.8	26.8	26.8
GUFSF	26.8	10.2	9.2	9.3
GUFNS	14.8	5.6	5.0	5.0
GUFSFNS	5.8	0.7	0.2	0.2
PLC Group				
PLC	54.3	50.9	51.0	51.0
PLCF	38.4	18.5	15.0	15.0
PLCSF	42.6	38.5	38.0	38.0
PLCNS	29.7	29.4	29.0	29.0
PLCFSF	25.0	9.2	8.0	8.1
PLCFNS	12.1	3.7	3.2	3.2
PLCFSFNS	4.2	0	0	0

Table 4. 3: Enthalpies (J/g) of the main phases in the cementitious matrix after acid exposure

Mixture ID.	After Phase I			After Phase II			After Phase III		
	Ettringite	**Gypsum**	**Portlandite**	**Ettringite**	**Gypsum**	**Portlandite**	**Ettringite**	**Gypsum**	**Portlandite**
GU Group									
GU	3.3	105.0	25.2	0.4	210.3	13.3	0.1	298.2	6.9
GUF	2.9	77.7	15.1	0.5	185.1	6.4	0	209.3	4.3
GUSF	3.3	76.5	18.2	0.1	182.4	9.5	0	254.4	5.2
GUNS	4.4	45.3	12.3	0	164.3	5.4	0	278.2	2.3
GUFSF	2.8	88.3	11.5	0	193.2	5.1	0	248.1	1.9
GUFNS	1.9	113.0	5.0	0	169.1	2.8	0	252.5	1.1
GUFSFNS	2.0	115.0	0.7	0	204.2	0.3	0	394.5	0.1
Plc Group									
PLC	4.3	54.2	23.1	1	188.3	12.1	0	224.8	5.8
PLCF	5.7	77.8	14.8	0	174.1	6.3	0	192.7	2.7
PLCSF	4.9	55.1	19.4	0	181.3	9.2	0	202.4	4.5
PLCNS	3.0	52.1	11.7	0	161.2	5.2	0	215.6	3.4
PLCFSF	4.3	61.5	10.5	0.2	182.2	4.4	0	210.4	2.4
PLCFNS	2.0	43.1	5.3	0	175.4	2.8	0	212.3	1.3
PLCFSFNS	3.9	60.5	0.8	0.2	192.5	0.6	0	368.7	0.4

Note: the temperature ranges for ettringite, gypsum and portlandite were 90-100ºC, 120-135ºC and 420-440ºC, respectively.

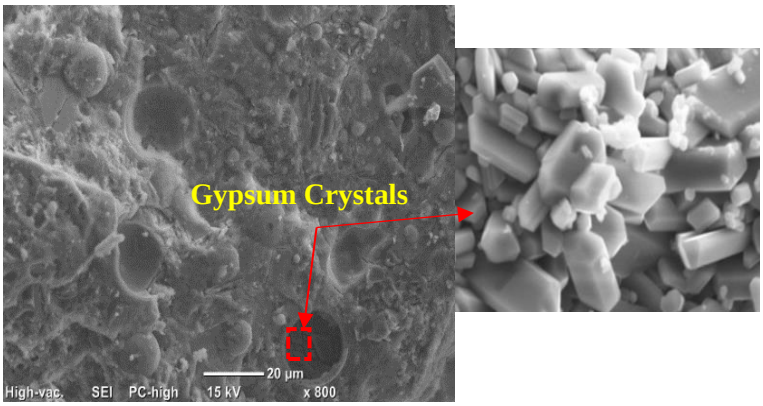

Fig. 4. 6: Exemplar micrographs from a GU specimen after Phase I showing gypsum in the reaction zone infilling air voids with higher magnification (x 3000).

After Phase II, all the specimens underwent surface deterioration [e.g. **Fig. 4.7(a)**] and mass loss due to severe sulfuric acid attack. The reaction zone consisted mainly of gypsum crystals in a deteriorated matrix [e.g. **Fig. 4.7(b)**]. Correspondingly, the DSC analysis (**Table 4.3**) for both the GU and PLC groups showed that the portlandite contents in specimens were significantly decreased (45-80% reduction in comparison with the corresponding specimens in the curing chamber). The amount of gypsum formed in the PLC group specimens was generally 5-10% lower

than those formed in the corresponding specimens in the GU group. As mentioned earlier, the slight improvement in the PLC specimens (less mass loss) might be due to the acid neutralization effect of the higher limestone component in PLC. After Phase II, the DSC results were generally comparable for all specimens made from the single and blended binders in the GU and PLC groups (**Table 4.3**). Compared to the single binder, the depletion of the amount of portlandite in the cementitious systems containing SCMs (**Table 4.2**) was due to increased pozzolanic activity, resulting in production of additional/secondary C-S-H gel, as reflected by the matrix densification observed in the RCPT and MIP results (**Table 4.1**). However, this led to more volume of cementitious gel directly vulnerable to direct attack and consequently decomposition of C-S-H in severely aggressive acidic media. This may compromise the possible benefit of improving physical resistance as recommend by building codes for concrete (CSA A23.1, 2014; BRE Special Digest, 2005), and hence most binders incorporating GU or PLC with SCMs, except for nanosilica, did not show notable improvement over the control specimens (GU and PLC) with comparable mass loss values. However, this may also imply that the concentration of the acid solution (aggression level) used in Phase II was inadequate to distinguish among the behaviors of the mixtures tested herein. In addition to the chemical degradation caused by sulfuric acid attack on cement paste, physical damage may occur due to the pressure resulting from gypsum precipitation in the pore structure of the degraded layer of the cement paste (Yuan et al., 2013, Beddoe, 2013). When the crystallization pressure exceeds the tensile strength of the weakened matrix, the degraded layer disintegrates. It was reported that gypsum formation resulting from reaction with acid will tend to precipitate faster in the coarser pores of the degraded layer rather than the finer pores (Beddoe, 2013). According to the crystal growth pressure theory, the equilibrium solubility product for solution in small pores is higher than the larger pores due to the action of the surface energy at the

solid/liquid interface (Scherer, 2004). Consequently, the small pores filled with gypsum are in equilibrium with higher acid concentrations than larger pores containing gypsum (Beddoe, 2013). The continuous precipitation of gypsum formed during sulfuric acid attack in larger pores can produce sufficient pressure to overcome the tensile strength of the weakened paste matrix, resulting in loss of surface. This may explicate the relative improvement in terms of mass loss **[Fig. 4.4 (a)]** of the binders blended with nanosilica in Phase II as these binders had very fine pore structure, as expressed by the RCPT and MIP results (**Table 4.1**).

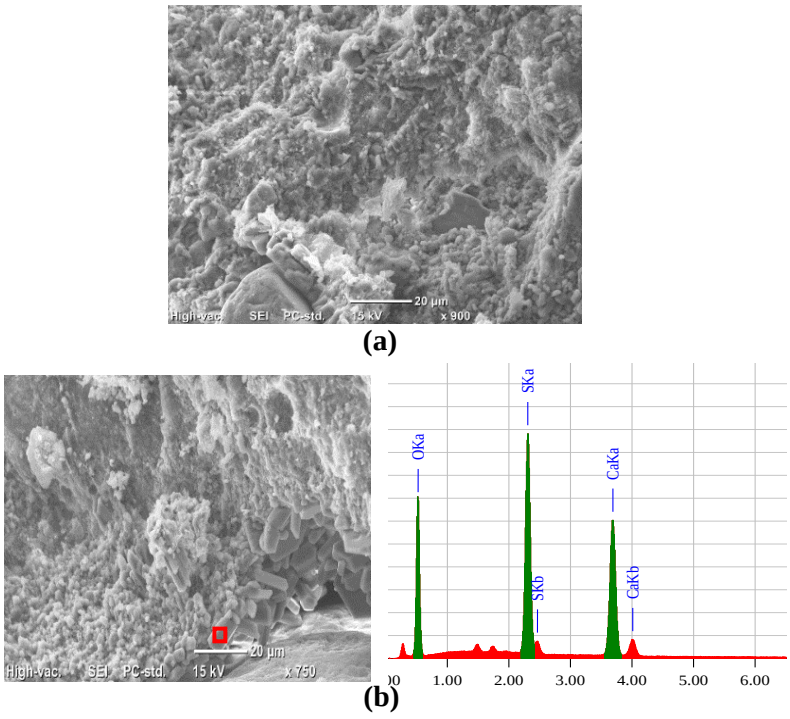

Fig. 4. 7: Micrographs of SEM and EDX analyses for a GUSF specimen after Phase II: (a) deteriorated surface, and (b) gypsum formation in the reaction zone (left) with corresponding EDX (right).

After Phase III, the amount of gypsum formed in all specimens were higher than that after Phase II, signifying the highest level of acidic aggression, in compliance with the mass loss results. The PLC group maintained lower gypsum contents compared to the GU counterparts, due to the effect of the limestone component as explained earlier. The micrographs taken from the fracture

surfaces (0–10 mm from the surface) of exposed specimens (e.g. GU) after Phase III indicated that the surface of concrete underwent significant deterioration and the reaction zone was composed mainly of gypsum crystals as confirmed by EDX [**Fig. 4.8(a)**] and DSC (**Table 4.3**). Incidental features of ettringite were found in areas towards the sound paste [more than 5 mm from the exposed surface, [e.g **Fig. 9(b)**], where the pH of the matrix was still sufficiently high [**Fig. 3(b)**] which maintained the stability of ettringite.

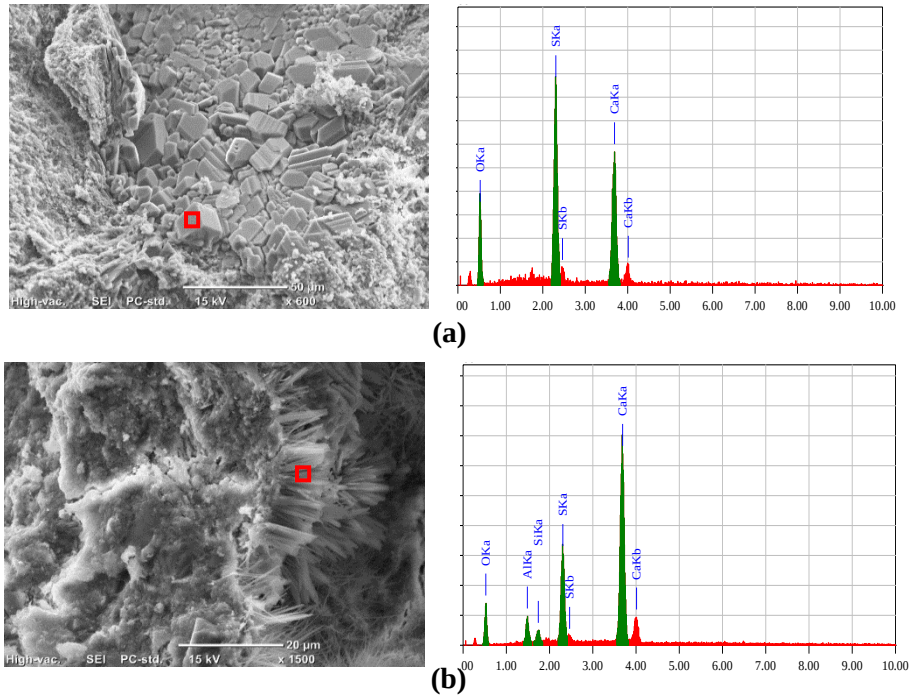

Fig. 4. 8: SEM and EDX analyses after Phase III for a GU specimen: (a) deteriorated surface showing gypsum formation in the reaction zone (left) with corresponding EDX (right), and (b) ettringite rosettes growing in an air void away from the surface (left) with corresponding EDX (right).

The quaternary binders (GUFSFNS and PLCFSFNS) exhibited the highest amounts of gypsum formation (**Table 4.3**), while the binary binders incorporating fly ash (GUF and PLCF) showed the lowest amounts of gypsum formation, corresponding to the highest and lowest mass losses, respectively [**Fig. 4.4 (b)]**. The micrographs taken from fractured surfaces of the quaternary binders (e.g. PLCFSFNS) after Phase III indicated that these binders showed the formation of large

parallel sheets of gypsum crystals as shown **Fig. 4.9(a)**, and the surface of concrete underwent significant deterioration with extremely coarse matrix due to sulfuric acid attack [**Fig. 4.9 (b)**]. The cracks and fishers propagated into the sound paste as shown in **Fig. 4.9(c)** facilitating direct ingress of the solution and resulting in significant level of deterioration. For the binders with silica fume or nanosilica, the amount of portlandite in the samples stored in the curing chamber did not show notable reduction beyond 28 days (**Table 4.2**). This might imply that the pozzloanic activity of 5% silica fume or nanosilica were exhausted by 28 days (before exposing the samples to the acid solution) due to the vigorous pozzloanic reactions of these fine or ultrafine SCMs. Greater reduction of portlandite were observed when blending SCMs together, especially in the quaternary binders, since the portlandite content was very low after 28 days. Indeed, this led to greater proportion of cement gel, as reflected by the densification of the matrix from RCPT and MIP results. However, this higher volume of cement gel, which was vulnerable to acid–base reactions especially in the very severe exposure in Phase III, led to increased amounts of gypsum in these binders (**Table 4.3**) and mass loss/deterioration (**Figs. 4.4(b) and 4.9**).

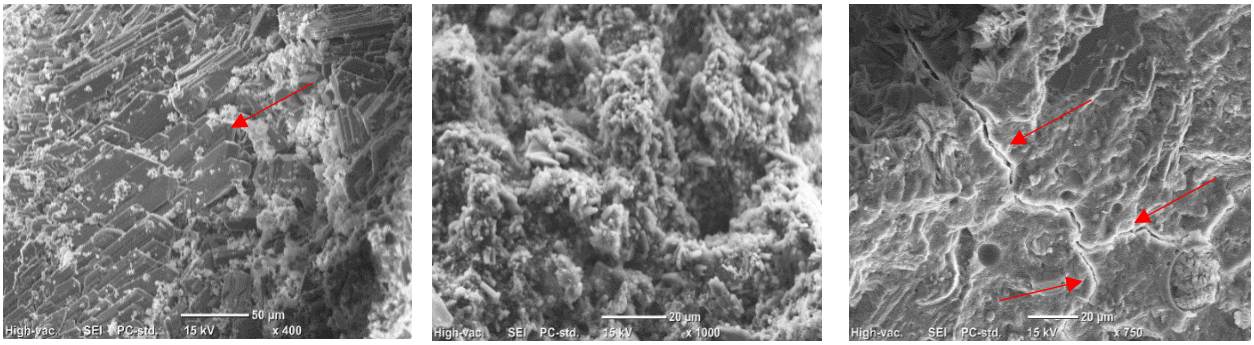

(a) **(b)** **(c)**

Fig. 4. 9: SEM and EDX analyses after Phase III for a PLCFSFNS specimen showing: (a) large gypsum crystals in the reaction zone, (b) deteriorated surface, and (c) cracks extending into the inner core.

Table 4.2 indicated significant reduction (about 50%) in portlandite after 118 days in the binary binders comprising 30% fly ash (GUF and PLCF) stored in the curing chamber and it remained constant afterwards up to 298 days. This indicated later-age pozzolanic activity of Type F fly ash (Mehta and Monteiro, 2014) between 28 and 118 days and implied availability of unreacted fly ash afterwards. The portlandite contents for these mixtures after Phase I in the acidic exposure were very close to those in the corresponding specimens stored in the curing chamber at 118 days (**Table 4.2**), reflecting the continuation of the pozzloanic activity during this mild exposure, in which no damage was observed. Subsequently, the DSC results (**Table 4.3**) for GUF and PLCF specimens showed that the amount of portlandite decreased markedly coupled with increasing gypsum formation, while the corresponding specimens in the curing room maintained their portlandite contents, signifying the dominant effect of the acid-base reactions in Phases II and III. The slow pozzloanic activity beyond Phase I in addition to the severe and very severe acid media used in Phases II and III impeded the reactivity of fly ash. This was augmented by the occurrence of unreacted fly ash particles at and within the surface of specimens (e.g. **Fig. 4.10**). Since fly ash particles are nearly inert in highly acidic solutions (Kim et al., 2003), their existence in the reaction zone minimized the surface of paste susceptible to the acid-base reaction, and thus reduced the rate of damage (inert-filler effect), in a manner similar to concrete comprising siliceous aggregates and exposed to sulfuric acid (Hughes and Guest, 1978; Fattuhi and Hughes, 1988).

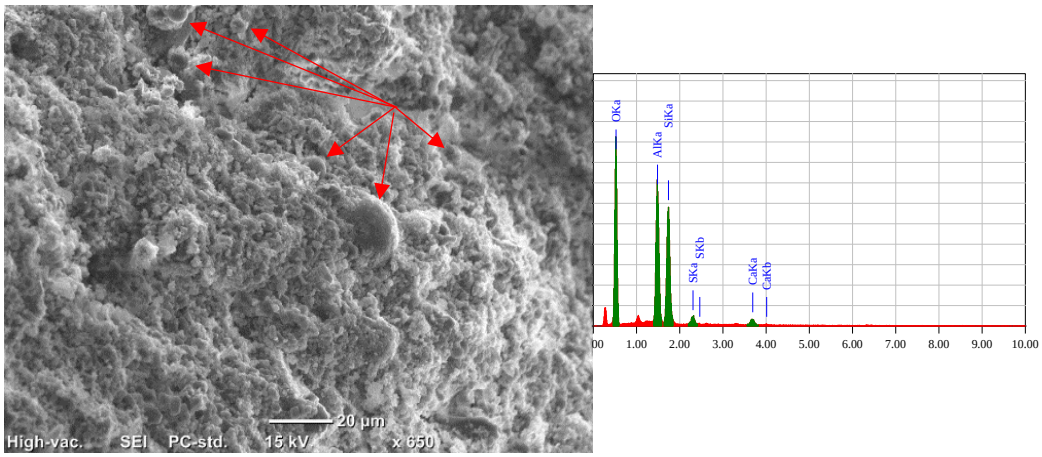

Fig. 4. 10: Unreacted fly ash particles within the reaction zone of a PLCF specimen (left) with corresponding EDX (right).

Chapter 5: Results and Discussion for Concrete with AAMs under Different Acidic Exposures

5.1 Absorption Test

Figure 5. 1 depicts the absorption depth versus time up to 360 min. The trends were mixed and overlapped during the first 40 min, as this initial absorption period is significantly affected by the composition of the skin layer (first few millimeters). This layer includes variations in paste content, aggregate distributions, sizes of capillary pores relative to the core of specimens which affected the behavior of absorption, giving inconclusive trends. Once this skin layer was saturated, the later absorption trends among the AAMs were distinctive between 40 to 360 min since they mainly governed by the proportion and sizes of accessible pores and their continuity (Tiznobaik and Bassuoni 2017a,b).

Specimens from the AAFA mixture experienced the highest total absorption depth after 360 min (about 1.35 mm), while AAS specimens exhibited the lowest total absorption depths (approximately 0.80 mm). This may suggest that slag based mixture had accelerated hydration and development of microstructure relative fly ash based mixtures, when cured at normal conditions (Lee and Lee, 2013). Incorporating 6% nanosilica in a binary system (AAFA-NS) led to some reduction (approximately 9%) in the total absorption depth relative to that of AAFA. This might be attributed to densification of the matrix, which is consistent with the slight increase in the compressive strength of AAAFA-NS. However, adding 6% nanosilica with slag in the binary slag system (AAS-NS) led to a minimal reduction in the total absorption depth relative to AAS, although AAS-NS showed significant improvement in compressive strength (37% increase). Adding 10% slag with fly ash in a binary system (AAFA-S) led to significant reduction in the

absorption depth (40%). This system showed the highest compressive strength among all mixtures, without the need for heat curing. Correspondingly, incorporating 6% nanosilica and 10% slag with fly ash in a ternary system (AAFA-S-NS) led to comparable results to that of the AAFA-S system.

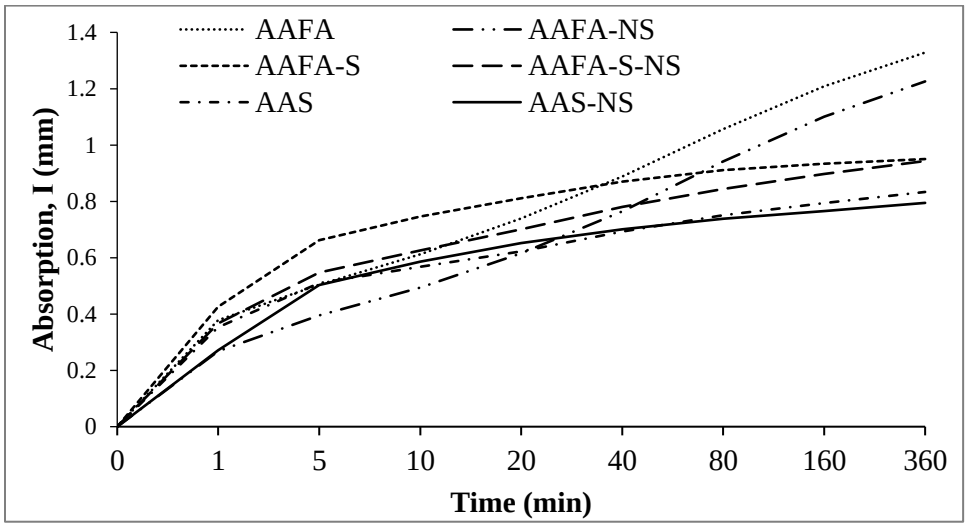

Fig. 5. 1: Absorption trends of all mixtures.

5.2 Visual Assessment

Throughout the duration of exposure (18 weeks), cubic specimens constantly immersed in the sulfuric acid solution were periodically (every 3 weeks) checked for visual assessment. All specimens from the fly ash group progressively lost parts of the exposed surface, and they eventually had uneven surfaces without change of color representing moderate deterioration at the end of exposure (**Fig. 5.2a**). The level of deterioration among specimens from the single binder (AAFA) and other blended binders (e.g. AAFA-NS, AAFA-S and AAFA-S-NS) was not visually distinguishable. On the other hand, since the start of exposure, progressive precipitation of soft whitish to yellowish layer (identified as gypsum by XRD) was observed on the surface of all specimens from the slag group and deposited in the bottom of containers, without distinctive

differences among specimens from the single or blended binders (**Fig. 5.2b**). These specimens also showed notable swelling.

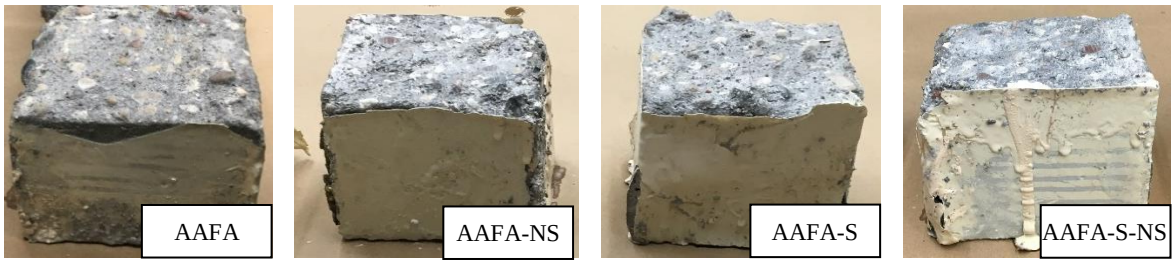

(a)

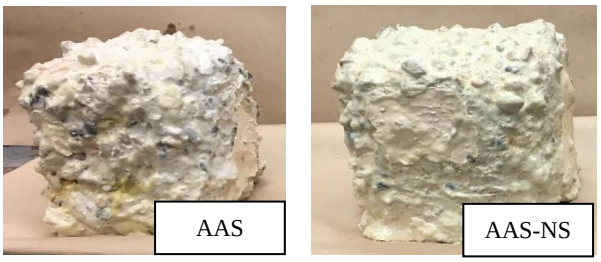

(b)

Fig. 5. 2*:* Appearance of concrete specimens after 18 weeks of immersion in 10% sulfuric acid: (a) fly ash based AAMs, and b) slag based AAMs

For the slabs exposed to the cyclic exposure combined with sulfuric acid solution, all the slabs from different mixtures experienced surface softening and scaling. At the end of the combined exposure, all the slabs were left to dry in laboratory conditions (20°C and 50% RH) followed by removing the loose materials from each slab using a nylon brush and recording their masses. It was notable that the deterioration was significant relative to that resulting from the continuous immersion of cubes in the acid solution. After removing the soft layer, the remaining concrete was intact, but the coarse aggregate appeared on the surface of all slabs as a consequence of surface scaling (e.g. **Fig. 5.3**). However, the visual assessment method could not distinctively capture the variable performance among the concrete mixtures after the combined exposure, and

thus it was complemented with physico-mechanical indicators reflecting the relative amount of scaled off material from each specimen and bond strength to parent concrete.

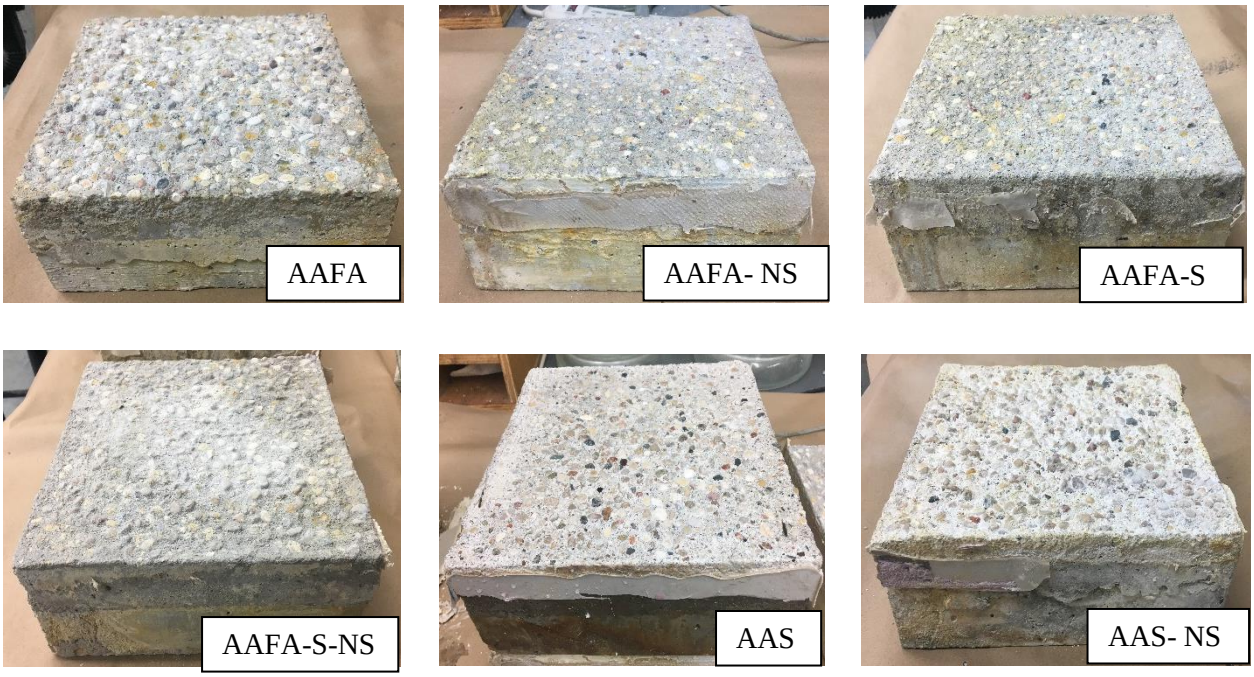

Fig. 5. 3: Degradation of slabs at the end of the cyclic exposure with the sulfuric acid.

5.3 Neutralization Depth

The neutralization depth gives a measure of the penetration depth of H^+ ions in concrete specimens, reflecting the loss of alkalinity due to acidic attack. In the fly ash and slag AAMs, the source of high alkalinity might originate from the sodium hydroxide and sodium silicate solutions (alkaline activators). For the full immersion exposure, the neutralization depth was determined periodically (every three weeks); specimens from different mixtures were cut across the middle and 1% phenolphthalein solution was sprayed on the freshly cut surfaces. The average depth of neutralization was measured from surface of colourless portion towards the magenta color front. **Fig. 5.4** shows the progress of the neutralisation depth in specimens with time. For the AAFA specimens, the neutralization depth increased rapidly with time, and the specimens were fully neutralized after nine weeks of exposure (**Figs. 5.4** and **5.5**). This trend was consistent with the

absorption test results (**Fig. 5.1**), since such mixture had porous microstructure. However, incorporating 6% nanosilica in the binary system (AAFA-NS) led to significant reduction in the neutralization depth by 55% (average 45 mm) relative to the AAFA mixture at the end of the exposure (**Fig. 5.4**). Also, specimens produced by adding 10% slag in the binary (AAFA-S) or ternary (AAFA-S-NS) systems with nanosilica comparably exhibited very low neutralization depths with an average of 20 mm, which was 80% lower than that of the AAFA specimens. Generally, the rate of increasing the neutralization depth for most of these specimens declined after 6 weeks, and became nil afterwards. These results suggest that the inclusion of nanosilica and/or slag might discount the transport properties of fly ash based AAMs and hence reducing the ingress of acidic solution into the specimens. The precipitation of reaction products or filler particles within the reaction zone might have led to this protection mechanism, as will be discussed in the microstructure section. On the other hand, binders from the slag group exhibited the lowest neutralization depths (average of 5 to 10 mm, throughout the entire exposure) relative to that from the fly ash group, without distinctive differences between the single and blended mixtures (AAS and AAS-NS). However, it should be noted that the reaction products (gypsum) were not periodically removed from the exposed surface of specimens in the full immersion exposure, which have contributed to this blocking behaviour.

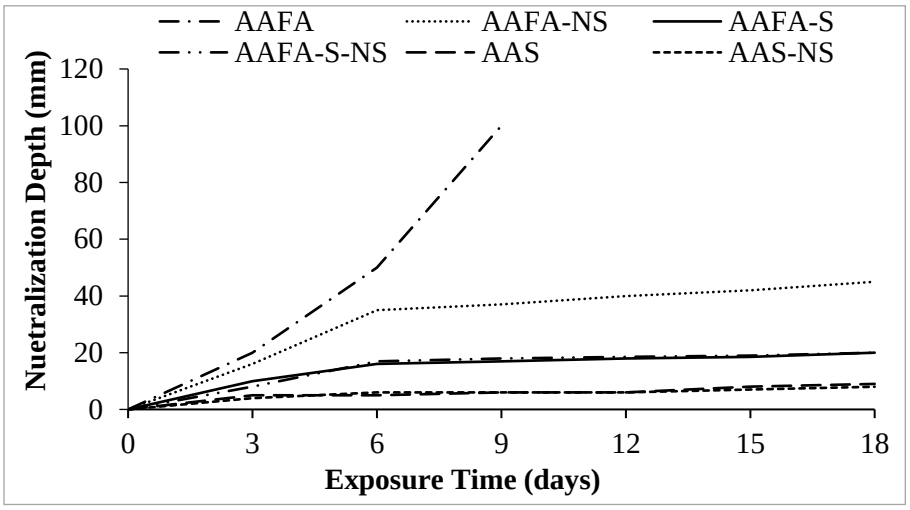

Fig. 5. 4: Neutralization depth versus time for the specimens in the full immersion exposure.

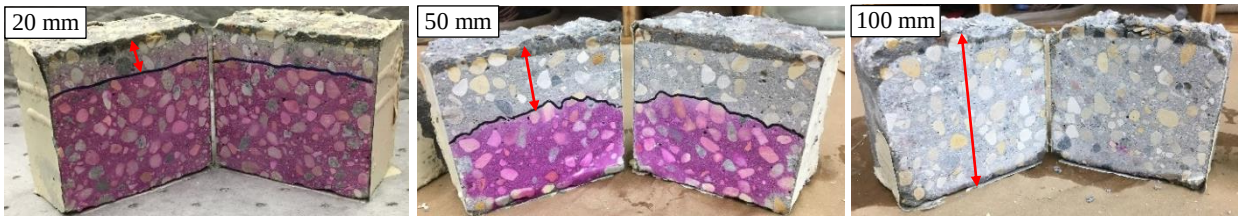

3 weeks 6 weeks 9 weeks

Fig. 5. 5: Progressive neutralization depth of specimens from the AAFA mixture at different ages in the full immersion exposure.

5.4 Mass Loss and Pull-off Test

The surface scaling of specimens was assessed by the mass loss of slabs per unit area at the end of the combined exposure as shown in **Fig. 5.6**. In general, the slabs from the slag group had higher mass losses relative to that from the fly ash group conforming to the visual assessment trends. Specimens from the single binder (AAFA) experienced the highest mass loss (900 g/m^2) compared to other specimens in the fly ash group. Adding nanosilica in the binary system (AAFA-NS) led to 11% reduction of mass loss compared to the AAFA slabs. Concrete specimens made from the binary (AAFA-S) and ternary (AAFA-S-NS) yielded lower mass losses, with an average reduction of 33% relative to the AAFA specimens. These trends were consistent with the neutralization depth results. For instance, concrete specimens AAFA-S and AAFA-S-NS had low neutralization depths

in the full immersion exposure and low mass losses in the combined exposure. Conversely, the slag based AAMs (AAS and AAS-NS), which had the lowest neutralization depths in the full immersion exposure, showed higher mass losses (average of 1000 g/m^2) in the combined exposure. It appears that the cyclic environmental actions (W/D, F/T and alternating cycles) in the combined exposure effectively washed away the gypsum residue precipitating on the surface of slag based specimens, which discounted the blocking effect observed in the full immersion exposure and made them vulnerable to further damage.

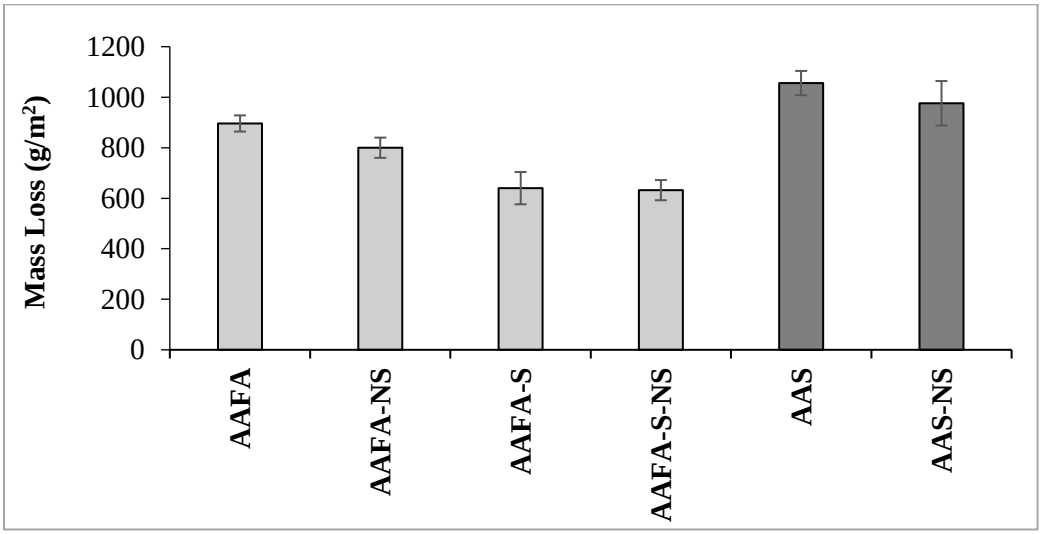

Fig. 5. 6: Mass loss of the fly ash and slag AAMs at the end of the combined exposure.

The pull-off test was used to evaluate the bond strength of the repair mixtures with substrate concrete before and after the combined exposure. It should be noted that the pull-off test represents an extreme loading configuration, by subjecting the deteriorating specimens to direct tensile stresses. The average bond strength values relative to substrate (parent) before and after the combined exposure are shown in **Fig. 5.7**. Generally, the average bond strength of all mixtures increased after the combined exposure, except for AAFA specimens. The bond strength of the AAFA specimens decreased significantly by approximately 50% after the combined exposure,

relative to the initial values at 28 days (1 MPa). The failure of these specimens occurred mainly at the repair material or the interface with the substrate concrete. This corresponded to the trends of the absorption and the neutralization depth in the sense that the high porosity of the AAFA mixtures (**Fig. 5.1**) led to a rapid ingress of the acid solution into the repair layer as expressed by the rapid/full neutralization of similar specimens (**Fig. 5.4** and **5.5**), which likely caused weakening of the interface surface and consequently low bond strength. Compared to AAFA, the bond strength for AAFA-NS, AAFA-S and AAFA-S-NS mixtures at 28 days exhibited increase by 35, 40 and 45% respectively; and it significantly increased by 68, 78 and 85%, respectively after the combined exposure, alluding to the continual reactivity of these binders. The presence of nanosilica and/or slag likely contributed to the geopolymerization reaction of fly ash (as confirmed by XRD analysis), and consequently improved the bond at the interface with substrate concrete since early age. For the slag group mixtures, their bond strengths before and after exposure were comparable. Also, incorporating nanosilica with slag in AAS-NS did not improve the bonding behaviour with the substrate concrete as observed in the fly ash group. The failure of these mixtures (AAS and AAS-NS) was mainly in the repair zone after the combined exposure, reflecting high level of deterioration with time. The trends of specimens from slag group were consistent with the high mass loss results in **Fig. 5.6**.

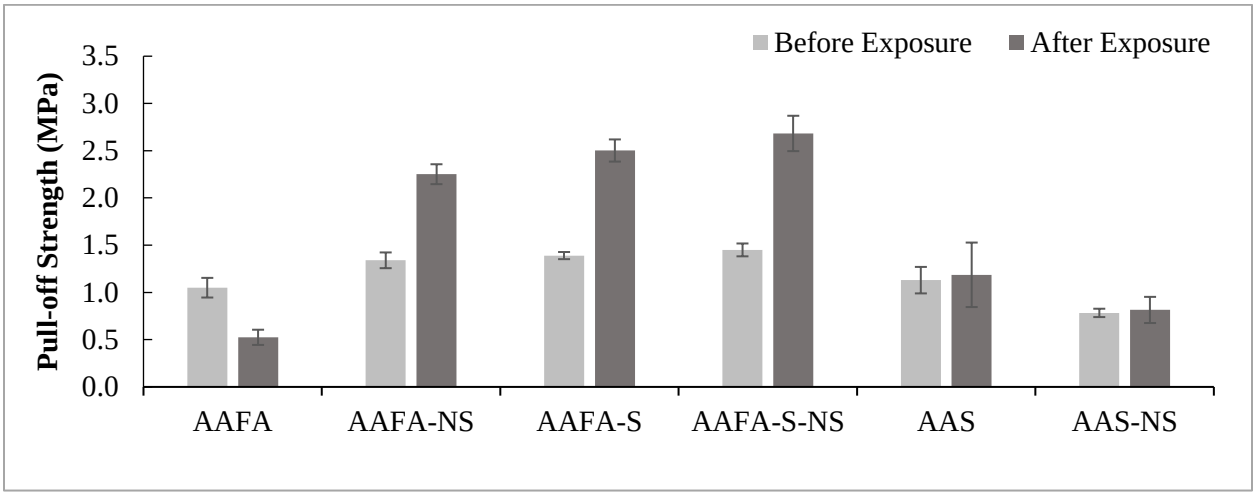

Fig. 5. 7: Bond strength of the repair assembly from the pull-off test.

.5 Discussion

The analysis of phase composition and microstructure were carried out by XRD, DSC and SEM. The XRD patterns of all mixtures at 28 days (before the acidic exposures) are presented in **Fig. 5.8a**. For the AAFA samples, the main crystalline phases present were quartz, mullite, calcite and dolomite. The peaks of quartz and mullite were from the mineralogical composition of fly ash as well as the siliceous coarse aggregate and sand used in all mixtures, while the dolomite and calcite likely occurred because the coarse aggregate contained a fraction of carboniferous aggregate. The main phase from the alkali activation of fly ash (geopolymerisation reaction) was microcrystalline sodium aluminosilicate hydrate gel (also known as N-A-S-H) identified by the broad hump (between 2θ of 20^{o} and 30^{o}) beneath the diffraction peaks of the crystalline phases, along with the formation of crystalline traces of zeolite-like phases centred around 28^{o}. Although the chemical composition of fly ash used herein included approximately 11% CaO, no portlandite peaks were observed in the XRD diffractograms of fly ash based AMMS. Oh et.al. (2010) attributed that to the possibility of a low degree of dissolution of calcium in fly ash, which seemed to remain unreacted after curing. The XRD pattern of AAFA-NS consisted mainly of amorphous sodium aluminosilicate hydrate gel products with a broader hump accompanied by a slight increase in the

intensity of zeolite peaks relative to AAFA. Besides its phylical filling effect, this implies that nanosilica accelerated/improved the geopolymerization reaction and hence led to reduction in absorption (**Fig. 5.1**) and increase in compressive strength (**Table 3.4**).

The XRD pattern of AAFA-S showed a shift in the amorphous hump compared to that of AAFA and AAFA-NS, indicating the formation of C–S–H like gel due to the presence of Ca^{2+} from slag giving crystallinity in C–S–H type gel centered at 2θ of 29.5° and overlapping with calcite. In addition, crystalline zeolitic products with structures resembling zeolite P1-Na similar to AAFA and AAFA-NS were identified along with the aluminosilicate gel phase. C-S-H phases formed due to the 10% substitution of fly ash with slag had a Ca/(Si+Al) ratio of 0.6, which was designated as C-A-S-H in the XRD pattern. Puligilla and Mondal (2013) reported that the availability of free calcium ions in the fly ash/slag blends may promote fly ash dissolution and geopolymer formation. It seems that this hybrid binding system led to a denser matrix, and consequently marked decrease in the total absorption and increase in compressive strength relative to AAFA and AAFA-NS. Accordingly, AAFA-S-NS showed similar XRD trends to that of AAS-S. Alkali activation of slag led to a denser matrix relative to fly ash AAMs as reflected by the lower absorption trends (**Fig. 5.1**). For the slag AAMs, the main reaction product from the alkali activation of slag was indicated by the broad hump between 2θ of 25–35°, resembling the diffraction pattern of a poorly crystalline phase of calcium silicate hydrate (C–S–H) with a riversideite type structure (Ismail et al, 2013). Also, peaks of portlandite were observed, due to the latent hydraulic reaction of slag. Incorporating nanosilica with slag in AAS-NS led to disappearance of the portlandite phases, due to the vigorous pozzolonic activity of nanosilica at early-age (Khater et al., 2012).

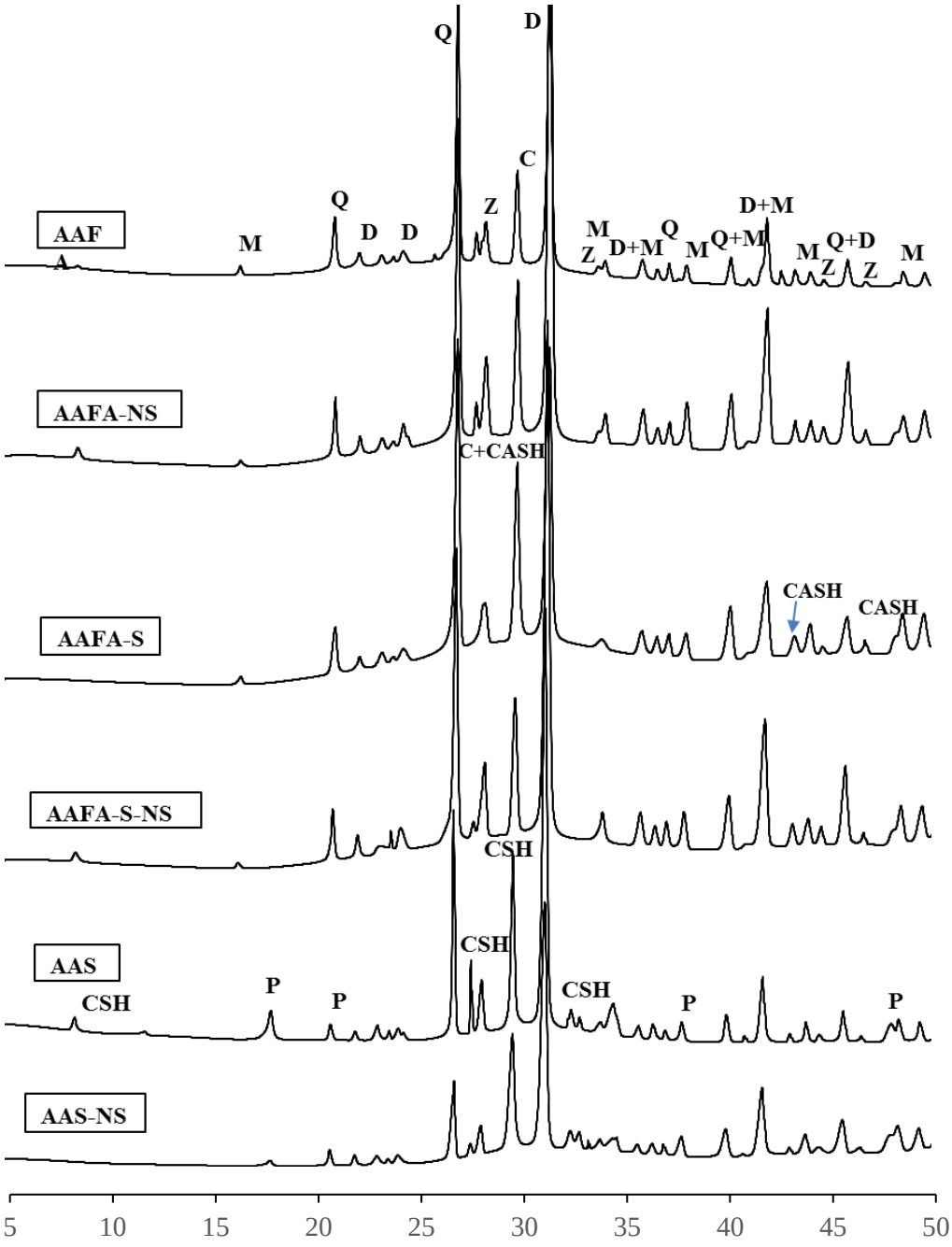

Fig. 5. 8: XRD patterns of specimens from different mixtures before exposure. (CSH: calcium silicate hydrate; Z: zeolite; CASH: calcium aluminate silicate hydrate; G: gypsum; P: portlandite; Q: quartz; D: dolomite; C: calcite; M: mullite)

The XRD patterns for specimens exposed to the combined acidic (aggravated) exposure are shown in **Fig. 5.9**, and the trends were corroborated by SEM DSC and analyses. From **Fig. 5.9**, it can be noted that gypsum were identified in all samples. The main source of gypsum was the

reaction of sulfuric acid with Ca^{+} ions originating from fly ash and/or slag systems. Also, it was noted that zeolite peaks decreased or diminished; correspondingly, the peaks of quartz and mullite reduced suggesting the dissolution of these crystalline phases. Complying with the neutralization depth trends, the SEM analysis showed that the AAFA system exhibited a porous and disintegrated matrix (**Fig. 5.10a**), with incidental occurrence of gypsum crystals. For the AAFA-NS, AAFA-S and AAFA-S-NS specimens, the matrix appeared denser (e.g. **Fig. 5.10b**) than that of the AAFA due the additional formation of geopolymer gel and/or C-A-S-H gel. For the slag group, gypsum was identified as the key reaction product with corresponding depletion of portlandite peaks and decalcification of C–S–H. There was a reduction in the intensity of the amorphous hump associated with disordered C–S–H type gels, suggesting the dissolution of the main binding phase in the material during the acidic exposure to sulfuric acid. SEM analysis of slag AAMs showed that the matrix was denser than that of fly ash AAMs; however, abundant cracks and fishers propagated into the sound paste which facilitating direct ingress of the solution, resulting in significant level of deterioration (**Fig. 5.11a)**. The reaction zone consisted mainly of a variety of small and large gypsum crystals in a deteriorated matrix (**Fig. 5.11b**).

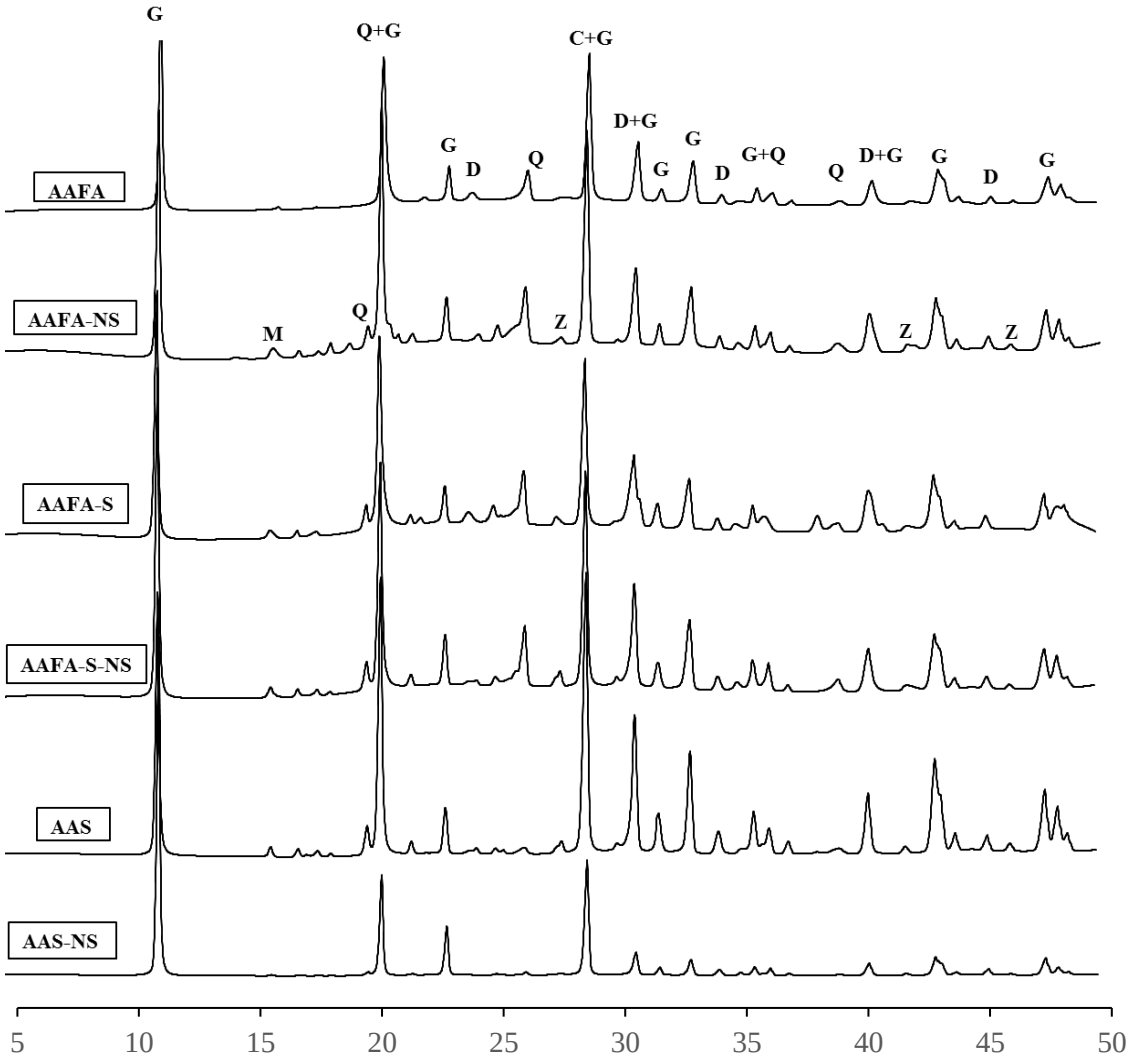

Fig. 5. 9: XRD patterns of specimens from different mixtures after the combined exposure. (Z: zeolite; M: mullite, G: gypsum; P: portlandite; Q: quartz; D: dolomite; C: calcite)

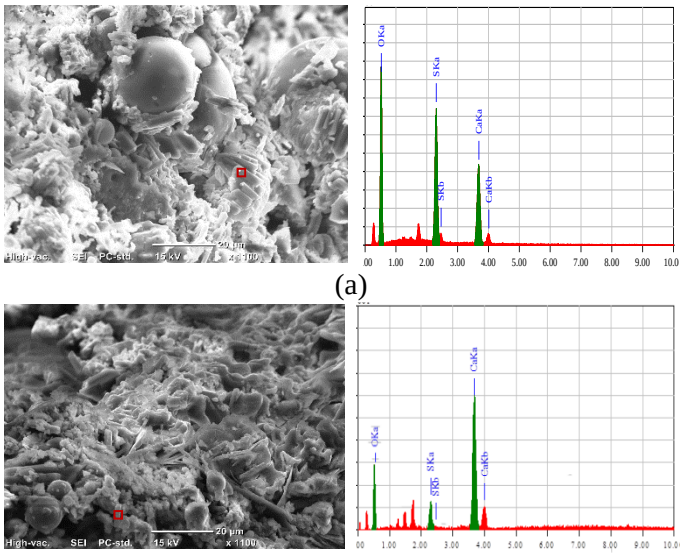

Fig. 5. 10: SEM images with EDX of deteriorated surface showing gypsum formation in the reaction zone (left) with corresponding EDX (right) after the combined exposure: (a) AAFA, and (b) AAFA-S

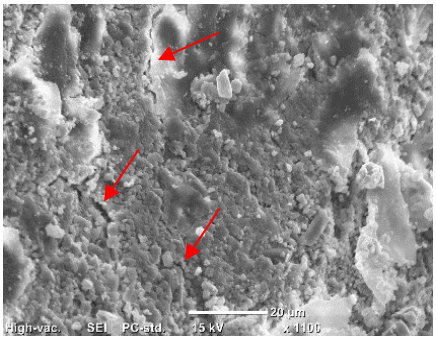

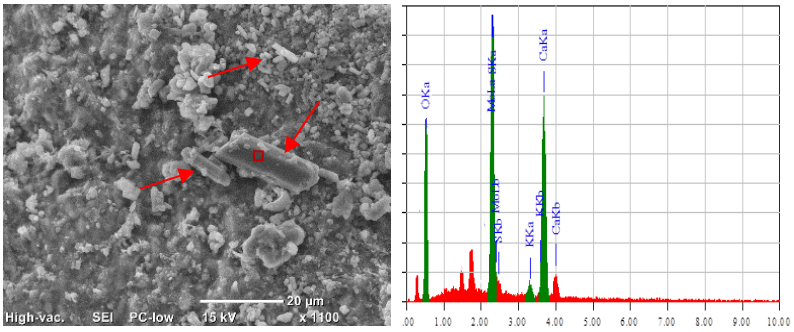

Fig. 5. 11: SEM and EDX analyses for AAS specimen showing: (a) cracks extending into the inner core, (b) small and large gypsum crystals in the reaction zone (left) with corresponding EDX (right).

In order to quantify the relative phase formation of gypsum among the different mixtures, DSC was used to determine the enthalpy (integration of the area contained by the flow curves) as depicted in **Fig. 5.12**. It can be noted that AAFA-NS, AAFA-S and AAFA-S-NS specimens showed lower gypsum formation relative to AAFA specimens. This might be attributed to the densification of the microstructure through blocking the pores or adding new binding gel as a result of incorporating nanosilica and/or slag, which led to reducing the penetrability, as reflected by the lower absorption and neutralization depth trends. On the other hand, the amounts of gypsum formed in specimens from the slag group were approximately three times that of specimens from the fly ash group, implying higher level and different mode of deterioration in these mixtures, in compliance with the mass loss results.

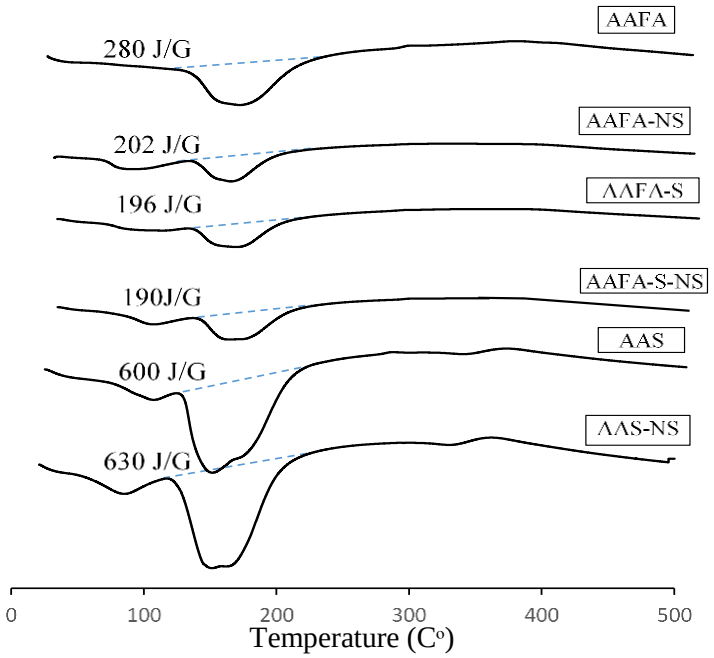

Fig. 5. 12: DSC curves of all mixtures showing quantities of gypsum formed after the combined exposure.

For the fly ash group, the reduction of the quartz and mullite peaks after the acidic exposure might be ascribed to the condensation of amorphous gel enriched with silicon on the surfaces of quartz and mullite as a result of the reaction of geopolymerization gel with sulfuric acid resulting in depolymerised gel (Bakharev, 2005b), thereby masking the XRD reflections. It is worth noting that this insoluble gel may contribute to the mass of the specimen after acidic attack, resulting in misleading conclusions on the performance of specimens, if mass change was used as the fundamental/sole criterion of assessment, especially in full immersion set-ups. For the AAFA specimens, it seems that this depolymerised gel did not provide a protective effect against further ingression of the acidic solution, as the neutralization depth increased markedly with time in the AAFA specimens (**Fig. 5.3** and **5.4**), which may be ascribed to the dominantly higher initial penetrability of this system (**Fig. 5.1**). Consequently, the ingress of further acid ions was observed and the bulk core experienced depolymerisation and loss mass and bonding with substrate concrete in the combined exposure (**Figs. 5.6-5.7**). These trends do not comply with that of reported by previous studies (e.g. Bakharev, 2005b; Song, 2005; Sata et al., 2012; Aliques-Granero et al., 2017; Mehta and Siddique, 2017) about the high durability of fly ash or slag AAMs to acids, as most of these studies were mainly based on recording the mass change over time during full immersion exposures. Adopting a normal temperature curing regime herein, compared to heat curing in most of the previous studies, produced systems with relatively higher porosity as heat curing can increase the rate of the geopolymerization process for AAMs. However, heat curing might not be feasible for AAMs in the repair field applications targeted in the current study.

Modifying fly ash based AAMs with nanosilica and/or slag (AAFA-NS, AAFA-S, AAFA-S-NS) led to significant improvement in the acidic exposures, without the need for heat curing. This was substantiated by the lower neutralization depth (**Fig. 5.5**) and mass loss of these systems

(**Fig. 5.6**) compared to AAFA, as well as the increase of bonding with substrate concrete after the combined exposure. This alludes to the potential success of these mixtures in repair applications of concrete elements serving in similar acidic environments. The effect of nanosilica was mainly ascribed to the particle packing/filler effects and enhancing the geopolymerization process, resulting in denser microstructure. This led to reducing the penetrability relative to the AAFA systems (**Fig. 5.1**), and consequently the neutralization depth decreased. The systems incorporating slag (AAFA-S) showed better performance than that with nanosilica as the presence of C-A-S-H gel phase along with the main geopolymerization gel, reduced the penetrability markedly (**Fig. 5.1).** Ismail et al. (2014) reported that the presence of low slag content in fly ash systems resulted in delaying the formation of C-A-S-H gel compared with higher slag substitution, leading to a higher degree of local structural ordering of this gel. Hence, the C-A-S-H gel resulted from low substitution of fly ash by slag might be relatively stable in acidic solutions, which contributed to improving the performance of AAFA-S and AAFA-S-NS herein.

When the fly ash was fully replaced with slag in the AAS and AAS-NS systems, an expansive corrosion product (gypsum) was a dominant feature in the specimens (**Fig. 11b**). The large amounts of gypsum formed in these systems (**Fig. 5.12**) suggested the contribution of portlandite and decalcification of C–S–H to the acid-base reactions. For AAS-NS there was some increase in the amounts of gypsum in this system, which was attributed to the increased volume of cementitious gel (due to the pozzolonic activity of nanosilica) vulnerable to decomposition in severely aggressive acidic media in a manner similar to blended portland cements incorporating high volume of supplementary cementitious materials (Amin and Bassuoni, 2017). In addition to the excessive gypsum precipitation in the confined pore space, the cracks observed in these systems might be ascribed to drying shrinkage. Many studies reported that slag based AAMs suffer

from drying shrinkage which causes micro-cracks in the matrix (Ye and Radlińska, 2016; Collins and Sanjayan, 1999; Neto et al, 2010). Likely these cracks were significant in the slabs exposed to the combined exposure, especially the drying cycles. Also, the nanosilica might have contributed to increasing the shrinkage effect (Ghazy and Bassuoni, 2017) in AAS-NS. Consequently, higher intensity of cracks may ease the acid ingress in the system, especially when the gypsum residue was constantly washed away in the combined exposure. Therefore, the repair zone made from AAS and AAS-NS was extremely vulnerable to loss of mass, expansion and softening, with pull-off failure mainly occurring in the repair zone.

Chapter 6: Summary, Conclusions and Recommendations

6.1. Summary

In this thesis, two experimental studies were conducted. The first one aimed at developing a test protocol for assessing the resistance of concrete to acidic attack, based on incremental levels of damage. Also, the physical and the chemical responses of different types of concrete made with general use or portland limestone cement [PLC] without or with SCMs (fly ash, silica fume and nanosilica) to progressive levels of sulfuric acid attack were investigated. The second study aimed at developing innovative types of concrete based on AAMs (AAFA, AAS and their blends incorporating nanosilica) and evaluatting their resistance to different exposures of acidic attack for potential use in repair of concrete elements vulnerable to acidic attack (e.g. wastewater facilities).

6.1.1 Conclusions of Concrete Mixtures Incorporating SCMs and Nanosilica under Incremental Acidic Attack

Considering the materials, mixture designs, and incremental test protocol implemented in this study, the following conclusions can be drawn:

- The results showed that all the GU and PLC specimens exposed to continuous immersion in the mild acidic environment (Phase I) remained intact without visible features of damage. However, during Phases II and III, progressive precipitation of gypsum was observed and the damage of specimens was sharply escalated. Phase III (very severe acidic exposure) gave the clearest distinction among the performance of concrete mixtures, as expressed by surface degradation and mass loss results.

- The relationship between the penetrability of specimens and their cumulative mass losses after Phases II and III was mixed and discordant. In Phase II, mixtures from blended binders with lower penetration depths (e.g. GUFSF, PLCFSF) had comparable mass losses to the control specimens from single binders. Also, some concrete mixtures (e.g. GUFSFNS and PLCFSFNS) with very low penetration depths exhibited the highest mass losses after Phase III, while others (e.g. GUF and PLCF) with higher penetration depths yielded the lowest mass losses. This shows that the notion adopted by building codes to improve the acidic resistance of concrete mainly by discounting its physical penetrability should be reconsidered.

- Specimens from the PLC group had lower mass losses (average of 24% and 15% reduction after Phases II and III, respectively) than that of corresponding specimens from the GU group due to the neutralization effect offered by the limestone component (chemical resistance).

- During Phase II (severe acidic attack), only systems with nanosilica, particularly in the GU group, led to relative improvement of the acidic resistance of concrete compared to control specimens; however, no such improvement was achieved for blended binary or ternary binders comprising silica fume and fly ash. This was ascribed to the further refinement of pore structure in systems containing nanosilica as gypsum formation, which can cause crystallization pressure and thus damage, tended to precipitate faster in coarser pore structures (systems with other SCMs).

- During Phase III (very severe acidic attack), the quaternary binders (GUFSFNS and PLCFSFNS) experienced the highest mass losses of 30-34%, signifying the dominance of

chemical vulnerability of binders at this stage, irrespective of the physical features of pore structure (physical resistance). This was due to the increased volume of cementitious gel exposed to deterioration in the sulfuric acid solution at this stage, as indicated by the increased gypsum formation in these specimens. Comparatively, GUF and PLCF binders exhibited the lowest mass losses due to occurrence fly ash particles within the surface of concrete, which acted as inert filler limiting the surface of paste susceptible to the acid-base reaction.

6.1.2. Conclusions of Concrete with AAMs under Different Acidic Exposures

Considering the materials, mixture designs, and acidic exposures implemented in this study, the following conclusions can be drawn:

- Visual assessment showed that all specimens from the fly ash group exposed to continuous immersion in a very severe acidic solution underwent moderate deterioration without distinguishable features among mixtures. Comparatively, specimens from the slag group experienced progressive precipitation of gypsum (blocking effect) on the surface with notable swelling.
- All slabs from the fly ash and slag groups exposed to the cyclic environments combined with sulfuric acid solution showed significant deterioration (surface softening and scaling), reflecting the high level of aggressing of this exposure.
- The results showed that the inclusion of nanosilica and/or slag discounted the transport properties of fly ash based AAMs, as expressed by lower absorption capacity. Accordingly, the neutralization depths for blended mixtures incorporating nanosilica and/or slag decreased relative to AAFA specimens, which had rapid/full neutralization depth. On the

other hand, specimens from the slag group exhibited the lowest absorption capacity and neutralization depths relative to that from the fly ash group, because of the blocking effect and lower initial absorption.

- Complying with the neutralization depth results, the mass loss results for the fly ash AAMs comprising slag and/or nanosilica (AAFA-S and AAFA-S-NS) showed lower mass loss compared to AAFA specimens in the combined exposure due to the lower penetrability and chemical stability of the geopolymerization products. Conversely, specimens from the slag group showed higher mass loss in the combined exposure, due to the continual wash out of the gypsum residue with cyclic environments and chemical vulnerability of their matrices to acidic deterioration.

- In comparison to AAFA, the pull-off test results showed that the bond strength of the AAFA-NS, AAFA-S, AAFA-S-NS increased after the combined exposure, due to the limited penetrability of the acid in the repair zone and continual geopolymerization activity at the interface with substrate concrete. Failure of specimens from slag group was mainly in the repair zone reflecting higher level of deterioration with time.

The overall results from this study suggest that fly ash based AAMs comprising slag and/or nanosilica, without heat curing after placement, are potentially a viable option for repair applications of concrete elements serving in acidic environments. Yet, field trials are still needed to document their performance, which is recommended for future research.

6.2 Recommendations for Future Work

The results and discussion presented in this thesis provide many useful insights for the extension of this research work. The following are recommendations for further investigations:

- Repeating the same incremental sulfuric acid exposure on mixtures composed of fly ash with different substitutions of slag and nanoparticles.
- Investigating the effect of different acidic concentrations and environmental conditions on the mechanisms of deterioration using similar mixtures.
- Calculating the diffusion coefficients of acidic solutions in alkali activated fly ash or slag based systems.
- Performing a field trial for the repair of concrete elements affected by acidic attack using AAMs incorporating fly ash and slag without and with nanosilica and monitoring its performance.

References

ACI 201.2R. (2016). Guide to durable concrete. Report by ACI Committee 201, MI. *American Concrete Institute*, Farmington Hills, USA.

ACI 515.1R. (1985). Guide to the use of waterproofing, damp proofing, protective, and decorative barrier systems for concrete. Report by ACI Committee 515, MI. *American Concrete Institute*, Farmington Hills, USA.

Adak, D., Sarkar, M., and Mandal, S. (2014). Effect of nano-silica on strength and durability of fly ash based geopolymer mortar. *Construction and Building Materials*, 70, 453-459.

Adam, A. (2009). Strength and durability properties of alkali activated slag and fly ash-based geopolymer concrete, Environment and Chemical Engineering. *RMIT University*, Melbourne, Australia.

Al Bakri Abdullah, M. M., Kamarudin, H., Khairul Nizar, I., Bnhussain, M., Zarina, Y., and Rafiza, A. R. (2012). Correlation between Na2SiO3/NaOH ratio and fly ash/alkaline activator ratio to the strength of geopolymer. *Advanced Materials Research*, 341, 189-193.

Alexander M, Bertron A, De Belie N. (2013) Performance of cement-based materials in aggressive aqueous environments. *RILEM TC 211-PAE. Springer*, Berlin

Alexander MG, and Fourie C. (2011). Performance of sewer pipe concrete mixtures with Portland and calcium aluminate cements subject to mineral and biogenic acid attack. *Materials and Structures*, 44(1), 313–30.

Aliques-Granero, J., Tognonvi, T. M., and Tagnit-Hamou, A. (2017). Durability test methods and their application to AAMs: case of sulfuric-acid resistance. *Materials and Structures*, 50(1), 36.

Al-Otaibi, S. (2008). Durability of concrete incorporating GGBS activated by water-glass. *Construction and Building Materials*, 22(10), 2059-2067.

Amin, M., and Bassuoni, M. T. (2017). Response of concrete with blended binders and nanoparticles to sulfuric acid attack. *Magazine of Concrete Research*, 1-16.

Al-Tamimi, A. K., and Sonebi, M. (2003). Assessment of self-compacting concrete immersed in acidic solutions. *Journal of Materials in Civil Engineering*, 15(4), 354-357.

Andrews-Phaedonos, F. (2014). Specification and use of geopolymer concrete. *Austroads Bridge Conference*, 9th, Sydney, New South Wales, Australia (No. 6.2).

ASTM C192-16. (2016). Standard Practice for Making and Curing Concrete Test Specimens in The Laboratory, Annual Book of ASTM Standards. *ASTM International*, West Conshohocken, PA, USA,

ASTM C1157 / C1157M. (2017). Standard Performance Specification for Hydraulic Cement. *ASTM International*, West Conshohocken, PA, USA.

ASTM C1202. (2015). Standard Test Method for Electrical Indication of Concrete's Ability to Resist Chloride Ion Penetration. *ASTM International*, West Conshohocken, PA, USA.

ASTM C267. (2012). Standard test methods for chemical resistance of mortars, grouts, and monolithic surfacings and polymer concretes. *ASTM International*, West Conshohocken, PA, USA.

ASTM C309. (2012). Standard Specification for Liquid Membrane-Forming Compounds for Curing Concrete. *ASTM International*, West Conshohocken, PA, USA.

ASTM C39. (2016). Standard Test Method for Compressive Strength of Cylindrical Concrete Specimens. *ASTM International*, West Conshohocken, PA, USA.

ASTM C494. (2016). Standard Specification for Chemical Admixtures for Concrete. *ASTM International*, West Conshohocken, PA, USA.

ASTM C496. (2011). Standard Sest Method for Splitting Tensile Strength of Cylindrical Concrete Specimens. *ASTM International*, West Conshohocken, PA, USA.

ASTM C666. (2015). Standard test method for resistance of concrete to rapid freezing and thawing. *ASTM International*, West Conshohocken, PA, USA.

Aydın, S., and Baradan, B. (2013). The effect of fiber properties on high performance alkali-activated slag/silica fume mortars. *Composites Part B: Engineering*, *45*(1), 63-69.

Azam, F., and Malfatti, F. (2007). Microbial structuring of marine ecosystems. *Nature Reviews Microbiology*, 5(10), 782.

Bakharev, T. (2005a). Geopolymeric materials prepared using Class F fly ash and elevated temperature curing. *Cement and Concrete Research*, 35(6), 1224-1232.

Bakharev, T. (2005b). Resistance of geopolymer materials to acid attack. *Cement and Concrete Research*, 35(4), 658-670.

Bakharev, T., Sanjayan, J. G., and Cheng, Y. B. (1999). Alkali activation of Australian slag cements. *Cement and Concrete Research*, 29(1), 113-120.

Bakharev, T., Sanjayan, J. G., and Cheng, Y. B. (2000). Effect of admixtures on properties of alkali-activated slag concrete. *Cement and Concrete Research*, 30(9), 1367-1374.

Bakharev, T., Sanjayan, J. G., and Cheng, Y. B. (2001). Resistance of alkali-activated slag concrete to carbonation. *Cement and Concrete Research*, 31(9), 1277-1283.

Bakharev, T., Sanjayan, J. G., and Cheng, Y. B. (2002). Sulfate attack on alkali-activated slag concrete. *Cement and Concrete Research*, 32(2), 211-216.

Bakharev, T., Sanjayan, J. G., and Cheng, Y. B. (2003). Resistance of alkali-activated slag concrete to acid attack. *Cement and Concrete Research*, 33(10), 1607-1611.

Bassuoni, M. T., and Nehdi, M. L. (2007). Resistance of self-consolidating concrete to sulfuric acid attack with consecutive pH reduction. *Cement and Concrete Research*, 37(7), 1070-1084.

Bassuoni, M. T., Nehdi, M. L., and Greenough, T. (2006). Enhancing the reliability of evaluating chloride ingress in concrete using the ASTM C 1202 rapid chloride penetrability test. *Journal of ASTM International*, 3, 13 p.

Bassuoni, M. T., Nehdi, M., and Amin, M. (2007). Self-compacting concrete: using limestone to resist sulfuric acid. *Proceedings of the Institution of Civil Engineers-Construction Materials*, 160(3), 113-123.

Bastidas, D. M., Fernández-Jiménez, A., Palomo, A., and González, J. A. (2008). A study on the passive state stability of steel embedded in activated fly ash mortars. *Corrosion Science*, 50(4), 1058-1065.

Beddoe, R. E. (2016). Modelling acid attack on concrete: Part II. A computer model. *Cement and Concrete Research*, 88, 20-35.

Beddoe, R. E., and Dorner, H. W. (2005). Modelling acid attack on concrete: Part I. The essential mechanisms. *Cement and Concrete Research*, 35(12), 2333-2339..

Bertron, A., Escadeillas, G., and Duchesne, J. (2004). Cement pastes alteration by liquid manure organic acids: chemical and mineralogical characterization. *Cement and Concrete Research*, 34(10), 1823-1835.

BRE Special Digest-1. (2005). Concrete in aggressive ground, *Building Research Establishment (BRE)*, Watford, UK. Publisher: HIS Rapidoc, Willoughby, Bracknall, Berks, UK.

Brough, A. R., and Atkinson, A. (2002). Sodium silicate-based, alkali-activated slag mortars: Part I. Strength, hydration and microstructure. *Cement and Concrete Research*, 32(6), 865-879.

BSI PAS 8820. (2016). Construction Materials. Alkali-activated Cementitious Material and Concrete Specification. *British Standards Institution*, London, UK.

BS EN 206-1. (2005). Concrete-specification. Performance, Production and Conformity. *British Standards Institution*, London, UK.

BS EN 12620. (2003). Aggregates for Concrete. *British Standards Institution*, London, UK.

BS EN 1504-10. (2003). Products and systems for the protection and repair of concrete structures. *British Standard European Norm*, London, UK.

BS EN 1504-2. (2004). Products and systems for the protection and repair of concrete structures. Definitions, requirements, quality control and evaluation of conformity. Surface protection systems for concrete. *British Standard European Norm*, London, UK.

Cartwright, C., Rajabipour, F., and Radlińska, A. (2014). Shrinkage characteristics of alkali-activated slag cements. *Journal of Materials in Civil Engineering*, 27(7), B4014007.

Chang, Z. T., Song, X. J., Munn, R., and Marosszeky, M. (2005). Using limestone aggregates and different cements for enhancing resistance of concrete to sulphuric acid attack. *Cement and Concrete Research*, 35(8), 1486-1494.

Chen, M. C., Wang, K., and Xie, L. (2013). Deterioration mechanism of cementitious materials under acid rain attack. *Engineering Failure Analysis*, 27, 272-285.

Chen, W., and Brouwers, H. J. H. (2007). The hydration of slag, part 1: reaction models for alkali-activated slag. *Journal of Materials Science*, 42(2), 428-443.

Cohen, M. D., and Mather, B. (1991). Sulfate attack on concrete: research needs. *Materials Journal*, 88(1), 62-69.

Collins, F. G., and Sanjayan, J. G. (1999). Workability and mechanical properties of alkali activated slag concrete. *Cement and Concrete Research*, 29(3), 455-458.

Collins, F., and Sanjayan, J. G. (2000). Effect of pore size distribution on drying shrinking of alkali-activated slag concrete. *Cement and Concrete Research*, 30(9), 1401-1406.

Criado, M., Palomo, A., and Fernández-Jiménez, A. (2005). Alkali activation of fly ashes. Part 1: Effect of curing conditions on the carbonation of the reaction products. *Fuel*, 84(16), 2048-2054.

CSA A23.1-14/A23.2-14. (2014). Concrete Materials and Methods of Concrete Construction/Test Methods and Standard Practices for Concrete. *Canadian Standards Association*, CSA, Mississauga, Ontario, Canada.

CSA A23.2-6B. (2014). Determination of Bond Strength of Bonded Toppings and Overlays and of Direct Tensile Strength of Concrete, Mortar, and Grout. *Canadian Standards Association*, CSA, Mississauga, Ontario, Canada.

CSA A3001-13. (2013) Cementitious Materials Compendium. *Canadian Standards Association*, CSA, Mississauga, Ontario, Canada.

CW 2160-R7. (2006). Concrete underground structures and works standard, construction specifications. City of Winnipeg, Manitoba, Canada.

Davidovits, J. (1991). Geopolymers: inorganic polymeric new materials. *Journal of Thermal Analysis and calorimetry*, 37(8), 1633-1656.

De Belie, N., Monteny, J., Beeldens, A., Vincke, E., Van Gemert, D., and Verstraete, W. (2004). Experimental research and prediction of the effect of chemical and biogenic sulfuric acid on different types of commercially produced concrete sewer pipes. *Cement and Concrete Research*, 34(12), 2223-2236.

De Vargas, A. S., Dal Molin, D. C., Vilela, A. C., Da Silva, F. J., Pavao, B., and Veit, H. (2011). The effects of Na2O/SiO2 molar ratio, curing temperature and age on compressive strength, morphology and microstructure of alkali-activated fly ash-based geopolymers. *Cement and Concrete Composites*, 33(6), 653-660.

Deb, P. S., Sarker, P. K., and Barbhuiya, S. (2015). Effects of nano-silica on the strength development of geopolymer cured at room temperature. *Construction and Building Materials*, 101, 675-683.

Deb, P. S., Sarker, P. K., and Barbhuiya, S. (2016). Sorptivity and acid resistance of ambient-cured geopolymer mortars containing nano-silica. *Cement and Concrete Composites*, 72, 235-245.

Diaz, E. I., Allouche, E. N., and Eklund, S. (2010). Factors affecting the suitability of fly ash as source material for geopolymers. *Fuel*, 89(5), 992-996.

Diercks, M., Sand, W., and Bock, E. (1991). Microbial corrosion of concrete. *Experiential*, 47(6), 514-516.

Dorner, H. (2000). Acid resistance of high performance concrete. *38th research colloquium, German Committee for Reinforced Concrete (DAfStb),* Munich, 77-86.

Dorner, H.W., and Beddoe, R. E. (2002). Prognosis of concrete corrosion due to acid attack, 9th Internat. *Conference Durability of Building Materials*, Brisbane.

Du, H., Du, S., and Liu, X. (2014). Durability performances of concrete with nano-silica. *Construction and Building Materials*, 73, 705-712.

Durning, T. A., and Hicks, M. C. (1991). Using microsilica to increase concrete's resistance to aggressive chemicals. *Concrete International*, 13(3), 42-48.

Elahi, A., Basheer, P. A. M., Nanukuttan, S. V., and Khan, Q. U. Z. (2010). Mechanical and durability properties of high performance concretes containing supplementary cementitious materials. *Construction and Building Materials*, 24(3), 292-299.

EPA. (1991). Hydrogen sulfide corrosion in wastewater collection and treatment system. EPA430/09-91-010, *Report to Congress.*

Escalante García, J. I., Fuentes, A. F., Gorokhovsky, A., Fraire Luna, P. E., and MendozaSuarez, G. (2003). Hydration products and reactivity of blast furnace slag activated by various aAlkalis. *Journal of the American Ceramic Society*, 86(12), 2148-2153.

Fan, Y. F., Hu, Z. Q., Zhang, Y. Z., and Liu, J. L. (2010). Deterioration of compressive property of concrete under simulated acid rain environment. *Construction and Building Materials*, 24(10), 1975-1983.

Fattuhi, N. I., and Hughes, B. P. (1988). The performance of cement paste and concrete subjected to sulphuric acid attack. *Cement and Concrete Research*, 18(4), 545-553.

Feret, R. (1939). Slags for the manufacture of cement. *Rev. Mater. Constr*. Tr. Publications, 1-145.

Fernández-Jiménez, A., and Palomo, A. (2005). Composition and microstructure of alkali activated fly ash binder: Effect of the activator. *Cement and Concrete Research*, 35(10), 1984-1992.

Fernández-Jiménez, A., and Puertas, F. (1997). Alkali-activated slag cements: kinetic studies. *Cement and Concrete Research*, 27(3), 359-368.

Fernández-Jiménez, A., Macphee, D. E., Lachowski, E. E., and Palomo, A. (2005). Immobilization of cesium in alkaline activated fly ash matrix. *Journal of Nuclear Mmaterials*, 346(2-3), 185-193.

Fernández-Jiménez, A., Palomo, J. G., and Puertas, F. (1999). Alkali-activated slag mortars: mechanical strength behaviour. *Cement and Concrete Research*, *29*(8), 1313-1321.

Fernández-Jiménez, A., Puertas, F., Sobrados, I., and Sanz, J. (2003). Structure of calcium silicate hydrates formed in alkaline-activated slag: influence of the type of alkaline activator. *Journal of the American Ceramic Society*, 86(8), 1389-1394.

Gao, X., Yu, Q. L., and Brouwers, H. J. H. (2015). Characterization of alkali activated slag–fly ash blends containing nano-silica. *Construction and Building Materials*, 98, 397-406.

GB/T 29423. (2012), Corrosion-resistant Products for Alkali-activated Slag Cement Fly Ash Concrete. *Standardization Administration of China*, Beijing, China.

Ghazy, A., and Bassuoni, M. T. (2017). Shrinkage of Nanomodified fly ash concrete as repair material. *ACI Materials Journal*, 144(6).

Glukhovsky, V. D., Rostovskaja, G. S., and Rumyna, G. V. (1980). High strength slag-alkaline cements. *Proceedings of the 7th international congress on the chemistry of cement, Paris*, 164-168.

Görhan, G., and Kürklü, G. (2014). The influence of the NaOH solution on the properties of the fly ash-based geopolymer mortar cured at different temperatures. *Composites Part b: Engineering*, 58, 371-377.

Gutberlet, T., Hilbig, H., and Beddoe, R. E. (2015). Acid attack on hydrated cement—Effect of mineral acids on the degradation process. *Cement and Concrete Research*, 74, 35-43.

Gutierrez-Padilla, M. G. D. (2007). Activity of Sulfur Oxidizing Microorganisms and impacts on concrete pipe corrosion. Thesis, University of Colorado at Boulder.

Hardjito, D., and Rangan, B. V. (2005). Development and properties of low-calcium fly ash-based geopolymer concrete, *Research Report GC 1*, Faculty of Engineering, Curtin University of Technology, Perth, Australia.

Hardjito, D., Wallah, S. E., Sumajouw, D. M., and Rangan, B. V. (2004). On the development of fly ash-based geopolymer concrete. *Materials Journal*, 101(6), 467-472.

Hewayde, E., Allouche, E. N., and Nakhla, G. F. (2003). Experimental investigations of the effect of selected admixtures on the resistance of concrete to sulfuric acid attack. *New Pipeline Technologies, Security, and Safety*, 504-513.

House, M., and Weiss, W. J. (2014). Review of microbially induced corrosion and comments on needs related to testing procedures. *4th International Conference on the Durability of Concrete Structures*, Purdue University, West Lafayette, IN, USA

Hughes, B. P., and Guest, J. E. (1978). Limestone and siliceous aggregate concretes subjected to sulphuric acid attack. *Magazine of Concrete Research*, 30(102), 11-18.

Ismail, I., Bernal, S. A., Provis, J. L., San Nicolas, R., Hamdan, S., and van Deventer, J. S. (2014). Modification of phase evolution in alkali-activated blast furnace slag by the incorporation of fly ash. *Cement and Concrete Composites*, 45, 125-135.

Ismail, I., Bernal, S. A., Provis, J. L., Hamdan, S., and van Deventer, J. S. (2013). Microstructural changes in alkali activated fly ash/slag geopolymers with sulfate exposure. *Materials and structures*, 46(3), 361-373.

Ivan Diaz-Loya, E., Allouche, E. N., and Vaidya, S. (2011). Mechanical Properties of Fly-Ash-Based Geopolymer Concrete. *ACI Materials Journal*, 108(3).

Jahani, F., Devinny, J., Mansfeld, F., Rosen, I. G., Sun, Z., and Wang, C. (2001). Investigations of sulfuric acid corrosion of concrete. I: modeling and chemical observations. *Journal of Environmental Engineering*, 127(7), 572-579.

Jalal, M., Mansouri, E., Sharifipour, M., and Pouladkhan, A. R. (2012). Mechanical, rheological, durability and microstructural properties of high performance self-compacting concrete containing SiO2 micro and nanoparticles. *Materials and Design*, 34, 389-400.

Kavalerova, E. S., Krivenko, P. V., and Rostovskaya, G. (2014). New National Standard of Ukraine for Heavy-weight Alkali Activated Cement Concretes. *Proceedings of the Second International Conference on Advances in Chemically-Activated Materials*, China, 449-459.

Khater, H. M., El-Sabbagh, B. A., Fanny, M., Ezzat, M., and Lottfy, M. (2012). Effect of nano-silica on alkali activated water-cooled slag geopolymer. *Proceedings of the Second International*

Conference on Microstructural-related Durability of Cementitious Composites, Amsterdam, the Netherlands, 1113.

Kim, A. G., Kazonich, G., and Dahlberg, M. (2003). Relative solubility of cations in class F fly ash. *Environmental science and technology*, 37(19), 4507-4511.

Kim, S. W., Jang, S. J., Kang, D. H., Ahn, K. L., and Yun, H. D. (2015). Mechanical properties and eco-efficiency of steel fiber reinforced alkali-activated slag concrete. *Materials*, 8(11), 7309-7321.

Krivenko, P.V., and Kovalchuk, G.Yu. (2002) Heat-Resistant Fly Ash Based Geocements. *Proceedings International Conference*, *Geopolymers*, Melbourne.

Krizan, D., and Zivanovic, B. (2002). Effects of dosage and modulus of water glass on early hydration of alkali–slag cements. *Cement and Concrete Research*, 32(8), 1181-1188.

Law, D. W., Adam, A. A., Molyneaux, T. K., and Patnaikuni, I. (2012). Durability assessment of alkali activated slag (AAS) concrete. *Materials and Structures*, 45(9), 1425-1437.

Lee, N. K., and Lee, H. K. (2016). Influence of the slag content on the chloride and sulfuric acid resistances of alkali-activated fly ash/slag paste. *Cement and Concrete Composites*, 72, 168-179.

Li, D., Xu, Z., Luo, Z., Pan, Z., and Cheng, L. (2002). The activation and hydration of glassy cementitious materials. *Cement and Concrete Research*, *32*(7), 1145-1152.

Mehta, A., and Siddique, R. (2017). Sulfuric acid resistance of fly ash based geopolymer concrete. *Construction and Building Materials*, 146, 136-143.

Mehta, P. K. (1985). Studies on Chemical Resistance of Low Water/Cement Ratio Concretes," *Cement and Concrete Research*, 15(6), 969-978.

Mehta, P. K., and Monteiro, P. J. M. (2014). Concrete: Structure, Properties, and Materials, Fourth Edition, Prentice Hall, Englewoods Cliffs, NJ.

Mindess, S., Young, J. F., and Darwin, D. (2003). Concrete, 2nd Edition, Pearson Education, Old Tappan, NJ.

Monteny, J., De Belie, N., and Taerwe, L. (2003). Resistance of different types of concrete mixtures to sulfuric acid. *Materials and Structures*, 36(4), 242-249.

Monteny, J., De Belie, N., Vincke, E., Verstraete, W., and Taerwe, L. (2001). Chemical and microbiological tests to simulate sulfuric acid corrosion of polymer-modified concrete. *Cement and Concrete Research*, 31(9), 1359-1365.

Monteny, J., Vincke, E., Beeldens, A., De Belie, N., Taerwe, L., Van Gemert, D., and Verstraete, W. (2000). Chemical, microbiological, and in situ test methods for biogenic sulfuric acid corrosion of concrete. *Cement and Concrete Research*, 30(4), 623-634.

Montes, C., Islam, R., Shi, J., Kupwade-Patil, K., and Allouche, E. N. (2013). Towards a pre-cast geopolymer concrete pipe. *Pipelines 2013: Pipelines and Trenchless Construction and Renewals—A Global Perspective*, 534-542.

Nath, P., and Sarker, P. K. (2014). Effect of GGBFS on setting, workability and early strength properties of fly ash geopolymer concrete cured in ambient condition. *Construction and Building Materials*, 66, 163-171.

Nath, P., and Sarker, P. K. (2015). Use of OPC to improve setting and early strength properties of low calcium fly ash geopolymer concrete cured at room temperature. *Cement and Concrete Composites*, 55, 205-214.

Neto, A. A. M., Cincotto, M. A., and Repette, W. (2010). Mechanical properties, drying and autogenous shrinkage of blast furnace slag activated with hydrated lime and gypsum. *Cement and Concrete Composites*, 32(4), 312-318.

NF P18-301. (1983). Granulats Naturels pour Bétons Hydrauliques. *French Standard*, 10 pp.

O'Connell, M., McNally, C., and Richardson, M. G. (2010). Biochemical attack on concrete in wastewater applications: A state of the art review. *Cement and Concrete Composites*, 32(7), 479-485.

Oh, J. E., Monteiro, P. J., Jun, S. S., Choi, S., and Clark, S. M. (2010). The evolution of strength and crystalline phases for alkali-activated ground blast furnace slag and fly ash-based geopolymers. *Cement and Concrete Research*, 40(2), 189-196.

Okochi, H., Kameda, H., Hasegawa, S. I., Saito, N., Kubota, K., and Igawa, M. (2000). Deterioration of concrete structures by acid deposition—an assessment of the role of rainwater on deterioration by laboratory and field exposure experiments using mortar specimens. *Atmospheric Environment*, 34(18), 2937-2945.

Pacheco-Torgal, F., Abdollahnejad, Z., Miraldo, S., Baklouti, S., and Ding, Y. (2012). An overview on the potential of geopolymers for concrete infrastructure rehabilitation. *Construction and Building Materials*, 36, 1053-1058.

Palomo, A., Alonso, S., Fernandez-Jiménez, A., Sobrados, I., and Sanz, J. (2004). Alkaline activation of fly ashes: NMR study of the reaction products. *Journal of the American Ceramic Society*, 87(6), 1141-1145.

Palomo, A., Grutzeck, M. W., and Blanco, M. T. (1999). Alkali-activated fly ashes: a cement for the future. *Cement and Concrete Research*, 29(8), 1323-1329.

Palacios, M., and Puertas, F. (2007). Effect of shrinkage-reducing admixtures on the properties of alkali-activated slag mortars and pastes. Cement and concrete research, 37(5), 691-702.

Parker, C. D. (1951). Mechanics of corrosion of concrete sewers by hydrogen sulfide. *Sewage and Industrial Wastes*, 23(12), 1477–1485.

Provis, J. L. (2014). Geopolymers and other alkali activated materials: why, how, and what? *Materials and Structures*, 47(1-2), 11-25.

Purdon, A. O. (1940). The action of alkalis on blast-furnace slag. *Journal of the Society of Chemical Industry*, 59(9), 191-202.

Puligilla, S., and Mondal, P. (2013). Role of slag in microstructural development and hardening of fly ash-slag geopolymer. *Cement and Concrete Research*, 43, 70-80.

Pye, K., and Miller, J. A. (1990). Chemical and biochemical weathering of pyritic mudrocks in a shale embankment. *Quarterly Journal of Engineering Geology and Hydrogeology*, 23(4), 365-382.

Ramezanianpour, A. M., and Hooton, R. D. (2014). A study on hydration, compressive strength, and porosity of Portland-limestone cement mixes containing SCMs. *Cement and Concrete Composites*, 51, 1-13.

Rangan, B. V., Hardjito, D., Wallah, S. E., and Sumajouw, D. M. (2005). Studies on fly ash-based geopolymer concrete. *Proceedings of the World Congress Geopolymer, Saint Quentin, France*, 28, 133-137.

Rattanasak, U., and Chindaprasirt, P. (2009). Influence of NaOH solution on the synthesis of fly ash geopolymer. *Minerals Engineering*, 22(12), 1073-1078.

Richardson MG. (2014). Fundamentals of durable reinforced concrete. London: Spon Press.

Rowles, M., and O'connor, B. (2003). Chemical optimisation of the compressive strength of aluminosilicate geopolymers synthesised by sodium silicate activation of metakaolinite. *Journal of Materials Chemistry*, 13(5), 1161-1165.

Roy, D. M. (1999). Alkali-activated cements opportunities and challenges. *Cement and Concrete Research*, 29(2), 249-254.

Roy, D. M., Arjunan, P., and Silsbee, M. R. (2001). Effect of silica fume, metakaolin, and low-calcium fly ash on chemical resistance of concrete. *Cement and Concrete Research*, 31(12), 1809-1813.

Ryu, G. S., Lee, Y. B., Koh, K. T., and Chung, Y. S. (2013). The mechanical properties of fly ash-based geopolymer concrete with alkaline activators. *Construction and Building Materials*, 47, 409-418.

Sagoe-Crentsil, K., and Weng, L. (2007). Dissolution processes, hydrolysis and condensation reactions during geopolymer synthesis: Part II. High Si/Al ratio systems. *Journal of materials science*, 42(9), 3007-3014.

Said, A. M., Zeidan, M. S., Bassuoni, M. T., and Tian, Y. (2012). Properties of Concrete Incorporating Nano-silica. Construction and Building Materials, 36, 838-844.

Saricimen, H., Shameem, M., Barry, M. S., Ibrahim, M., and Abbasi, T. A. (2003). Durability of proprietary cementitious materials for use in wastewater transport systems. *Cement and Concrete Composites*, 25(4-5), 421-427.

Sata, V., Sathonsaowaphak, A., and Chindaprasirt, P. (2012). Resistance of lignite bottom ash geopolymer mortar to sulfate and sulfuric acid attack. *Cement and Concrete Composites*, 34(5), 700-708.

Scherer, G. W. (2004). Stress from crystallization of salt. *Cement and Concrete Research*, 34(9), 1613-1624.

Schmidt, T., Neuenschwander, J., Romer, M., and Luthi, T. (2006). Investigation of physical and microstructural changes in the surface of mortar samples exposed to sulphuric acid. *Special Publication*, 234, 561-570.

SIA. (2014). Anforderungen an neue Zemente (Merkblatt 2049). *Schweizerisches Ingenieur and Architektenverein*. Zürich, Switzerland.

Shi, C. (1996). Strength, pore structure and permeability of alkali-activated slag mortars. *Cement and Concrete Research*, 26(12), 1789-1799.

Shi, C., and Stegemann, J. A. (2000). Acid corrosion resistance of different cementing materials. *Cement and Concrete Research*, 30(5), 803-808.

Shi, C., Roy, D., and Krivenko, P. (2006). *Alkali-activated cements and concretes*. CRC press.

Sofi, M., Van Deventer, J. S. J., Mendis, P. A., and Lukey, G. C. (2007). Engineering properties of inorganic polymer concretes (IPCs). *Cement and Concrete Research*, 37(2), 251-257.

Song, X. J., Marosszeky, M., Brungs, M., and Munn, R. (2005). Durability of fly ash based geopolymer concrete against sulphuric acid attack. *International Conference on Durability of Building Materials and Components*, Lyon, France, 17-20.

Sunshine, R. A. (2009). The Budget and Economic Outlook: Fiscal Years 2009 to 2019. *Testimony Before the Committee on the Budget*, United States Senate, 2009.

Sumajouw, M., and Rangan, B. V. (2006). Low-calcium fly ash-based geopolymer concrete: reinforced beams and columns.

Tagnit-Hamou, A., Saric-Coric, M., and Rivard, P. (2005). Internal deterioration of concrete by the oxidation of pyrrhotitic aggregates. *Cement and Concrete Research*, 35(1), 99-107.

Talling, B. (1989). Effect of curing conditions on alkali-activated slags. *Special Publication*, 114, 1485-1500.

Talling, B., Brandstetr, J. (1989). Proceedings 3rd International Conference on Fly Ash, Slag, and Natural Pozzolans in Concrete, Trondheim, Norway, ACI SP 114.

Taylor, H. F. W. (1997). *Cement chemistry*, London, T. Telford.

Thistlethwayte, D. K. B. (1972). Control of sulfides in sewerage systems, Butterworth, Melbourne, Australia

Teychenne, D. C., Franklin, R. E., and Erntroy, H. C. (1988). Design of normal concrete mixes

(rev. ed.), Great Britain. Department of the Environment.

Tiznobaik, M., and Bassuoni, M. T. (2017a). A test protocol for evaluating absorption of joints in concrete pavements. *Journal of Testing and Evaluation*, 46(4).

Tiznobaik, M., and Bassuoni, M. T. (2017b). Investigation into enhancing and evaluating curing efficiency of joints in concrete pavements. *Road Materials and Pavement Design*, 1-17.

Torii, K., and Kawamura, M. (1994). Effects of fly ash and silica fume on the resistance of mortar to sulfuric acid and sulfate attack. *Cement and Concrete Research*, 24(2), 361-370.

Van Deventer, J. S., Provis, J. L., and Duxson, P. (2012). Technical and commercial progress in the adoption of geopolymer cement. *Minerals Engineering*, 29, 89-104.

Van Jaarsveld, J., and Van Deventer, J. S. J. (1999). Effect of the alkali metal activator on the properties of fly ash-based geopolymers. *Industrial and Engineering Chemistry Research*, 38(10), 3932-3941.

Vincke, E., Boon, N., and Verstraete, W. (2001). Analysis of the microbial communities on corroded concrete sewer pipes–a case study. *Applied Microbiology and Biotechnology*, 57(5-6), 776-785.

Wallah, S.E. and Rangan, B.V. (2006). Low-Calcium Fly Ash-Based Geopolymer Concrete: Long Term Properties, *Research Report GC2*, Faculty of Engineering, Curtin University of Technology, Perth.

Wang, S. D., Scrivener, K. L., and Pratt, P. L. (1994). Factors affecting the strength of alkali-activated slag. *Cement and Concrete Research*, 24(6), 1033-1043.

Wardhono, A., Law, D. W., and Strano, A. (2015). The strength of alkali-activated slag/fly ash mortar blends at ambient temperature. *Procedia Engineering*, 125, 650-656.

Wei, S., Jiang, Z., Liu, H., Zhou, D., and Sanchez-Silva, M. (2013). Microbiologically induced deterioration of concrete: a review. *Brazilian Journal of Microbiology*, 44(4), 1001-1007.

Winnefeld, F., Leemann, A., Lucuk, M., Svoboda, P., and Neuroth, M. (2010). Assessment of phase formation in alkali activated low and high calcium fly ashes in building materials. *Construction and Building Materials*, 24(6), 1086-1093.

Xie, S., Qi, L., and Zhou, D. (2004). Investigation of the effects of acid rain on the deterioration of cement concrete using accelerated tests established in laboratory. *Atmospheric Environment*, 38(27), 4457-4466.

Ye, H., and Radlińska, A. (2016). Shrinkage mechanisms of alkali-activated slag. *Cement and Concrete Research*, 88, 126-135.

Yuan, H., Dangla, P., Chatellier, P., and Chaussadent, T. (2013). Degradation modelling of concrete submitted to sulfuric acid attack. *Cement and Concrete Research*, 53, 267-277.